TECHNISCHE
UNIVERSITÄT
DRESDEN

Fakultät Umweltwissenschaften, Fachrichtung Hydrowissenschaften

Modeling the effects of Transient Stream Flow on Solute Dynamics in Stream Banks and Intra-meander Zones

DISSERTATION

Zur Erlangung des akademischen Grades
Doktoringenieur (Dr.-Ing.)
in der Wissenschaftsdisziplin Wasserwirtschaft

vorgelegt von
M.Sc. WRM. **MUHAMMAD NASIR MAHMOOD**
Geboren am 10. September 1984 in Kotli-AJK

Tag der Verteidigung: **06. März 2020**

Gutachter:

Prof. Dr. Rudolf Liedl
Technische Universität Dresden, Institut für Grundwasserwirtschaft

Prof. Dr. Jan. H. Fleckenstein
Helmholtz-Zentrum für Umweltforschung, Department für Hydrogeologie

JProf. Dr. rer. nat. Marc Walther
Technische Universität Dresden, Institut für Grundwasserwirtschaft

To my big brother and the first mentor, ***Khurshid Anwer***

&

To ***Hanzala****, my son, the best thing happened to me during these times*

Erklärung des Promovenden

Die Übereinstimmung dieses Exemplars mit dem Original der Dissertation zum Thema:
“Modeling the effects of Transient Stream Flow on Solute Dynamics in Stream Banks and Intra-meanderZones”
wird hiermit bestätigt.

Leipzig,

Ort, Datum

Unterschrift

“ Do not you see that the heavens and the Earth were
meshed together then We ripped them apart?
And then We made of water everything living.”
[Quran 21.30]

“And We sent down from the sky water (rain) in measure,
and We gave it lodging in the earth, and verily,
We are Able to take it away.”
[Quran 23:18]

Abstract

Waters from various sources meet at the interface between streams and groundwater. Due to their different origins, these waters often have contrasting chemical signatures and therefore mixing of water at the interface may lead to significant changes in both surface and subsurface water quality. The riparian zone adjacent to the stream serves as transition region between groundwater and stream water, where complex water and solute mixing and transport processes occur. Predicting the direction and the magnitude of solute exchanges and the extent of transformations within the riparian zone is challenging due to the varying hydrologic and chemical conditions as well as heterogeneous morphological features which result in complex, three-dimensional flow patterns.

The direction of water flow and solute transport in the riparian zone typically varies over time as a result of fluctuating stream water and groundwater levels. Particularly, increasing groundwater levels can mobilize solutes from the unsaturated zone which can be subsequently transported into the stream. Such complex, spatially and temporally varying processes are hard to capture with field observations alone and therefore modeling approaches are required to predict the system behavior as well as to understand the role of individual factors.

In this thesis, we investigate the inter-connectivity of streams and adjacent riparian zones in the context of water and solute exchanges both laterally for bank storage and longitudinally for hyporheic flow through meander bends. Using numerical modeling, the transient effect of stream flow events on solute transport and transformation within the initially unsaturated part of stream banks and meander bends have been simulated using a systematic set of hydrological, chemical and morphological scenarios.

A two dimensional variably saturated media groundwater modeling set up was used to explore solute dynamics during bank flows. We simulated exchanges between stream and adjacent riparian zone driven by stream stage fluctuations during stream discharge events. To elucidate the effect of magnitude and duration of discharge events, we developed a number of single discharge event scenarios with systematically varying peak heights and event duration. The dominant solute layer was represented by applying high solute concentration in upper unsaturated riparian zone profile. Simulated results show that bank flows generated by high stream flow events can trigger solute mobilization in near stream riparian soils and sub-

sequently export significant amounts of solutes into the stream. The timing and amount of solute export is linked to the shape of the discharge event. Higher peaks and increased duration significantly enhance solute export, however, peak height is found to be the dominant control for overall lateral mass export. The mobilized solutes are transported towards the stream in two stages (1) by return flow of stream water that was stored in the riparian zone during the event and (2) by vertical movement to the groundwater under gravity drainage from the unsaturated parts of the riparian zone, which lasts for significantly longer time (> 400 days) resulting in a theoretically long tailing of bank outflows and solute mass outfluxes. Our bank flow simulations demonstrate that strong stream discharge events are likely to mobilize and export significant quantity of solutes from near stream riparian zones into the stream. Furthermore, the impact of short-term stream discharge variations on solute exchange may sustain for long times after the flow event.

Meanders are prominent morphological features of stream systems which exhibit unique hydrodynamics. The water surface elevation difference across the inner bank of a meander induces lateral hyporheic exchange flow through the intra-meander region, leading to solute transport and reactions within intra-meander region. We examine the impact of different meander geometries on the intra-meander hyporheic flow field and solute mobilization under both steady-state and transient flow conditions. In order to explore the impact of meander morphology on intra-meander flow, a number of theoretical meander shape scenarios, representing various meander evolution stages, ranging from a typical initial to advanced stage (near cut off) meander were developed. Three dimensional steady-state numerical groundwater flow simulations including the unsaturated zone were performed for the intra-meander region for all meander scenarios. The meandering stream was implemented in the model by adjusting the top layers of the modeling domain to the streambed elevation. Residence times for the intra-meander region were computed by advective particle tracking across the inner bank of meander. Selected steady state cases were extended to transient flow simulations to evaluate the impact of stream discharge events on the temporal behavior of the water exchange and solute transport in the intra-meander region. Transient hydraulic heads obtained from the surface water model were applied as transient head boundary conditions to the streambed cells of the groundwater model. Similar to the bank storage case, a high concentration of solute (carbon source) representing the dominant solute layer in the riparian profile was added in the unsaturated zone to evaluate the effect of stream flow event on mobilization and transport from the unsaturated part of intra-meander region. Additionally, potential chemical reactions of aerobic respiration by the entry of oxygen rich surface water into subsurface as well denitrification due to stream and groundwater borne nitrates were also simulated. The results indicate that intra-meander mean residence times ranging from 18 to 61 days are influenced by meander geometry, as well as the size of the intra-meander area. We found that, intra-meander hydraulic gradient is the major control of RTs. In general, larger

intra-meander areas lead to longer flow paths and higher mean intra-meander residence times (MRTs), whereas increased meander sinuosity results in shorter MRTs. The vertical extent of hyporheic flow paths generally decreases with increasing sinuosity. Transient modeling of hyporheic flow through meanders reveals that large stream flow events mobilize solutes from the unsaturated portion of intra-meander region leading to consequent transport into the stream via hyporheic flow. Advective solute transport dominates during the flow event; however significant amount of carbon is also consumed by aerobic respiration and denitrification. These reactions continue after the flow events depending upon the availability of carbon source. The thesis demonstrates that bank flows and intra-meander hyporheic exchange flows trigger solute mobilization from the dominant solute source layers in the RZ. Stream flow events driven water table fluctuations in the stream bank and in the intra-meander region transport substantial amount of solutes from the unsaturated RZ into the stream and therefore have significant potential to alter stream water quality.

Zusammenfassung

An der Schnittstelle zwischen Grund- und Oberflächenwasser vermischen sich Wässer aus verschiedenen Quellen. Aufgrund ihrer unterschiedlichen Herkunft weisen diese oft gegensätzliche chemische Signaturen auf, so dass der Austausch zwischen Grund- und Oberflächenwasser zu erheblichen Veränderungen der Wasserqualität beider Wasserkörper führen kann. Die Uferzone ist der Übergangsbereich zwischen Grund- und Oberflächenwasser, indem die Mischungs- und Transportprozesse vorwiegend ablaufen. Aufgrund der unterschiedlichen hydrologischen und chemischen Bedingungen sowie der heterogenen morphologischen Merkmale, die zu komplexen, dreidimensionalen Strömungsmustern führen, ist die Vorhersage der Richtung und der Stärke des Austauschs von Wasser und gelösten Stoffen in der Uferzone schwierig. Die Richtung des Wasserflusses und damit des Stofftransports in der Uferzone variiert typischerweise auch mit der Zeit aufgrund schwankender Fluss- und Grundwasserstände. Insbesondere steigende Grundwasserspiegel können gelöste Stoffe aus der ungesättigten Zone mobilisieren, die anschließend in Richtung Fluss transportiert werden können. Solche räumlich und zeitlich variierenden Prozesse sind allein mit Feldbeobachtungen schwer zu erfassen, daher bieten sich Modellierungsansätze an, um das Systemverhalten vorherzusagen und die Rolle der einzelnen Faktoren zu verstehen. In dieser Arbeit untersuchen wir den Wasser- und Stoffaustausch sowohl lateral als Interkonnektivität zwischen Fluss und Uferzone als auch longitudinal entlang von Mäanderbiegungen. Mittels numerischer Modellierung wurden transiente Effekte von Abflussereignissen auf Transport und Reaktion von gelösten Stoffen einschließlich des ursprünglich ungesättigten Teils von Uferzone und Mäanderbiegungen für verschiedene hydrologische, chemische und morphologische Szenarien untersucht. Für die Modellierung der Uferzone wurde ein zweidimensionales, variabel gesättigtes Grundwassermodell verwendet, um die Dynamik der gelösten Stoffe zu untersuchen. Der simulierte Wasser- und Stoffaustausch zwischen Fluss und der angrenzenden Uferzone wird durch Schwankungen der Wasserstände während der Abflussereignisse angetrieben. Um die Auswirkungen von Höhe und Dauer der Abflussereignisse systematisch zu untersuchen, wurden eine Reihe von Einzelereignisszenarien mit systematisch unterschiedlichen Spitzenhöhen und -dauer verwendet. Um die Mobilisierung von gelösten Stoffen aus dem Uferbereich im Modell abzubilden, wurde eine Schicht mit hoher Konzentration in der ungesättigten Zone implementiert. Die Ergebnisse zeigen, dass Ereignisse mit hohem Durchfluss eine Mobilisierung von gelösten Stoffen in der Uferzone bewirken, die anschließend bei fallenden Wasserständen und umgekehrten hydraulischen Gradienten in den Fluss transportiert werden. Der Zeitpunkt und die Menge des Exports von gelösten Stoffen hängt von der Form des Abflussereignisses ab. Höhere Abflussspitzen und eine längere Dauer erhöhen den Export von gelösten Stoffen erheblich, jedoch ist die Höhe der Abflussspitze die Hauptkontrollgröße für den gesamten lateralen Massenexport. Die mobilisierten gelösten Stoffe werden in zwei Phasen in Richtung Fluss transportiert, (1) durch den Rückfluss von Flusswasser, das während des Ereignisses in der Uferzone gespeichert wurde, und (2) durch vertikale, ungesättigte Strömung. Die Effekte des Abflussereignisses dauern in der 2. Phase teilweise länger als 400 Tage an. Es kommt zu einer langfristigen Verlagerung von gelösten Stoffe aus der Uferzone in den Fluss, ausgelöst durch kurzzeitige Abflussereignisse. Mäander sind häufig vorkommende morphologische Strukturen von Flusssystemen. Der Höhenunterschied der Wasseroberfläche entlang des Gleithangs eines Mäanders induziert einen lateralen hyporheischen Austauschfluss durch die Intramäanderregion. In dieser Arbeit wurden die Auswirkungen verschiedener Mäandergeometrien auf das hyporheische Strömungsfeld und den Intramäander-Stofftransport sowohl unter stationären als auch unter transienten Strömungsbedingungen untersucht. Um den Einfluss der Mäandermorphologie auf die Intramäanderströmung systematisch zu quantifizieren, wurden eine Reihe von theoretischen Mäanderform-Szenarien entwickelt, die verschiedene Entwicklungsstadien der Mäander repräsentieren. Diese reichen von einem typischen Anfangs- bis zu einem fortgeschrittenen Stadium (near cut off). Zunächst wurden stationäre dreidimensionale Grundwassermodelle einschließlich der ungesättigten Zone verwendet. Der mäandrierende Fluss wurde im Modell implementiert, indem die oberen Schichten der Modelldomäne an die Höhe des Bachbettes angepasst wurden. Die Verweilzeiten für die Intramäanderregion wurden durch Partikeltracking ermittelt. Ausgewählte stationäre Fälle wurden dann auf transiente Strömungssimulationen erweitert, um den Einfluss von Abflussereignissen auf das zeitliche Verhalten des Wasseraustausches und des Stofftransports in der Intramäanderregion zu untersuchen. In den transienten Modellläufen wurde die obere Druckrandbedingung des Grundwassermodells aus den Wasserständen eines Oberflächenwassermodells abgeleitet und iterativ auf das Grundwassermodell übertragen. Ähnlich wie Modell der Uferzone wurde in der ungesättigten Zone eine hohe Konzentration (gelöster organischer Kohlenstoff) implementiert, um den Einfluss eines Abflussereignisses auf die Mobilisierung und den Transport aus dem ungesättigten Teil der Intramäanderregion zu bewerten. Zusätzlich wurden die Effekte auf aerobe Respiration durch den Eintrag von sauerstoffreichem Oberflächenwasser in den Untergrund sowie auf die Denitrifikation durch fluss- und grundwasserbürtiges Nitrat simuliert. Die Ergebnisse deuten darauf hin, dass die mittleren Intramäander-Verweilzeiten

(MRTs) im Bereich von 18 bis 61 Tagen von der Mäandergeometrie sowie der Größe der Intramäanderfläche beeinflusst werden, wobei der hydraulische Gradient innerhalb des Mäanders die wichtigste Kontrollgröße der Verweilzeiten ist. Im Allgemeinen führen größere Intramäanderflächen zu längeren Fließwegen und höheren mittleren Intramäander-Verweilzeiten, während eine erhöhte Mäander-Sinuosität zu kürzeren MRTs führt. Die vertikale Ausdehnung hyporheischer Fließwege nimmt im Allgemeinen mit zunehmender Sinusförmigkeit ab. Die transiente Modellierung der hyporheischen Strömung durch Mäander zeigt, dass große Abflussereignisse gelöste Stoffe aus dem ungesättigten Teil der Intramäanderregion mobilisieren, was zu einem Transport aus der Intramäanderregion in den Fluss führt. Während des Abflussereignisses dominiert der advektive Transport. Jedoch wird auch durch erhöhte aerobe Respiration und Denitrifikation eine beträchtliche Menge an Kohlenstoff verbraucht. Diese Reaktionen setzen sich nach den Abflussereignissen in Abhängigkeit von der Verfügbarkeit der Kohlenstoffquelle fort. Die Arbeit zeigt, dass Abflussereignisse die Mobilisierung von gelösten Stoffen aus der ungesättigten Zone bewirken können. Abflussereignisse führen zu Schwankungen des Grundwasserspiegels in der Uferzone und im Intramäanderbereich. Dadurch werden gelöste Stoffe aus der ungesättigten Zone mobilisiert und beim Abklingen des Abflussereignisses in Richtung Fluss transportiert. und so die Wasserqualität beeinflusst werden kann.

Contents

Declaration **V**

Abstract **IX**

Zusammenfassung **XIII**

1 General Introduction **1**
- 1.1 Background and Motivation 1
- 1.2 Hydrology and Riparian zones 4
  - 1.2.1 Transport processes driven by fluctuation in riparian water table depth 5
    - 1.2.1.1 Upland control 6
    - 1.2.1.2 Stream control 6
  - 1.2.2 Biochemical Transformations within the Riparian Zone 6
- 1.3 Types and scales of stream-riparian exchange 8
  - 1.3.1 Hyporheic Exchange 8
    - 1.3.1.1 Small Scale Vertical HEF 9
    - 1.3.1.2 Large Scale lateral HEF 9
  - 1.3.2 Bank Storage 10
- 1.4 Methods for estimation of GW-SW exchanges 11
  - 1.4.1 Field Methods 11
    - 1.4.1.1 Direct measurement of water flux 12
    - 1.4.1.2 Tracer based Methods 13
  - 1.4.2 Modeling Methods 14
    - 1.4.2.1 Transient storage models 15
    - 1.4.2.2 Physically based models 15
- 1.5 Research gaps and need 16
- 1.6 Objectives of the research 20
- 1.7 Thesis Outline 21

2 Flow and Transport Dynamics during Bank Flows **23**
- 2.1 Introduction 24
- 2.2 Methods 26
  - 2.2.1 Concept and modeling setup 26

2.2.2 Numerical Model 27
2.2.3 Stream discharge events 28
2.2.4 Model results evaluation 29
2.3 Results and discussion 31
2.3.1 Response of water and solute exchange to stream discharge events 31
2.3.1.1 Water exchange time scales 31
2.3.1.2 Stream water solute concentration 32
2.3.2 Solute mobilization within the riparian zone 34
2.3.3 Influence of peak height and event duration on solute mass export towards the stream 38
2.3.4 Effects of event hydrograph shape on stream water solute concentration 39
2.3.5 Model limitations and future studies 41
2.4 Summary and Conclusions 43

Appendix 2 **45**

3 Flow and Transport Dynamics within Intra-Meander Zone **49**
3.1 Introduction 49
3.2 Methods 54
3.2.1 Meander Shape Scenarios 54
3.2.2 Surface Water Simulations 56
3.2.3 3D Groundwater Flow Simulations with Modeling code MIN3P 58
3.2.3.1 Steady Flow Simulations 59
3.2.3.2 Stream flow event and Solute Mobilization Set-up . . 60
3.2.4 Reactive Transport 61
3.3 Results and Discussion 64
3.3.1 Groundwater heads and flow paths in the saturated intra-meander zone 64
3.3.1.1 Groundwater heads 64
3.3.1.2 Flow paths and isochrones 64
3.3.1.3 Vertical extent of flow paths 66
3.3.2 Intra-Meander Residence Time Distribution 67
3.3.3 Factors affecting intra-meander flow and residence times . . . 70
3.3.3.1 intra-meander hydraulic gradient 70
3.3.3.2 Maximum penetration depth 72
3.3.3.3 Meander sinuosity 72
3.3.3.4 intra-meander area (A) 73
3.3.4 Influence of Discharge Event on intra-meander Flow and Solute Transport 74

3.3.4.1 Spatial distribution of groundwater head and solute concentration 74
3.3.4.2 Time scales of intra-meander groundwater heads and solute transport 78
3.3.4.3 Solute export during stream discharge event 81
3.3.5 Intra-meander reactive transport during stream discharge event 83
3.3.5.1 Impact of stream discharge on aerobic respiration and denitrification 83
3.3.5.2 DOC mass removal during stream discharge event . . 87
3.4 Summary and Conclusions 89

Appendix 3 **92**

4 General Summary and Conclusions **101**
4.1 Summary 101
4.2 Conclusions 103
4.2.1 Flow and Transport Dynamics in Near Stream Riparian Zone (Bank Flows) 103
4.2.2 Flow and Transport Dynamics within Intra-Meander Zone . . 104
4.3 Model Limitations and Future Studies 105

Bibliography **109**

Acknowledgement **127**

List of Figures

1.1 River scale groundwater-surface water interactions and hyporheic flow. 8

1.2 Simulation results of bedforms induced hyporheic flow paths (black) (Stonedahl et al., 2010). 9

1.3 Conceptual representation of quasi-horizontal water exchange at scale of meander wavelength. The brown colored part represents unsaturated part of intra-meander zone. 10

2.1 Cross sectional view of the model setup (not to scale). Filled area represents the extent of the solute layer. The stream is represented by the time varying head (TVH) boundary (from $z = 0.26$ to 1.22 m) at the right boundary. At the left boundary of the domain, a fixed head boundary is assigned, representing the ambient groundwater level ($z = 0.3$ m) at the outer bound of the riparian zone. The dots represent observation points referred to in the subsequent figures where changes in groundwater head (black dots) and detailed solute mobilization process in unsaturated zone (blue dot) are observed. . . 28

2.2 Time scales of water and solute fluxes during a bank flow event of 0.96 m peak height above base flow and duration of 100 h.(a) stream discharge normalized to the base flow (Q/Q_b), (b) stage and groundwater heads at 5, 10 and 20 m distance from stream boundary (black dots in Figure 2.1), (c) hydraulic gradient at stream-riparian interface, i_{50} is the hydraulic gradient between the stream stage and the ambient groundwater head at the left boundary, while i_5 is the local gradient between the stream stage and the groundwater head at a distance of 5 m from stream (dotted blue line represents the hydraulic gradient in absence of the flow event), (d) water fluxes into (Q_{in}) and out (Q_{out}) of the riparian zone, (e) change in saturation during the flow event, (f) Concentration (C_{str}) in stream water. The red dotted vertical lines across the figures show the relative position of fluxes at these time steps. 33

2.3 Solute mass ($M[mol]$) in the part of riparian zone at various time steps. The solid and dotted blue lines show the 100 % (water level) and 5 % water saturation respectively. The black dots indicate the locations of the observation points for groundwater heads, while the blue dot shows the location for which a detailed description of the solute mobilization process in unsaturated zone follows in the next section. 36

2.4 Water saturation (a), solute concentration (b), solute mass (c) and vertical velocity component (d) at one individual cell at location $x = 5$ m and $y = 0.9$ m (indicated by the blue dot in Figure 2.3. 37

2.5 Total solute mass exported into stream in 4000 h (166 days) as a fraction of total solute mass in the domain at pre-event conditions, (a) combined effect of event peak height and duration, (b) effect of event peak height, and (c) effect of event duration. 38

2.6 Stream discharge $Q/Q_b[-]$ versus solute concentration in stream $C_{str}[mol/m^3]$ for (a-c) increasing discharge event duration (30, 60, and 90 h, respectively) for a fixed maximum peak height (0.96 m) (d-f) increasing maximum peak height (0.18, 0.54, 0.96 m) above base flow level respectively) for a fixed event duration (100 h). 41

2.1A Selected discharge scenarios of varied peak height and duration used in simulations (shortened list). Tick marks on x and y axes indicate duration of events [h] and peak height [m] respectively. 45

2.2A Effects of event hydrograph shape on stream water solute concentration [a, b]: Peak concentration in stream (C_{str}) with increasing peak discharge and duration [c, d]: Time lag in starting time of bank outflow (Q_{out}) and stream concentration (C_{str}) 47

2.3A Fraction of bank inflow water remaining in the riparian zone (green line), corresponding solute export (orange line) out of the riparian zone (top) and change in saturation within the riparian zone during and after the flow event (bottom).The vertical line indicate starting time of bank outflow, end time of flow event and time when major part of the outflow has discharged back to the stream respectively. . . 48

3.1 Basic form parameters of a meander, wavelength (λ), height or amplitude (H), radius of curvature (R_c) and meander length (L). 55

3.2 Three of the meander shape scenarios developed using different values of ω. The sinuosity increases with increasing value of ω. 56

3.3 Model set-up showing the extent of modeling domain with incised meandering channel and location of solute source. The domain area between two dotted lines parallel to Y direction is used for results evaluation. Two (XZ) cross sections on the right side show vertical profile of simulated water saturation (bottom) and solute concentration (top) under steady state conditions at the section XX' (marked in yellow). 58

3.4 Groundwater heads (GWH) distribution at a depth 0.25 m below the streambed for the scenarios $\omega = 60°$, $\omega = 90°$ and $\omega = 115°$ respectively (first row, sub-figures a1, b1, c1). Flow paths of the particles released from the upstream segment (segment AC in Figure 3.1) of the meander at the same depth are shown in second row (sub-figures a2, b2, c2). The blue lines show the particle paths in [XY] plane. Vertical extent of flow paths with colored lines are also shown in [XZ] plane (row 3, sub-figure a3, b3, c3). The arrows show the direction of flow paths. The dotted line perpendicular to flow paths in the second row represents 10 h isochrones while the gray dots show the locations of deepest points of flow path. 65

3.5 Residence time distributions (obtained through forward advective particle tracking) of the particle released from upstream segment of the meander for initial stage (a - d), middle stage (e - i) and advanced stage (j - l) meander scenarios. 68

3.6 (a) Cumulative distribution functions (CDF) for selected scenarios (early, middle and advanced stage meanders). (b) Probability distribution functions (PDF) of the residence times for early and middle stage meander scenarios. 70

3.7 Effect of meander sinuosity ($\omega[-]$), intra-meander area ($A[m^2]$) and hydraulic gradient ($Grad[-]$), on mean intra-meander residence times ($\mu RT[d]$) and maximum depth of flow paths ($D_{max}[m]$). 71

3.8 Effect of meander sinuosity ($\omega[-]$) and intra-meander area ($A[m^2]$) on intra-meander residence times ($\mu RT[d]$). Figure (a) shows relation between meander sinuosity ($\omega[-]$) and mean residence times ($\mu RT[d]$), Figure (b) shows relation between intra-meander area ($A[m^2]$) and mean residence time ($\mu RT[d]$). 73

3.9 Influence of discharge event on intra-meander flow and solute mobilization (scenario ω 60). Horizontal [XY] cross sections show groundwater head distribution (row 1) and solute mobilization (row 2) at a depth of 0.75 m below surface. The vertical [XZ] section of groundwater heads (row 3) and solute mobilization (row 4) are also shown at Y = 20 m (indicated by white lines in [XY] section (row 2)). 75

3.10 Influence of discharge event on intra-meander flow and solute mobilization (scenario ω 90). Horizontal [XY] cross sections show groundwater head distribution (row 1) and solute mobilization (row 2) at a depth of 0.75 m below surface. The vertical [XZ] section of groundwater heads (row 3) and solute mobilization (row 4) are also shown at Y = 20 m (indicated by white lines in row 2). 77

3.11 Influence of discharge event on intra-meander flow and solute mobilization (scenario ω 115). Horizontal [XY] cross sections show groundwater head distribution (row 1) and solute mobilization (row 2) at a depth of 0.75 m below surface. The vertical [XZ] section of groundwater heads (row 3) and solute mobilization (row 4) are also shown at Y = 20 m (indicated by white lines in row 2). 78

3.12 Stream stage above base flow $[H - H_b]$ at the upstream end of the meander (row 1), groundwater heads (row 2) $[GWH]$ and solute concentration $[Conc.]$ (row 3) at three locations marked as dots in in Figures 3.9, 3.10 and 3.11 for scenarios ω 60, ω 90 and ω 115 . The letters 'L', 'M' and 'R' represent the location of left, middle and right observation point along the XZ cross section. 79

3.13 Conservative solute exported to stream during the flow event for three meander shape scenarios i.e. ω 60, ω 90, ω 115. T_p and T_{end} indicate the peak and the ending time of the flow event respectively. 82

3.14 XZ-sections (at Y = 20 m) of intra-meander area for scenarios ω 60, 90 and 115 showing concentrations of CH_2O conserv. (R1), CH_2O reactive (R2), O_2 influx (R3), $S - NO_3$ (R4) at different time steps of stream discharge event. 84

3.15 Time frames of aerobic respiration (AR) and denitrification (DEN) via stream and groundwater borne oxygen and nitrates during the flow event for meander scenarios ω 60, ω 90, ω 115. T_p and T_{end} indicate the peak and the ending time of the flow event respectively. . 86

3.16 Cumulative reactive solute transport during the flow event for three meander shape scenarios i.e. ω 60, ω 90, ω 115. Solid and dotted lines represent fraction of solute remaining for conservative and reactive transport respectively. 87

3.1A XY- cross sections (at Z = 0.75 m below surface) for scenario ω 60 showing concentrations of CH_2O conserv. (R1), CH_2O reacted (R2), O_2 influx (R3) and $S - NO_3^-$ influx (R4) at various stages of stream flow event. 92

3.2A XY- cross sections (at Z = 0.75 m below surface) of intra-meander area for scenario ω 90 showing concentrations of CH_2O conserv. (R1), CH_2O reacted (R2), O_2 influx (R3) and $S - NO_3^-$ influx at various stages of stream flow event. 93

3.3A XY-cross sections (at Z = 0.75 m below surface) of intra-meander area for scenario ω 115 showing concentrations of CH_2O conserv. (R1), CH_2O reacted (R2), O_2 influx (R3) and $S-NO_3^-$ influx (R4) at various stages of stream flow event. 94

List of Tables

2.1 Hydrologic Properties of the Porous Medium. 29
2.1A Simulated discharge Scenarios of systematically increasing event peak height and duration 46

3.1 Hydraulic parameters for surface water model [HEC RAS]. 57
3.2 Meander shape scenarios for steady and unsteady flow simulations. . 59
3.3 Flow and transport parameters for the groundwater model [MIN3P]. . 62
3.4 Parameters of fitted probability density functions (pdf) to the residence time distributions for meander shape scenarios. 69

Chapter 1

General Introduction

1.1. Background and Motivation

The resources of fresh water on the earth can be broadly divided into two categories, a) surface water which includes all surface water bodies in liquid form such as rivers, lakes etc. as well as in solid form e.g. ice at poles and other snow covered areas, b) the water stored in the subsurface as soil water and groundwater. The largest portion of fresh water (around 68 %) exists in the forms of ice caps and glaciers e.g. at the poles and therefore is not readily accessible as a water resource. The total available surface water comprised of rivers, lakes and other isolated surface water bodies is estimated to 1.2 % whereas groundwater resources are estimated to 30 % of the total fresh water, making it almost 25 times bigger than all fresh surface water bodies combined (Gleick, 1993). A large portion of domestic and agricultural water needs are fulfilled by groundwater extraction across the world. Hence, the water beneath the surface is perhaps the most important fresh water resource.

Most surface water (SW) bodies are hydraulically connected with adjacent groundwater (GW) bodies. Surface bodies exchange water to groundwater bodies through their beds and banks. In fact, a large portion of water in perennial streams originates from the seepage from groundwater storage. Conversely, surface bodies also serve as recharge source of groundwater bodies in many geological settings (e.g., Winter, 1998). Hence, changes in one resource are translated into other resource and vice versa. Besides the natural exchanges between surface and groundwater bodies, human activities also influence the interactions between surface and groundwater bodies. For example, excessive withdrawal from surface bodies results in water influx from surrounding riparian zone towards stream. Similarly, excessive pumping of groundwater near streams will induce increased flow from the stream to the surrounding riparian zone (e.g., Döll, 2009).

Perhaps the most important aspect of GW-SW exchange is its roles in altering water quality for both GW and SW. Since GW-SW exchanges continuously occur in nature, solute contamination in one source can potentially lead to the contamination in other source due to transformation and exchange of solutes (Winter, 1998). In most cases, SW and GW have completely different chemical compositions, thus exchange across GW-SW interface often has profound influence on chemistry of both surface water bodies and groundwater (Boulton et al., 1998). Natural and man made stresses on one or both components of fresh water can alter the extent and direction of water and associated contaminant fluxes across GW-SW interface (e.g., Bencala, 1993; Valett et al., 1997).

Contamination sources of the fresh water may be categorized as following:

1. **Natural causes:** A major portion of run off generated from precipitation travels through the subsurface before reaching the stream. Depending upon the composition of soils around the surface and subsurface flow paths of run off, a variety of dissolved and undissolved species such as organic carbon (OC) and nitrogen species etc. are transported with the water flow to surface water bodies (Wood, 1977). Nitrate concentrations in the streams in agricultural catchments are found to be positively related to the discharge events (Krause, 2005). Similarly increase in stream DOC loads has been observed with flow events e.g. (Laudon et al., 2004; Inamdar and Mitchell, 2006). Catchment characteristics such as land cover i.e type of vegetation (e.g., Reddy et al., 1999), land use (Pratt and Chang, 2012), topography (e.g., Sliva and Williams, 2001), climate (e.g., Hanrahan et al., 2003), soil properties (Franklin et al., 2013) in combination with the hydrology (e.g., Hrachowitz et al., 2016) etc. strongly influence the amount of nutrient loads and suspended solid in the stream.

2. **Anthropogenic activities:** Besides natural causes, human activities such as industrial and municipal wastes as well as the use of fertilizers in agriculture are sources of a variety of pollutants into both surface and subsurface waters. Intensive and persistent use of agricultural fertilizers has become a major source of contaminants into surface and subsurface water (Suarez and Puertas, 2005). Excess nitrogen and phosphorous are accumulated in the soils from where they are transported to surface and groundwater causing eutrophication of surface waters (Carpenter et al., 1998). The species like ammonia are leached down to groundwater through various sources of recharge such as precipitation and irrigation (e.g., Hallberg, 1989; Galloway et al., 2004) etc. In cases where groundwater discharges to the surface water, it serves as a contamination source to the surface water. Since, the velocities of groundwater are considerably lower than that of surface water, groundwater borne solutes serve as long term contamination source for surface water. Moreover, sewage and industrial waters also release various type of harm-

ful chemicals including carbon, sulphur and nitrogen compounds as well as hazardous substances such as heavy metals into surface and subsurface water bodies (e.g., Pye and Patrick, 1983). Similarly extraction and use of fossil fuel is also linked to increased quantities of variety of contaminants to the fresh water resource ranging from DOC and nitrate loads to hazardous metals (e.g., Seitzinger et al., 2002).

Hence, understanding the processes involved in river scale GW-SW interactions is crucial for integrated water resource management as well as for preservation and management of groundwater dependent ecosystems and riparian habitat (e.g., Krause et al., 2009). The increasing demand of fresh water as a result of changes in hydrologic cycle associated with regional/global climate change (Barnett et al., 2005; Cisneros et al., 2014) as well as due to over exploitation of these resources by human activities, (e.g., Wang and Qin, 2017) is leading to the disturbance of GW-SW exchange balance. Especially, GW-SW interactions are the focus of the current hydrological research (e.g., Fleckenstein et al., 2010; Boano et al., 2014) due to their practical implications on fresh water chemistry such as adverse effects on stream ecology and drinking water reservoirs (Bencala, 1993). Nitrogen (N) release into the surface and groundwater bodies activities has been identified as one of the major water quality problem in agricultural catchments (e.g., Grizzetti et al., 2011). Similarly, in the recent past, a persistent trend of increased concentrations of dissolved organic carbon (DOC) has been observed in the European and North American streams (Rinke et al., 2013; Camino Serrano et al., 2016). In a field study of northern Sweden catchments, Laudon and Buffam (2007) showed that even a smaller change in the DOC concentration during the spring floods could impact acid sensitive aquatic biota in stream network. Both nitrogen (N) and DOC serve as an energy source for aquatic life (e.g., Berman and Bronk, 2003), leading to eutrophication. Furthermore, stream DOC has been also known for its role in nutrient transport (Schlesinger and Bernhardt, 2013), controlling the metal loads e.g. mercury (Mierle and Ingram, 1991) etc. One of the most critical concern of increased fluxes of nitrogen (N) and DOC in the stream is the rise in the cost of drinking water treatment (Ulrich et al., 2006; Grizzetti et al., 2011; Ledesma et al., 2012; Rinke et al., 2013). When treated with conventional methods like chlorination practices, drinking water with elevated DOC concentration can produce harmful by-products including infamous trihalomethane (THM) (USEPA, 2002).

In context of above mentioned scenario, a better understanding of transformation and exchange of organic matter and nutrients at GW-SW interface i.e. mixing zone between streams and groundwater is required for efficient management of stream water quality as well as for broader aspects of clean environment (Lintern et al., 2018). However, the temporal and spatial patterns of water and chemical exchange across the stream-groundwater interface are still poorly understood (Boano et al., 2014). The role of hydrological and chemical conditions across GW-SW interface, impact of morphological setting as well as identification of flow paths patterns and their residence times are the main focus of current GW-SW exchange research and will be addressed also in this thesis.

1.2. Hydrology and Riparian Zones

Riparian zones are land strips surrounding the river which serve as a transition zone between terrestrial and aquatic environment. On a broader scale, we can assume riparian zone as the interface between the terrestrial and aquatic environment. Although riparian zones are a small portion of the total watershed area, they play crucial role in the riverine ecosystem and are known to have disproportionate influence on aquatic environment due to their unique hydrological and chemical functions (e.g., Hill, 2000; Naiman et al., 2010). For example, unique riparian zone environment support vegetation which regulates stream temperatures (e.g., Barling and Moore, 1994) as well as reduces run off velocities and entraps sediments (e.g., Tabacchi et al., 2000). In addition to that, riparian zones also entrap variety of nutrients carried by run off from upland and therefore also serve as nutrient filter (Karr and Schlosser, 1978). As a result, a variety of nutrients such as carbon, nitrogen and phosphorous species are accumulated in the riparian zones, providing a major source of energy for aquatic life. A combination of climatic conditions and availability of life supporting nutrients makes the riparian zones a suitable place for high metabolic activity and extended plant growth (Swanson et al., 1982).

Being at the junction of aquatic and terrestrial environment, the complex riparian processes vary both in space and time and are influenced by a variety of factors including temperature, variability in soil moisture, presence and type of biota, type and concentration of chemical species and difference in solute concentration in various sources of water (Hedin et al., 1998; Vidon and Hill, 2004a) etc. However, primary control for riparian functionality is the dynamic hydrologic conditions of the riparian zone because pathways of water through riparian zone are strongly influenced by the hydrological conditions (Vidon and Hill, 2004b) such as fluctuations of riparian water table due to complex exchange processes between surface and groundwater (Bencala and Walters, 1983; Harvey and Bencala, 1993; Boulton et al., 1998). Therefore in order to understand the processes at riparian zone, we first need to understand riparian zone hydrology.

The riparian hydrology is strongly influenced by its connectivity to the stream and upland (Brinson, 1993; Baker et al., 2001; Laudon et al., 2004). For example, Hill (2000) showed that the size of upland aquifer is an important control of the magnitude of subsurface flow and nutrient inputs to the riparian zone. Moreover the riparian water table is also influenced by the size and seasonal changes in the upland hydrology (e.g., Hill and Devito, 1997). Similarly, Vidon and Hill (2004b) found that the upland topography and riparian sediment lithology influence riparian groundwater flow patterns. In the hydraulically connected stream and groundwater systems, the hydraulic gradient at the interface controls magnitude and direction of exchange (Duval and Hill, 2006). In addition to that, the type of sediments at the interface determines the connectivity between SW and GW and therefore controls the extent of exchanges. If the streambed is composed of impervious material e.g. rock, the exchange will be limited. In contrast, presence of sand at the streambed will insure high exchange of water and chemicals (Packman and Salehin, 2003). Hence, interactions of surface water bodies i.e. streams, lakes, and wetlands with surrounding groundwater are defined by their mutual positions, geologic characteristics of the area as well as their climatic settings (Winter, 1999).

Dissolved organic carbon (DOC) and nitrogen (N) species are important nutrients which are accumulated in the riparian zone e.g. during run off from upland and entrapment of nutrients from shallow subsurface flow. The riparian vegetation takes up significant amount of nitrogen (e.g., Lowrance et al., 1984; Kaushal and Lewis, 2005, etc.) and carbon (e.g., Tank et al., 2010) that otherwise would discharge to stream. On the other hand, accumulation process results in abundance of these nutrients in the riparian zone. The portion of nutrients that is taken by the the riparian species such as plants, is also reintroduced to the riparian soils e.g. by decomposition of biomass (Webster et al., 1999). The potential of accumulation of organic matter is further enhanced by the high nitrogen availability which supports high productivity (Jansson et al., 2007). These nutrient stored within the riparian zone can undergo transformations through continuous interactions of stream and groundwater and therefore these zones are seen as areas of large geochemical reaction potential and can also serve as nutrient source to stream water (e.g., Bishop et al., 1994) under dynamic water table conditions.

1.2.1. Transport Processes driven by Fluctuation in Riparian Water Table Depth

As a result of continuous accumulation of nutrients, upper horizons of soil profile of riparian zones are often enriched with nutrients such as organic matter (Parkin, 1987; Hill, 2000). Under normal flow riparian water table is usually below this nutrient rich zone. However, a rise in water table in riparian zone may result in the infiltration of water into the nutrients rich soils, resulting in mobilization and transport of nutrients (e.g., Bishop et al., 1994; Vidon and Hill, 2004b; Boutt and Fleming, 2009). The chemical composition of riparian zone is mainly controlled by both stream and upland sub-surface flow.

1.2.1.1. Upland Control

A rise in water table due to the increased subsurface flow from upland (e.g. in case of precipitation event etc.) could lead to the water infiltration into the unsaturated zone. The infiltration into the nutrient rich layers may result in mobilization and consequent transport of solutes into the stream. Many studies have suggested that during precipitation events, subsurface flow paths passing through nutrient rich layers of riparian zone significantly increase nutrient loads into the stream. In a meta-study of forested watersheds, Raymond and Saiers (2010) concluded that 86 % of total annual DOC load was exported during precipitation events, and major portion (about 57 %) of it was transported in larger precipitation events. Similarly, Yoon and Raymond (2012) found that about 40 % of annual export of DOC from Esopus Creek was released to the stream within 5 days of Hurricane Irne. Moreover, DOC dynamics in peat lands are also been found to be strongly controlled by site hydrology, especially by the water table depth (Blodau and Moore, 2003).

1.2.1.2. Stream Control

Besides the ambient groundwater discharge, stream stage fluctuations e.g. in case of stream flow event can also lead to the mobilization of organic matter in the riparian zone. For example, stream water is temporarily stored in stream banks or riparian zones during storm events. These bank flows have potential to exchange solutes between stream and and adjacent riparian zone (Vidon and Hill, 2004a; McCallum et al., 2010; Welch et al., 2015, etc.).

1.2.2. Biochemical Transformations within the Riparian Zone

In addition to the water table driven nutrient transport, stream-riparian exchange also creates a conducive environment for important biogeochemical activity of microorganisms which may biogeochemically transform the species and even may permanently remove them (Battin et al., 2003). One of the major reasons for high interest of researchers in riparian zone (RZ) dynamics is the unique biogeochemical environment of RZ and its significant effect on surface and groundwater quality.

Chemical composition of stream water is significantly different than groundwater. For example, surface waters are typically enriched in dissolved oxygen (DO), whereas groundwater possesses little to no amount of DO (Robertson et al., 2010). On the other hand, riparian water is enriched in nutrients such as carbon and nitrogen species (Valett et al., 1994; Jones Jr et al., 1995). Mixing of surface and groundwater at RZ leads to interactions between stream and groundwater borne solutes (Boulton et al., 1998). Entry of DO rich surface water into the riparian zone triggers microbial heterotrophic respiration in presence organic matter. In addition to that, DO also facilitates nitrification, a process where aerobic bacteria transform subsurface ammonia into soluble form of (NO_3^-) in presence of oxygen (O) and in the meanwhile consume DOC as their energy source (Bencala, 2000). The process of nitrification is very important for the removal of N because transformation of insoluble nitrogen to the soluble form (NO_3^-), provides opportunity of denitrification under suitable conditions. Since, riparian zones generally have shallow groundwater table, which create anoxic conditions limiting degradation processes like aerobic respiration and therefore reducing consumption of organic matter (e.g., Munch and Ottow, 1983). At this stage, anaerobic conditions favour denitrification, a process of reducing NO_3^- into gaseous N (Hedin et al., 1998). However, for anaerobic denitrification, availability of soluble carbon is a limiting factor as often at higher depths there is low soluble carbon content. Limited availability of carbon means low energy for anaerobic organism and therefore little denitrification potential (Burt et al., 1999). For example Hill (2000) found that most of NO_3^- removal occurred where groundwater was enriched with organic matter. Similarly, Correll et al. (1997) found that in a soil with low organic matter, limited denitrification occurred. Hence, for denitrifcation, shallow water table conditions are necessary, which ensure energy source (carbon matter) for denitrifying bacteria. The reactions involved in the decomposition of organic carbon by consumption of oxygen (O) and nitrogen (N) are given below.

$$\mathrm{CH_2O + O_2 \longrightarrow CO_2 + H_2O} \text{ (Aerobic respiration)}$$

$$\mathrm{2\,NH_4{}^+ + 3\,O_2 \longrightarrow 2\,NO_2{}^- + 4\,H^+ + 2\,H_2O} \text{ (Nitrification step-1)}$$

$$\mathrm{2\,NO_2{}^- + O_2 \longrightarrow 2\,NO_3{}^-} \text{ (Nitrification step-2)}$$

$$\mathrm{5\,CH_2O + 4\,NO_3{}^- + 4\,H^+ \longrightarrow 5\,CO_2 + 2\,N_2 + 7\,H_2O} \text{ (Denitrification)}$$

The complex biogechemical processes in RZ are controlled by various combination of diverse factors including temporal and spatial variability of riparian soil moisture (McClain et al., 2003), redox potentials (Vidon et al., 2010), temperature (Hedin et al., 1998), spatail and temporal variations in the riparian hydrology (Hill, 2000; Vidon and Hill, 2004b), flow rates and residence times (Trauth et al., 2014; Trauth and Fleckenstein, 2017) as well as chemical compositions of riparian zone. The role of riparian zone for regulating and transporting nutrient is well known, however the relative importance of individual factors on reactive efficiency e.g. role of dynamic flow conditions, are not clear. A detailed look into the mechanism of water mixing and their effects on regulating nutrients in the near stream-riparian zone is required for better management of stream water quality.

1.3. Types and Scales of Stream-Riparian Exchange

The scales of stream-riparian exchange vary in both space and time. Depending upon the topographical and hydrological features as well as climatic conditions and their specific functions, these interactions may range from small scale vertical exchanges across the streambed to the large scale lateral exchanges such as sinuosity driven exchange and bank storage processes. Besides, the characterization of stream connection with surrounding riparian environment also varies depending upon the prospective of investigator and the specific study goals (Boano et al., 2014). The functions of these exchange processes also differ on the basis their scales and deriving factors. Commonly known river scale GW-SW exchange processes are illustrated in the Figure 1.1.

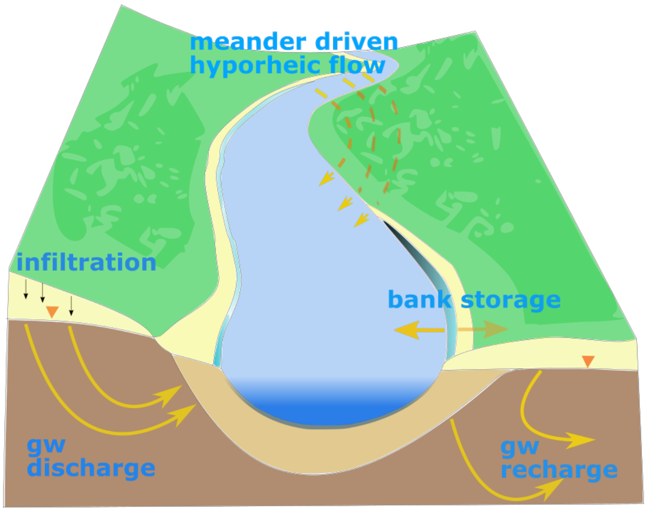

Figure 1.1: River scale groundwater-surface water interactions and hyporheic flow.

1.3.1. Hyporheic Exchange

The exchange of surface water with the surrounding sediments in defined flow paths that return back to surface water is termed as the hyporheic flow (Harvey et al., 1996; Winter, 1998). The subsurface area beneath the streambed and around the banks penetrated by these flow paths is called hyporheic zone. This continuous forth and back exchange from and to the stream is a key difference of hyporheic exchange flow (HEF) from normal groundwater flow which is often one way flow on a much larger scale e.g. groundwater originated by recharge during a precipitation event, travels to discharge into a gaining stream. Similarly, it is also possible for groundwater to move away from the stream depending upon hydrologic and climatic conditions (Figure 1.1), whereas the hyporheic exchange flow is strictly the flow which originates from the stream and after spending sometimes in the sediments returns back to stream. Hyporheic exchange is the primary mechanism by which oxygen rich surface water interacts with the streambed sediments (e.g., Elliott and Brooks, 1997). The hyporheic exchange may range from very small scale i.e. a few centimeters around the bed in vertical extent to the hundreds of meters in lateral extent e.g. through meander bends. The hydraulic forces of stream in combination with the morphological features, define the type and extent of hyporheic flow (Boano et al., 2014).

1.3.1.1. Small Scale Vertical HEF

The most commonly known hyporheic flow paths are vertical exchanges across the streambed. Pressure variations caused by small topographical features e.g. bedforms and other obstacles along the bed induce hyporheic flow across the streambed. At such as small scale hydrodynamically driven forces are more dominant e.g. in submerged bedforms changes in stream velocity define the energy head at the streambed. The Figure 1.2 shows simulated results of hyporheic flow paths (black) induced by small bedforms (Stonedahl et al., 2010). The head distribution at the streambed is influenced by the temporal variations of stream flow properties. This type of hyporheic exchanges are usually both smaller in terms of extent (usually in centimeters), shallow in depth as well as shorter in terms of residence times.

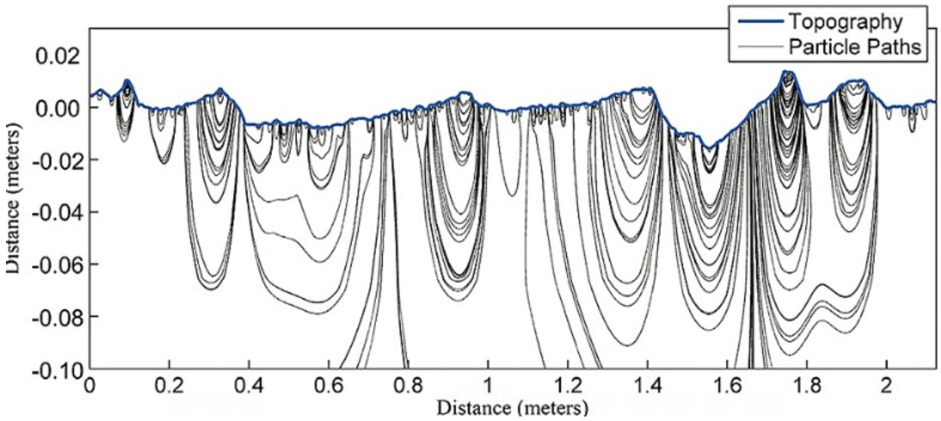

Figure 1.2: Simulation results of bedforms induced hyporheic flow paths (black) (Stonedahl et al., 2010).

1.3.1.2. Large Scale Lateral HEF

In addition to the small scale vertical hyporheic flow induced by submerged bed features, lateral hyporheic exchanges on medium and larger scale also occur within stream reaches. The topographical features of river induce hydraulic differences across in-stream structures, e.g. across the in-stream gravel bars and meander bends. The HEF across larger morphological features is usually driven by hydrostatic head difference which causes the flow to enter the bed at locations of higher water surface (usually upstream side of structure) and exit at the lower water surface level (Boano et al., 2006). For example, in case of intra-meander flow, the flow paths leave from upstream bank of meander bed and, passing through subsurface intra-meander region, exit at downstream bank of the meander (Figure 1.3). This type of hyporheic exchanges are characterized by the larger spatial extent and very long residence times and therefore have important implications for biochemical transformations. Furthermore, flow paths are predominately longer in lateral extent as compared with the vertical extent. Such lateral exchanges have been found to occur throughout the stream network (e.g., Kiel and Cardenas, 2014), thus water reaching the outlet has been laterally circulated multiple times through riparian zone around streambed, where it undergoes biogeochemical transformations.

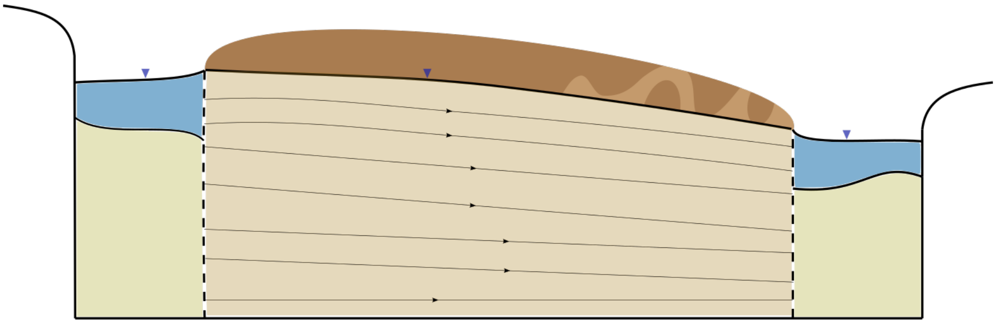

Figure 1.3: Conceptual representation of quasi-horizontal water exchange at scale of meander wavelength. The brown colored part represents unsaturated part of intra-meander zone.

1.3.2. Bank Storage

Besides the above mentioned vertical and horizontal scale HEF, other kind of connections between streams and surrounding riparian zones also exist, e.g. temporary storage of stream water into bank soils during high stream stage. During stream discharge events, a rise in stream stage leads to the movement of stream water into surrounding unsaturated riparian area perpendicular to the stream flow direction, where this water is stored for some times and discharges back to the river after the flow event. This temporary storage of stream water in the surrounding riparian zone is termed as the bank storage (BS).

The exchange processes during bank flows are not included in hyporheic flow types because of their contrasting driving mechanism. Hyporheic exchange flow (HEF) is caused due to hydrostatic head difference induced by the topographical features of the stream and therefore occurs under all conditions and throughout the length of rivers (Buffington and Tonina, 2009). The changing hydrologic conditions such as flow event may further influence the exchange by altering the extent of exchange and cycling of nutrients. On the other hand, bank storage (BS) is exclusively associated with flow events which result in temporary reversal of gradient at GW-SW interface.

Even though HEF and BS are two separate processes in terms of their driving mechanism, they have similar implications for solute mobilization, transport and transformations (e.g., Shuai et al., 2017). Similar to the HEF, BS enables delivery of surface water nutrients and oxygen into subsurface, in presence of oxygen, these nutrients interact with groundwater borne nutrients resulting in their retention, cycling and transformation (Gu et al., 2012). Although bank storage (BS) is a well known classical phenomenon (Cooper and Rorabaugh, 1963; Pinder and Sauer, 1971), relatively small number of studies have explored its potential for solute transport and resulting influence on ground and surface water quality. A few studies have focused on the influence of BS on solute transport processes and have indicated that river fluctuations increase physical connectivity and biogeochemical transformation between rivers and RZ (e.g., Sawyer et al., 2014; Musial et al., 2016; Stegen et al., 2016; Shuai et al., 2017). Gu et al. (2012) simulated the effect of BS on nutrient transport during stream flow events and found that near stream RZ are biogeochmically active during bank flows. Shuai et al. (2017) simulated the influence of dam induced BS on the fate of stream borne nitrogen. They found that near stream RZ, where oxygen rich surface water penetrates, facilitates nitrification whereas the deeper anoxic RZ promotes denitirifcation. They also found that nitrates removal is positively related to stream stage fluctuations and sediment hydraulic conductivity.

Due to their similar potential of biogeochmical activity, i.e. nutrient cycling, retention and transformation, and their implications on both stream and groundwater quality, the line between hyporheic exchange flow (HEF) and classical bank storage phenomenon is becoming blurred with the advancement of the research (Boano et al., 2014). In recent studies, the term BS and HEF have been alternatively used (e.g., Shuai et al., 2017) while others have merged the large scale HEF and BS (e.g., Gomez-Velez et al., 2017).

1.4. Methods for Estimation of GW-SW Exchanges

1.4.1. Field Methods

The spatial and temporal extent of GW-SW interactions and their implications is hard to quantify due to the complexity of mechanisms involved. The main controls of water flux across the interface include hydraulic head gradient at the interface (e.g., Welch et al., 2015; Mahmood et al., 2019) and sediment hydraulic conductivity (e.g., Salehin et al., 2004). Biogeochemical transformations within the riparian zone depend on the chemical composition of both surface and groundwater, temperature, flow paths of water entering and exiting the riparian zone and the contact time (residence time) between the stream borne and riparian borne solutes. An accurate description of underlying mechanism is pre-requisite in order to estimate the water exchange as well as the solute transport and reactions.

Various direct and indirect methods for estimation of the exchange fluxes and associated biochemical activity have been developed over the years. The choice of method is dictated by the spatial extent of the exchange as well as the specific research question (e.g., Kalbus et al., 2006). A short overview of the commonly used methods and their limitations is discussed in the following.

1.4.1.1. Direct Measurement of Water Flux

The direct measurement of water flux is the most suitable for measuring GW-SW exchange at point scale. Hydrometric measurements e.g. by installation of seepage meters (Lee, 1977) at streambed help in the identification of groundwater recharge or discharge zones. These techniques provide the direction of exchange as well as the rate of exchange at a specific location of streambed. In the most simplified form, a seepage meter consists of a bottomless cylinder connected to a deflated plastic bag via a vent. The cylinder is submerged into the sediments to collect upwelling groundwater in the bag. The seepage flux can be calculated by measuring the volume of collected water, cross sectional area of cylinder and the duration of collection. For estimation of SW flux into groundwater, a known volume is filled in the plastic bag and infiltration rate is estimated by measuring the volume loss.

However, their applicability is limited, e.g. in streams, water flow can affect the hydraulic head in the bag, leading to over or underestimation of the flux. Higher flow velocities can destabilize the streambed due to scour and therefore can influence the hydraulic head and seepage flow (Brunner et al., 2017). To overcome these issues, many modification and improvement have been made over the years. For example, Kelly and Murdoch (2003) proposed installation of piezometers with seepage meter in order to measure vertical hydraulic conductivity and head gradient for the better estimation of seepage flux. Similarly many other automated versions of seepage meter have been developed such as heat pulse meter (Taniguchi and Fukuo, 1993), which utilizes the travel time of heat pulse, the ultrasonic meter (Paulsen et al., 2001) based on the travel time of ultrasonic signal and electromagnetic meter (Rosenberry and Morin, 2004) that measures flow velocity by detecting voltage induced by the water passing through a magnetic field. The direct measurement methods are simple, inexpensive and do not require additional information such as sediment hydraulic conductivity, however, they are mostly suitable for still waters such as lakes or flowing water with very small velocities. In addition to that application of these methods is limited for the estimation of vertical exchange at small scales and in very shallow surface bodies. As the exchange fluxes are highly dynamic over space and time, a very fine resolution of measurement points is required to predict reasonably accurate exchange direction and rates (Stonedahl et al., 2013).

1.4.1.2. Tracer Based Methods

Alternatively tracer based techniques are widely used for the estimation of flux exchanges and are found more reliable at larger scale (e.g., Cook, 2013; Kalbus et al., 2006). Some of the widely used tracer techniques are presented in following.

1. **Heat as a tracer:** Stream temperatures strongly vary in time on daily and seasonal basis whereas the groundwater temperature remains stable throughout the season, hence this phenomenon of difference in temperature can be utilized to quantify the water fluxes across the GW-SW interface. For example, relatively stable sediment temperatures have been observed in gaining reaches due to influx of ground water into the streambed, whereas losing reaches usually exhibit highly variable sediment temperature (Winter, 1998). Heat transport in the subsurface can be described by the heat transport equation (Domenico et al., 1998). Temperature is a robust and easily measurable parameter, therefore are suitable for long term monitoring. Hence, temperature based methods have been widely used as the measure of flux exchanges across GW-SW interface (e.g., Constantz, 1998; Constantz et al., 2001; Becker et al., 2004; Schmidt et al., 2007; Constantz, 2008; Krause et al., 2011; Munz and Schmidt, 2017). However, due to heat retardation in sediments, this method has been found to underestimate the exchange rates (e.g., Engelhardt et al., 2011). Similarly under low flow velocities, the results have been found unreliable (Rau et al., 2014). High resolution temperature logging are required for estimation of low fluxes.

2. **Environmental chemical tracers:** Another commonly used method to distinguish the various sources of streamflow is the use of environmental tracers. Both surface water and groundwater contain different quantities of naturally existing stable isotopes such as O^{18} and Deuterium. These isotopes are conservative (i.e. non-reactive) in nature, therefore are easy to evaluate (Engelhardt et al., 2011). The difference between chemical signature of stream and surrounding riparian water exchanges is widely used to differentiate various sources of water (e.g., Harvey and Bencala, 1993; McCallum et al., 2010; Fowler and Scarsbrook, 2002, etc.). Some of the commonly used tracer include electrical conductivity (EC) (Vogt et al., 2010), background chemical concentrations such as stable isotopes of deuterium, O^{18} (Kendall, 1998), chlorofluorocarbons (CFCs) (Cook et al., 2003) etc. Similarly non-stable (radioactive) isotopes are also used to predict travel times and chemical activities within hyporheic zone e.g. isotopes of Radon (e.g., Cook et al., 2003; Wu et al., 2004) and Radium (Kraemer, 2005). With the advancement of technology automated sampling techniques have been developed enabling continuous sampling of river stage, EC, pH, temperature, DO and DOC etc. for longer time periods. However, environmental tracers have their drawbacks, for example, it is often impossible to trace the contribution from individual location due

to widespread injection locations of environmental tracers (Leibundgut et al., 2011). For reliable results, the environmental tracers require a very precise assessment of sources and sinks of the tracer in the targeted area, which could be very challenging as often different sources have similar concentrations (e.g., Burnett et al., 2006).

3. **Artificial Tracers:** Besides the naturally existing environmental tracers, substances are intentionally injected in the hydrological systems in planned experiments. The artificial tracers are used to identify the flow paths, flow direction, residence times and containment transport in subsurface flow. Unlike the environmental tracers, artificial tracers are injected at specific points, therefore they are useful in detecting individual sources of flow. On the other hand, artificial tracers are scale limited both temporally and spatially. Artificial tracers include fluorescent tracers e.g. Uranine, Pyranine (Einsiedl, 2005) etc., salt tracers such as Sodium/Potassium chloride (Lange et al., 1998), radioactive tracer e.g. Tritium, Bromide-82 (Bolin, 1959; Leibundgut et al., 2011) etc. and trace particulate such as bacteria and viruses (Harvey, 1997) etc.

Although a variety of methods have been developed for estimating the GW-SW exchange processes, they all have inherent uncertainties (Brunner et al., 2017; Kalbus et al., 2006; Engelhardt et al., 2011; Leibundgut et al., 2011) due to the spatial and temporal diversity in the exchange processes. For example, Engelhardt et al. (2011) compared various tracer methods to quantify the GW-SW exchange within riparian zone and concluded that relying on temperature and hydraulic data alone will result in inaccurate representation of GW-SW exchange dynamics. Furthermore, available techniques are not suitable to distinguish between groundwater discharge to stream and hyporheic flow (e.g., Kalbus et al., 2006). For reliable results, researchers often emphasize the combination of various tracers along with observation data (e.g., Kalbus et al., 2006; Engelhardt et al., 2011; Leibundgut et al., 2011). In addition to the coupling of multiscale sampling and monitoring methods, the use the numerical modeling is increasing for improving our understanding of the water and solute exchange mechanism (Derx et al., 2010; Cardenas, 2010; Fleckenstein et al., 2010).

1.4.2. Modeling Methods

With increasing awareness of the importance of GW-SW interactions, methods for quantification of exchange fluxes have been improved over the time. In addition to field methods, modeling techniques have been developed to better understand the exchange processes and their implications. It is not always possible to fully understand the complex exchange processes through field measurements alone. For example hyporehic flow paths and their travel times are important variables in context of biogechemical implications of hyporheic zone (Boano et al., 2014). The hyporheic flow paths may range from the centimeters to the tens of meters and corresponding residence times may range from minutes to ten of years, making it hard to fully capture the spatial and temporal extent of HEF. Therefore modeling approaches are used in combination of observed field data to better represent exchange processes associated to nearly all morphological scales (Boano et al., 2014).

1.4.2.1. Transient Storage Models

The modeling of exchange across GW-SW started as early as 1960's after Cooper and Rorabaugh (1963) developed an analytical method to estimate bank storage. However these models were initially limited to the bank flows, as the concept of hyporheic exchange was not realized at that time. The earliest concept of modeling hyporeheic exchange was introduced by Bencala and Walters (1983) when they proposed a transient storage model (TSM) of solute transport. The TSM is based on the 1 D advection and dispersion model that assumes a transient storage zone connected with stream, where solute is temporarily stored and released back to stream after some time. This simple lumped representation of transient storage and its modified versions have been widely used to predict mass transport (Bencala and Walters, 1983; Runkel, 1998), hydrological functioning (Harvey et al., 1996), nutrient cycling (Edwardson et al., 2003) and ecological processes (Mulholland et al., 1997) within the hyporheic zone. In TSM, the parameters which cannot be directly measured, are obtained through inverse modeling, i.e., calibration of field tracer experiments. The TSM approach oversimplifies the complex environment where many diverse processes occur e.g. in TSM the surface and subsurface storage zones are represented as a single transient storage. Surface storage zone have different conditions than the subsurface zone and therefore have different biogeochemical functions. As a result, models based on the concept of transient storage although show excellent fit to the observed tracer data, often fail to capture key information e.g. relative importance of surface and subsurface storage (Neilson et al., 2010; Bencala et al., 2011). Therefore these models are not suitable for predicting role of individual drivers and the representation of small scale processes.

1.4.2.2. Physically Based Models

An alternate modeling framework is physically based models. The physical based models use the physical principle of mass and momentum balance to link forces acting on surface and subsurface flow. A number of physically based models have developed in the past two decades to understand the exchange processes at different morphological scales (e.g., Zolezzi and Seminara, 2001; Harvey et al., 1996; Elliott and Brooks, 1997; Cardenas and Wilson, 2007; Tonina and Buffington, 2011; Marzadri et al., 2012; Boano et al., 2006; Stonedahl et al., 2010; Han and Endreny, 2014; Konsoer et al., 2016, etc.).

A physical based model proposed by Elliott and Brooks (1997) to analyze the pressure induced small scale hyporheic exchange induced by bedforms is regarded as first physical based hydrodynamic model of hyporheic exchange. Small scale, dune and ripple shaped bedforms are the first exchange processes which were predicted by the physical based model due to relatively simple geometry which can be represented as quasi 2D geometry (Elliott and Brooks, 1997; Cardenas and Wilson, 2007).

After successful application of the physical based model on small scale bedforms i.e. dunes, relatively larger morphological features such as bar induced bedforms were modeled. Unlike dunes, the larger bedforms cannot be fully represented as a 2D problem, instead a three dimensional approach is required, adding complexities to the physical model. As a result fewer models are available to predict large scale bedform induced exchanges. For example Boano et al. (2010) and Marzadri et al. (2010) proposed physically based models to better understand the exchange induced by large bedforms. Similarly attempts have been made to model lateral exchange induced by large stream features (e.g., Boano et al., 2006; Cardenas, 2009; Gomez et al., 2012; Trauth et al., 2015; Gomez-Velez et al., 2017).

Physical based modeling approach requires detailed hydrological and morphological data. If the data is available, these models are useful for predicting flow and exchange patterns of water and solute as well as their residence times, however, their applicability to real field settings is often hindered by the scarcity of data required. Another useful application of the physical based model is their use as explorative tools where processes are simulated in controlled scenario settings (Boano et al., 2006; Cardenas, 2009; Fleckenstein et al., 2010; Trauth et al., 2015; Trauth and Fleckenstein, 2017). The role of individual parameters is hard to distangle in the field as well as in the lumped modeling approaches. This kind of explorative modeling enables the identification of the role of individual parameters in a process.

1.5. Research Gaps and Need

The interactions between streams and connected riparian zones occur at variety of scales ranging from small scale vertical exchanges across streambed to large scale lateral exchanges through meander bends and stream banks. However, early HEF research focus remained largely limited to small scale vertical fluxes across streambed. Harvey and Bencala (1993) simulated hyporheic exchange flow paths through streambed using numerical modeling backed by the field data. Elliott and Brooks (1997) proposed a physically based model to analyze the pressure induced small scale hyporheic exchange induced by bedforms. Since then, the influence of various factors on the magnitude of hydrodynamically driven hyporheic flow at streambed have been extensively investigated such as sediment permeability and bed shear stress (e.g., O'Connor et al., 2012), wavelength of roughness features (e.g., Cardenas and Wilson, 2007), vertical and horizontal hydraulic conductivity (Rosenberry and Pitlick, 2009), residence times (e.g., Stonedahl et al., 2010), influence of flow conditions such as steps/hydraulic jumps (e.g., Hassan et al., 2015). Furthermore, many studies have also investigated the influence of small scale vertical exchanges on chemical transformations. For example, Brunke and Gonser (1997) explored how stream borne solutes are transformed during bedform induced hyporheic exchange. Hence, HEF processes through streambed are well known.

More recently, the HEF research focus was shifted to medium and large scale morphological features induced exchange such as pool and riffle (Tonina and Buffington, 2007), gravel bars (Cardenas, 2010) and meander bends (Boano et al., 2006; Cardenas, 2008). The solute transformations under steady flow conditions during hyporheic exchange flow has also been modelled for pool riffle morphology (Marzadri et al., 2012; Trauth et al., 2013, 2014) and as well as sinuosity driven hyporheic exchange through meander bends (e.g., Boano et al., 2010; Gomez et al., 2012, etc.)

Most of the available large scale HEF studies assume steady state flow, whereas, steady flow conditions are rare in natural systems. Assumption of steady state flow may lead to reasonably accurate results for vertical HEF through small scale submerged bed features as previous studies indicate that bedform driven exchanges are larger in magnitude under steady state conditions resulting in higher chemical transformation efficiency (e.g., Gomez-Velez et al., 2015; Stonedahl et al., 2013). However, for lateral stream-riparian exchanges such as meander bends and bank storage, the relation of surface water level and groundwater level at the stream-riparian interface cannot be ignored because changes in stream water level e.g. due to a stream discharge event, may alter hydraulic head gradients in near stream-riparian zone, influencing direction, magnitude and timing of exchange (e.g., Vidon and Hill, 2004a; Duval and Hill, 2006, etc.). Furthermore, in case of partially submerged features such as meander bends, changes in stream water level add further complexity to stream-riparian exchange processes because hydraulic head gradient is not only influenced by morphological feature (Boano et al., 2006; Cardenas, 2008) alone, but additionally due to the changes in degree of submergence with changes in stream water level. Furthermore, dynamic stream flow conditions can potentially mobilize and transport solutes from initially unsaturated near stream-riparian zones.

Recent attempts on modeling the effect of dynamic stream flow conditions on hyporheic exchange flow (e.g., Schmadel et al., 2016; Ward et al., 2017) in absence of morphological controls, show that dynamic stream conditions can increase length and residence times of hyporheic flow paths. Trauth and Fleckenstein (2017) showed that discharge event increased reactive efficiency of a partially submerged gravel bar induced HEF. They have simulated reaction possibilities among stream and groundwater borne species in saturated zone but did not account for solute source initially residing within unsaturated part of the feature. Gomez-Velez et al. (2017) have recently attempted to evaluate impact of stream discharge on sinuosity and bank storage driven exchanges using a two dimensional model. In their study, using a two dimensional modeling concept of Cardenas (2009), they found that stream discharge events have long term influence on residence times of sinuosity driven exchange. However, they did not simulate the influence of flow event on mobilization and transport of solute within the intra-meander zone. These studies indicate that the dynamic flow conditions on solute can have significant impact on mobilization and transport of solutes in large scale partially submerged features like meander bends and therefore cannot be ignored.

A number of bank flow studies have evaluated the importance of stream stage variation on the exchange between stream and adjacent riparian soils. However, these studies are more focused towards the water exchanges only (e.g., Burt et al., 2002; Chen and Chen, 2003; Doble et al., 2012; Schmadel et al., 2016; Ward et al., 2017, etc.). A few studies have also explored the biological implications of stream discharge event such as dam oscillation induced solute injection to the aquifer (Boutt and Fleming, 2009) and effect of stream discharge event on the denitrification in the near stream riparian zone (Gu et al., 2012). However, these studies are limited to the solute transport from stream to the riparian zone during high flow, whereas the effect of bank flows on riparian solute dynamics and subsequent transport back to the stream have not been investigated.

Overall, most of the available studies of stream-riparian exchange are focused on the exchanges through submerged features such as streambed under steady flow assumption. A few studies dealing the event driven exchange processes in partially submerged features, do not address stream flow event induced transformation and transport within the initially non-submerged unsaturated zone. Another limitation of existing work is that most of the physical modeling studies treat hyporheic exchange as a 2D problem. While small scale vertical exchanges or bank flows can be correctly predicted through 2D models, the more complex large scale hyporheic exchanges such as through meander bends require 3D model conceptualization for better representation of HEF and transport processes (Boano et al., 2014).

Hence, there is a knowledge gap in understanding the role of dynamic stream flow conditions on solute mobilization and transport at bank storage and meander scale lateral exchange processes. Especially, the role of stream discharge events on horizontal transport of solute from riparian zone during bank and intra-meander flow has not been fully explored yet. It is not known how bank flows influence the solute residing in the initially unsaturated riparian zone during stream flow events and what is the relative importance of event peak and duration for solute mobilization and transport? Furthermore, the role of meander geometry in combination with changing stream water level on intra-meander HEF and solute transport is obscure. For example, it is unclear whether intra-meander hyporheic flow enhances nutrient load such as DOC into the stream by transporting nutrients from the initially non-submerged nutrient rich layers of riparian zone or conversely acts as a sink by depositing stream borne solute into the riparian zone? Moreover, during the flow event, stream and groundwater borne solutes may come into contact with nutrient rich layers of initially unsaturated riparian zone, providing an opportunity of chemical transformation of nutrients, that may have long term effects on both stream and groundwater (Kiel and Cardenas, 2014; Trauth et al., 2015).

1.6. Objectives of the Research

In this thesis, lateral exchanges during bank flows and sinuosity driven hyporheic flow through meander bends have been explored using numerical approaches. Particular focus has been put on the role of stream discharge events on the mobilization and transport of riparian solute residing initially in the non-submerged portion of the riparian soils. Since hydrological and morphological variability can be difficult to study in a systematic way from field studies, a simulation approach is adopted. In the first part, an explorative modeling framework was developed, where controlled hydrological scenarios have been applied to explore influence of bank flows on solute mobilization and transport in near stream-riparian zone. In the second part, intra-meander flow has been simulated for varying meander sinuosity scenarios in order to develop a predictive understanding of the factors that control hyporheic flow patterns. Furthermore, influence of dynamic flow conditions on intra-meander solute transformations and transport are also evaluated.

The following specific objectives have been developed on the basis of research gaps identified in the previous section.

1. Developing a generic modeling framework for the simulation of flow and resulting solute transport at bank and meander scale lateral exchanges with focus on solute dynamics within the unsaturated riparian zone.

2. Evaluation of the role of stream stage fluctuations on the flow and transport processes in the near stream-riparian zones during bank flows with a particular focus on the relative importance of event peak and duration on mobilization and potential transport of riparian solute towards stream.

3. Evaluation of the role of meander sinuosity on intra-meander hyporheic exchange flow and residence times.

4. Evaluation of the role of stream flow events and meander sinuosity on conservative solute export from variably saturated intra-meander zone.

5. Evaluating the chemical transformation of stream and groundwater-borne solutes and of solutes residing in the initially unsaturated portion of intra-meander zone during a stream flow event.

1.7. Thesis Outline

- In chapter 1, the general introduction of the GW-SW exchange processes, mechanism and drivers of these exchange processes as well as approaches to estimate GW-SW exchange are briefly discussed. Furthermore, after identifying the research gaps, the objectives of the study have been stated.

- Chapter 2, is based on an individual manuscript published in the journal *"Groundwater"* under the title ***Modeling the Impact of Stream Discharge Events on Riparian Solute Dynamics***. In this chapter, the role of stream discharge event on solute dynamics within the unsaturated riparian zone are analyzed by developing systematic stream discharge scenarios of varying duration and peaks.

- In chapter 3, meander driven hyporheic exchange is investigated by developing a coupled groundwater and surface water model. The meander shape scenarios representing the various evolutionary stages are developed and the intra-meander flow is simulated. The role of meander sinuosity on intra-meander residence times under steady state conditions are explored. Furthermore, the influence of discharge events on conservative transport of intra-meander solute are also investigated. In addition to that, biogeochemical transformations during intra-meander flow are evaluated by simulating reactions between stream and groundwater borne species as well as solutes laying within non-submerged portion of the intra-meander region.

- In chapter 4, the outcomes of the research, general conclusions and their potential implication are discussed.

Chapter 2

Flow and Transport Dynamics during Bank Flows

An article with equivalent content has been published as: Mahmood, M. N., C. Schmidt, J. H. Fleckenstein, and N. Trauth. ***Modeling the impact of stream discharge events on riparian solute dynamics.Groundwater.***

Abstract:

The biogeochemical composition of stream water and the surrounding riparian water is mainly defined by the exchange of water and solutes between the stream and the riparian zone. Short-term fluctuations in near stream hydraulic head gradients (e.g., during stream flow events) can significantly influence the extent and rate of exchange processes. In this study, we simulate exchanges between streams and their riparian zone driven by stream stage fluctuations during single stream discharge events of varying peak height and duration. Simulated results show that strong stream flow events can trigger solute mobilization in riparian soils and subsequent export to the stream. The timing and amount of solute export is linked to the shape of the discharge event. Higher peaks and increased durations significantly enhance solute export, however, peak height is found to be the dominant control for overall mass export. Mobilized solutes are transported to the stream in two stages (1) by return flow of stream water that was stored in the riparian zone during the event and (2) by vertical movement to the groundwater under gravity drainage from the unsaturated parts of the riparian zone, which lasts for significantly longer time (> 400 days) resulting in long tailing of bank outflows and solute mass outfluxes. We conclude that strong stream discharge events can mobilize and transport solutes from near stream riparian soils into the stream. The impact of short term stream discharge variations on solute exchange may last for long times after the flow event.

Keywords: riparian zone, solute mobilization, solute exchange, stream discharge variations, hydraulic gradient, bank flows

2.1. Introduction

Water fluxes in riparian zones often vary strongly in time and space, altering solute transport across the river-groundwater interface. Fluctuations in the direction and magnitude of hydraulic gradients between the stream and the connected groundwater lead to complex water exchange patterns enhancing mixing of groundwater and stream water (Vidon and Hill, 2004a; Boutt and Fleming, 2009; Welch et al., 2015). These hydraulic gradients are induced by morphological features at various scales such as river bed dunes (Cardenas and Wilson, 2007), gravel bars (e.g., Trauth et al., 2015) and meander bends (e.g., Boano et al., 2006).

Besides flow driven by morphological features, transient stream stage variations drive varying hydraulic head gradients which in turn control water and matter exchanges between streams and riparian zones (Cooper and Rorabaugh, 1963; Sandén et al., 1997; Rassam et al., 2006). Stream stage fluctuations can occur at different time scales caused by dam regulation (Gerecht et al., 2011; Sawyer et al., 2014), rain events (McCallum et al., 2010; Vidon et al., 2017) and seasonal variations (Bartsch et al., 2014). These variations in stream stage induce the well-studied bank storage effect where water is temporarily stored in the riparian zone during high stream stage and subsequently released back to the stream when stream stage recedes to pre-event conditions (Squillace et al., 1993; Chen and Chen, 2003; McCallum et al., 2010; Doble et al., 2012; Grabs et al., 2012; McCallum and Shanafield, 2016). Along with the infiltration of river water into the riparian zone, river water constituents are transported into the riparian aquifer (Boutt and Fleming, 2009; Sawyer et al., 2014), where they potentially undergo transformations (Gu et al., 2012; Diem et al., 2013). For instance, riparian zones are known to be capable of removing elevated nutrient concentrations, like nitrogen species (Hill, 1996). In contrast, riparian zones can act as net source of solutes for the receiving streams such as for organic carbon or nitrate carried by groundwater (Bishop et al., 1994; Inamdar et al., 2004; Pellerin et al., 2012).

Hornberger et al. (1994) proposed that DOC flushing from the unsaturated riparian soils to the stream occurs during high flow events. Wondzell and Swanson (1996) demonstrated in a field study that flood events facilitated nitrogen fluxes from riparian zones to the stream. Sawyer et al. (2014) observed increase in solute concentration in both riparian water and stream during a strong stream discharge event.

The changes in stream stage induce variations in near stream water table and therefore in the vertical extent of unsaturated zone. Consequently, the solutes stored in the unsaturated zone (e.g., nitrogen species and organic carbon) are tapped by the rise in groundwater level (Creed et al., 1996; Biron et al., 1999; Hill,

2000) leading to their dissolution and mobilization as well as potential transport into the groundwater and adjacent stream (Creed and Band, 1998). As a result, the increased solute concentration leads to a changing hydrochemical system which may fuel biogeochemical processes e.g., an increased denitrification activity, which has strong implications on the status of the entire aquatic ecosystem (Simmons et al., 1992; Burt et al., 2002; Hefting et al., 2004; Gift et al., 2010).

Despite such an important interplay between transient stream conditions and the availability of solutes in riparian zone, only a few studies have systematically investigated the implications of stream stage variation on solute dynamics in variable saturated riparian zone. Boutt and Fleming (2009) found that diurnal stream stage oscillations caused by dam regulations, enhance mass transport into the banks compared to the base flow conditions. McCallum et al. (2010) focused on the influence of bank inflows on the chemical base flow separation method. They found that bank flows during stream discharge events significantly alter the chemical signature of groundwater discharge which in turn leads to incorrect estimation of baseflow. Gu et al. (2012) found that biogeochemical activity in the near stream riparian zone is enhanced by the bank storage process. However, the impact of different types of stream stage variations on riparian solute export to the stream has not yet been explored.

This paper aims at evaluating the effect of stream stage variations on the mobilization of solutes residing in the unsaturated part of the riparian zone and resultant solute mass export to the stream. We use a generic setup with a conservative solute initially stored in the unsaturated part of the riparian zone as we focus on the hydraulic effects of solute dynamics in the riparian zone. The processes are elucidated by means of numerical simulations of flow and conservative solute transport scenarios. The effects are evaluated by investigating the time scales of bank inflow; outflow and the resulting solute mass outfluxes into the stream during and after stream flow events. To differentiate the influence of magnitude and timing of stream stage on exchange processes, the flow scenarios were systematically varied in terms of peak streamflow height and event duration.

2.2. Methods

2.2.1. Concept and Modeling Setup

In natural systems, riparian bank storage processes are controlled by various factors like changing hydraulic gradients, heterogeneity of the subsurface sediments, groundwater recharge and evapotranspiration (Vidon and Hill, 2004b; Duval and Hill, 2006; Grabs et al., 2012) . Accounting for all existing factors in a model would lead to a very complex setup and model parameterization, where the role of a single factor is difficult to identify. Therefore, in our modeling setup only the effect of changing stream stages is considered, whereas all other parameters were kept constant for the range of the scenarios. By using such kind of a simplified model, we can evaluate the effect of stream stage fluctuations on solute mobilization in the riparian zone. The simplification of the natural processes allows us to investigate the sensitivity of solute mobilization to discharge events. This type of "explorative numerical modeling" has been very common recently (Cardenas and Wilson, 2007; McCallum et al., 2010; Frei et al., 2012; Trauth et al., 2014) because it enables the evaluation of individual effects of multiple factors of a process, which are hard to disentangle otherwise in the field and fully representative modeling studies.

The conceptual model consists of three major components: (1) a variably saturated riparian zone (unconfined aquifer) which is hydraulically connected to (2) a gaining stream, and (3) a layer of a conservative solute residing in the upper, unsaturated part of the riparian zone.

The domain geometry is similar to the one described for the analytical solution of bank storage flow by Cooper and Rorabaugh (1963). The domain extends 50 m in horizontal (x) and 1.26 m in vertical (z) direction (Figure 2.1). The domain length was selected after performing test-simulations considering various domain lengths for stream stage event scenario of the highest peak height and the longest duration. Based on these model runs, we found that at distance of more than 50 m from the stream the effect of stream stage variations on groundwater level was negligible. Increasing the length of the model domain would not affect the overall results, but would increase computational effort. The model geometry is a generic representation of a typical riparian zone observable at river corridors of third to fourth order streams in humid regions (perennial rivers) (Bishop et al., 1990; Castelle et al., 1994; Mayer et al., 2005).

The main enhancement compared to previous studies, is the addition of an unsaturated zone containing a solute layer, which has been observed during many riparian zone field studies (Bishop et al., 1990, 1994; Wondzell and Swanson, 1996; Grabs et al., 2012; Gassen et al., 2017). During groundwater level rise induced by stream flow events, the high solute concentrations can be mobilized and consequently, solutes can be potentially exported to the stream (Bishop et al., 1994). These observations are represented in our model concept by implementing a 0.66 m thick and 30 m long (66% of total domain length) layer of a conservative solute source of uniform concentration in the unsaturated zone ranging from z = 0.6 m to z = 1.26 m and x= 0 to x= 33 m.

The solute layer was not extended over the entire length of the domain in order to observe the movement of solute within the bank as well as to avoid loss of solute mass across the left boundary. In all scenarios, bank overflows were not considered ($h \leq 1.26$ m). The porous medium was assumed to be homogenous and isotropic, whereas dispersivity in horizontal direction was assumed to be one order of magnitude higher than in the vertical direction. Hydraulic properties of the porous medium represent sand (see Table 2.1).

2.2.2. Numerical Model

Flow and transport simulations for the variably saturated media were performed with the multicomponent reactive transport modeling code MIN3P. It solves the Richards equation for water flow simulation and the advection-dispersion equation for solute transport. The van Genuchten-Mualem approach is utilized for the estimation of the unsaturated hydraulic conductivity (Mualem, 1976; Van Genuchten, 1980) whereas tortuosity is calculated by Millington Formula (Millington, 1959). The MIN3P code has been used for simulating a variety of problems in contaminant transport and stream-groundwater interaction studies (Mayer et al., 2002; Trauth et al., 2014, 2015; Trauth and Fleckenstein, 2017). Although MIN3P is fully capable of simulating reactive transport, in this study we are focusing on non-reactive solute transport because the objective of this study is to investigate how conservative solute transport is affected by changing hydraulic conditions.

For the simulation of base flow conditions, a constant head boundary condition (Dirichlet boundary) representing ambient groundwater level of 0.3 m was assigned at the land side of the riparian zone (left boundary) whereas a constant head of 0.26 m was assigned at the interface between the stream and the riparian zone (right boundary) to obtain the gaining conditions (groundwater is feeding the stream) under base flow. For simulation of stream flow events, a time varying head boundary was applied at the stream-riparian interface (along z direction) that enables a simulation of changes in hydraulic head caused by the stream stage fluctuations. The head at inflow boundary (stream end) was varied between base flow condition ($h_o = 0.26$ m) and the peak stage height (h), to represent the stream flow event. No flow boundaries were assigned at top and bottom of the model domain. A uniform grid size of 0.04 m was used both along z (perpendicular to stream section) and x direction in all simulation runs. Third kind boundary conditions were applied for solute exchange at inflow and outflow boundaries, enabling the transport of solutes in both directions. A relatively high solute concentration of 100 mg/L was initially assigned to the solute source layer. In the rest of the model domain, initial concentration was set to zero. Similarly nearly zero solute mass flux was assigned to both groundwater (left) and stream water (right) boundaries, leaving the solute source layer as the only source of solute concentration.

A long simulation time of 1000 days was selected to account for expected long tailing of solute breakthrough curves. In the transient scenarios, flow events were introduced after 41.6 days (1,000 h) of simulation time when the outflux of water and solute from the riparian zone had reached a constant value.

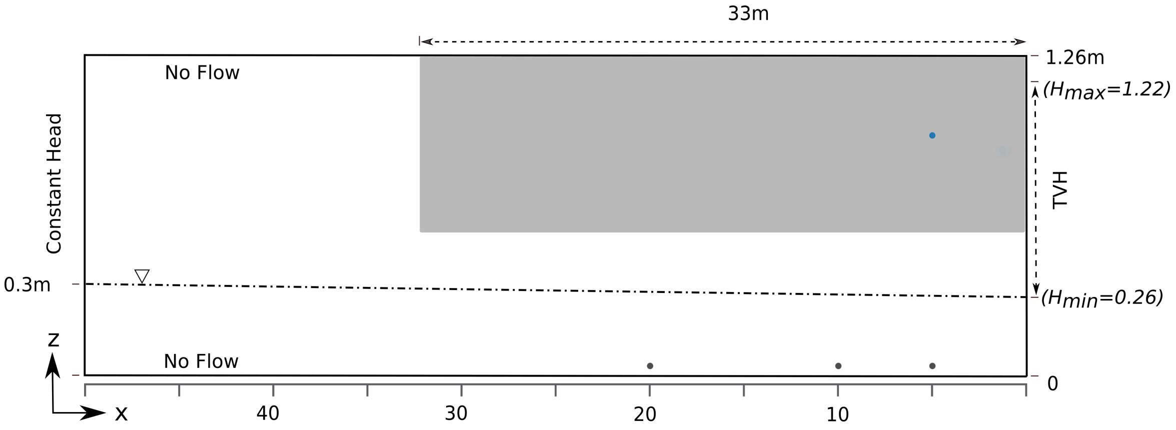

Figure 2.1: Cross sectional view of the model setup (not to scale). Filled area represents the extent of the solute layer. The stream is represented by the time varying head (TVH) boundary (from $z = 0.26$ to 1.22 m) at the right boundary. At the left boundary of the domain, a fixed head boundary is assigned, representing the ambient groundwater level ($z = 0.3$ m) at the outer bound of the riparian zone. The dots represent observation points referred to in the subsequent figures where changes in groundwater head (black dots) and detailed solute mobilization process in unsaturated zone (blue dot) are observed.

2.2.3. Stream Discharge Events

Stream stage fluctuations during flow events were represented by applying a stream hydrograph at the right boundary (stream-aquifer interface) of the model (Figure 2.1). The flow event is characterized by (1) the peak of the hydrograph representing the maximum stream stage, (2) the time length of the hydrograph corresponding to the duration of the event. These two parameters determine the magnitude, height and the timing of water entering into the riparian zone.

Parameter	Unit	Value
Hydraulic Conductivity ($K_{sx} = K_{sy} = K_{sz}$)	ms^{-1}	10^{-03}
Specific Storage	m^{-1}	10^{-04}
Effective porosity (n)	–	0.3
Residual saturation (θ_r)	–	10^{-02}
Van Genuchten -n	–	3.5
Van Genuchten -α	m^{-1}	8.5
longitudinal dispersivity	m	10^{-02}
Transversal vertical dispersivity	m	10^{-04}

Table 2.1: Hydrologic Properties of the Porous Medium.

A typical single peak hydrograph derived from a real flow event of a third order stream was adjusted to a set of flow scenarios where variants of changing maximum peak and event duration were applied. Discharge for each hypothetical event scenario is calculated by the rating curve equation:

$$Q(t) = (G(t) - a)^b \tag{2.1}$$

where 'G' is the stream stage and 'a' is the gauge reading against zero discharge while 'b' is the rating curve constant. In our hypothetical case $a = 0$ and $b = 0.11$. A total of 160 input hydrograph scenarios were developed, organized in a matrix of combinations of 16 peak heights and 10 event durations. Peak heights ranging between 0.06 to 0.96 m above base flow level were equally spaced at 0.06 m interval. Similarly event durations were also equally spaced at 10 h intervals between 10 to 100 h. Table 2.1A and Figure 2.1A represent the combination and shape of discharge scenarios simulated in this study.

2.2.4. Model Results Evaluation

The influence of stream stage variation on riparian solutes is evaluated in terms of mass balance of solutes and the temporal behavior of solute outfluxes with respect to stream discharge. Assuming that all of the solute outflux (J) from the riparian zone is entering the stream, the total solute mass outflux (J_{tot}) from riparian zone caused by the stream stage fluctuations over the entire simulation period (τ) can be estimated as:

$$J_{tot} = \int_0^{\tau} J(t)dt \tag{2.2}$$

Addition of solute mass into the stream results in increased stream concentration. Considering the initial solute concentration in the stream is zero, the resulting stream concentration of the solute in the stream water (C_{str}) can be calculated as:

$$C_{str}(t) = \frac{J(t)}{Q(t)} \tag{2.3}$$

Where $J(M/T)$ is the solute outflux into the stream, from the unit cross sectional area of the domain perpendicular to the river. $Q(L^3/T)$ is the stream discharge and $C_{str.}$ (M/L^3) is the solute concentration in the stream at time (t). Solute mass export was evaluated in terms of peak height and duration of the corresponding flow event.

2.3. Results and Discussion

2.3.1. Response of Water and Solute Exchange To Stream Discharge Events

2.3.1.1. Water Exchange Time Scales

The time scales of water infiltration and exfiltration to and from the riparian zone induced by a stream flow event are presented in Figure 2.2. In our model setup the 100 h stream event starts at 41.66 days (1000 h) of the simulation in order to account for the effect of initial conditions (Figure 2.2a). The flow event reaches peak flow height above base flow level at about 9 h, then slowly recedes, terminating at about 100 h (at 45.83 days) after the beginning of the flow event. Groundwater hydraulic heads (Figure 2.2b) respond to the stream discharge variation with delay depending upon the distance from stream-riparian interface (black dots in Figures 2.1, 2.3 indicate the location of observation points). The effect of the stream stage fluctuation is most pronounced in the near stream riparian zone. This effect is the result of the spatial and temporal variation of the hydraulic gradients in the domain (Figure 2.2c). Prior to the event, the stream is slightly gaining (positive i) due to lower stream stage compared to the ambient groundwater head. With the beginning of the flow event, the direction of the hydraulic gradient is changing towards losing conditions, indicating that stream water flows into the riparian zone (negative i). The shift in the near stream hydraulic gradient i_5 is earlier and higher than the respective changes in the hydraulic gradient over the entire modeling domain (i_{50}). In turn, the change in the hydraulic head difference between the stream and the near stream groundwater during the flow event controls the timing and magnitude of Q_{in} and Q_{out} (Figure 2.2d). The time of peak Q_{in} coincides with the time of the strongest negative value of i_5. After the peak of the event, both i_5 and Q_{in} start declining towards pre-event value. The i_5 switches to positive on the falling limb of the stream flow event, causing a reversal in the direction of the exchange flow, marking the termination of net Q_{in} and the beginning of a net Q_{out}. In contrast, the negative value of i_{50} slowly declines reaching the pre-event value at the end of flow event. The peak value for positive i_5 is only 0.23 times that of the peak negative i_5, however a positive i_5 is maintained for more than 6-times the duration of the negative hydraulic gradient forcing substantially lower Q_{out} rates for long duration compared with Q_{in}. The peak Q_{out} in this case is 16 % of peak Q_{in}. After the end of flow event a rapid decline in Q_{out} is observed which is driven by decrease in i_5. During Q_{in} the total water saturation within the domain increases, reaching the peak value of 1.6 times higher at the end of Q_{in} than its pre-event value (Figure 2.2e). Q_{out} starts before the end of the event at the falling limb, which leads to an overall decline in saturation within the domain. At the end of the flow event about 60 % of Q_{in} is already released back to the stream. After 12 days (T= 53 hrs), Q_{out}

rate as well as saturation drop to very small values, however they do not reach their pre-event values. After a quick initial release of the bulk of the stored water, a relatively small amount remains in the riparian zone which is released subsequently over a long period of time due to slow unsaturated zone drainage. Even after 50 days of the start of the flow event, still 2 % of Q_{in} is present in the unsaturated riparian zone (Figure 2.3A), resulting in a slightly higher saturation (0.2 %) than the pre-event value. These higher and shorter Q_{in}, lower but longer Q_{out} and long tailing of Q_{out} are consistent with other bank flow studies (McCallum et al., 2010; Doble et al., 2012; McCallum and Shanafield, 2016).

2.3.1.2. Stream Water Solute Concentration

Figure 2.2f represents theoretical changes in stream water solute concentrations (C_{str}) derived from solute mass outflux simulations (J) (see section 2.2.4). Stream water is assumed to be free of solute concentration prior to the event, therefore change in solute concentration in the stream is solely caused by the solute mass exported with Q_{out} from the riparian zone to the stream. The onset of C_{str} is approximately 15 h later than the start of Q_{out}. The delayed response of J from the riparian zone is due to the fact that Q_{in} initially mobilizes and transports solutes from the near stream riparian zone deeper into the domain, therefore the last part of Q_{in} does not come into contact with riparian solute. When Q_{out} starts, newly infiltrated water with no solute concentrations drains out of the domain during first few hours. This lag between the starting times of Q_{out} and J depends on the duration of the flow event. C_{str} increases until the end of the flow event, even though Q_{out} is discharged at a nearly constant rate. This is because of the fact that mobilization of riparian solute increases with time, therefore the later part of Q_{out} carries more solute mass. At the end of the flow event, the turning point in near stream hydraulic gradient results in decreased Q_{out} as well as corresponding J. That is why the peak concentration is observed exactly at the end of flow event (Figure 2.2f). Similar to Q_{out}, the pre-event conditions for C_{str} are not reached long after the flow event.

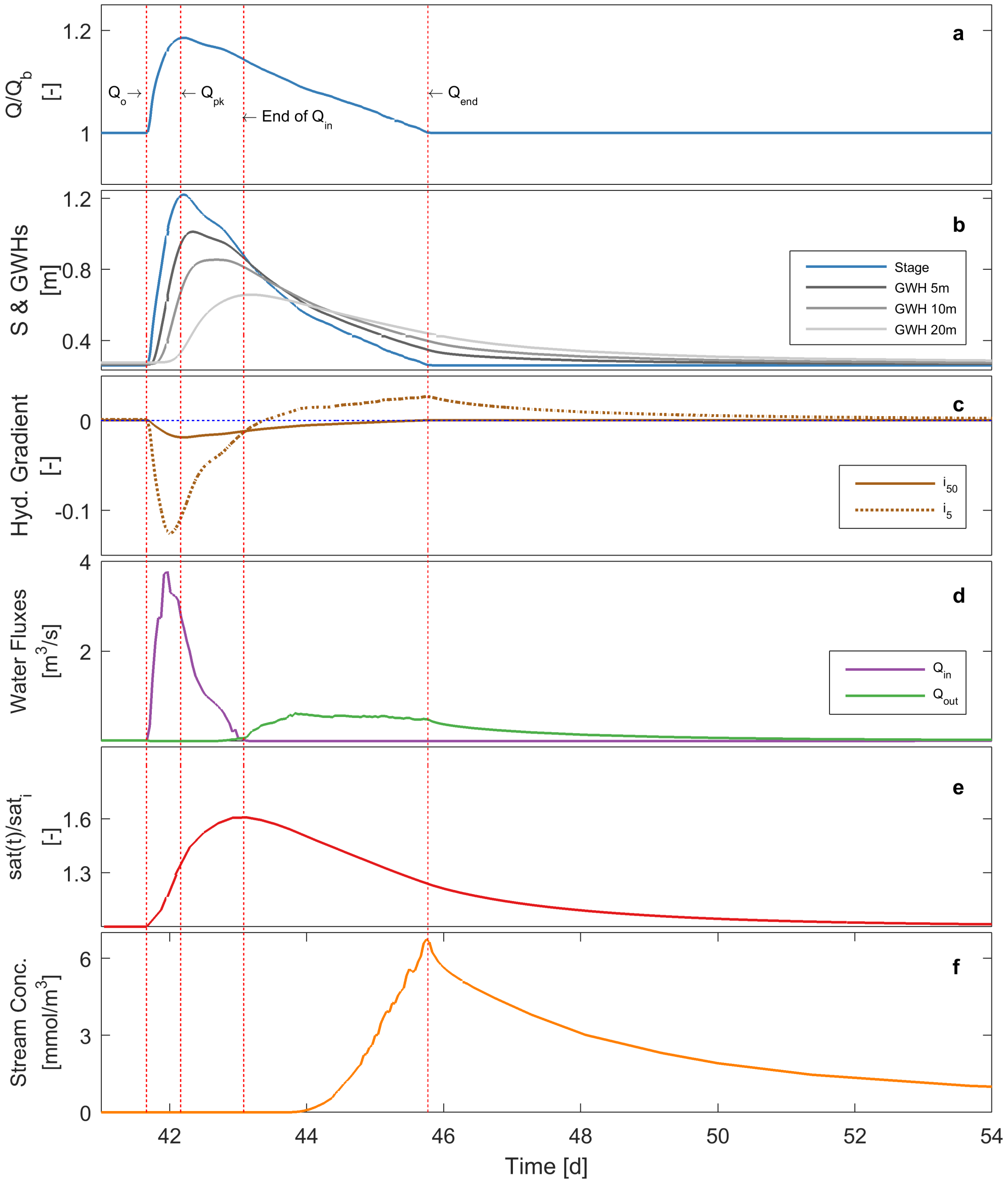

Figure 2.2: Time scales of water and solute fluxes during a bank flow event of 0.96 m peak height above base flow and duration of 100 h.(a) stream discharge normalized to the base flow (Q/Q_b), (b) stage and groundwater heads at 5, 10 and 20 m distance from stream boundary (black dots in Figure 2.1), (c) hydraulic gradient at stream-riparian interface, i_{50} is the hydraulic gradient between the stream stage and the ambient groundwater head at the left boundary, while i_5 is the local gradient between the stream stage and the groundwater head at a distance of 5 m from stream (dotted blue line represents the hydraulic gradient in absence of the flow event), (d) water fluxes into (Q_{in}) and out (Q_{out}) of the riparian zone, (e) change in saturation during the flow event, (f) Concentration (C_{str}) in stream water. The red dotted vertical lines across the figures show the relative position of fluxes at these time steps.

.

2.3.2. Solute Mobilization within the Riparian Zone

During the flow event, infiltrating stream water results in an increase in water saturation in the upper riparian zone leading to mobilization of riparian solutes. In Figure 2.3 this solute mass within the riparian zone is shown at various time steps of the simulation period during and after the flow event. The actual mass of solute in each cell is calculated in terms of water content:

$$M = V.C.S_w.n \tag{2.4}$$

where M is the actual mass of solute, C is the concentration at the point, S_w is the water content in the mesh cell, V is the volume of the cell and n is the effective porosity of the aquifer.

At pre-event conditions ($T < 1000$ h) more solute mass is concentrated in lower part of the solute layer. The zone above water level is variably saturated. We applied a uniform solute concentration throughout the layer, resulting in a higher solute mass in the areas of higher water content (lower part). During the rising limb until the peak of the event (1006 and 1012 h) the water levels in the near stream zone rise to a maximum level while in the more distant domain it remains nearly unaffected. Water inflow into the unsaturated zone during Q_{in} creates strong horizontal as well as vertical water flow component in near stream riparian zone. This results in complete flushing of the solute source layer from the near stream zone where the unsaturated zone is filled with recently entered stream water. Solutes from the near stream area are mobilized and transported away from the bank both vertically upward by a capillary rise effect as well as horizontally away from the stream. The highest solute mass is observable directly in areas where saturation is high (dark red area around the 100 % saturation line), while there is also visible increase in solute mass in areas between 5 (blue dashed line in Figure 2.3) and 100 % saturation.

To illustrate the effect of Q_{in} on riparian solute mobilization, we observe the water and solute mass changes in a near stream cell located within the unsaturated zone at $x = 5$ m and $y = 0.9$ m (indicated by the blue dot in Figure 2.3). The change in saturation (S_w), solute concentration (C), solute mass (M) and vertical velocity (V_z) within the cell are shown in Figure 2.4. Clearly at the time, when the S_w within the cell starts increasing (Figure 2.4 a) by vertical water flow (indicated by V_z in Figure 2.4 d), concentration C (Figure 2.4 b) decreases but solute mass M (Figure 2.4 c) increases within the cell at the same time, indicating that additional solute mass is received from the cell below by upward movement of water (positive V_z in Figure 2.4 d). The solute mass keeps increasing in the cell until the cell reaches nearly full saturation. At this stage water flow starts transporting mass to neighboring cell which is evident from declining mass in Figure 2.4 c) until water within the cell is completely replaced by river water of zero solute concentration. The observed vertical water flow can be explained by capillary rise effect on commencement of Q_{in}. Similar behavior of flow and solute movement in variably saturated zone was observed by Silliman et al. (2002) in a laboratory study.

The mobilization of solute within the domain shown in Figure 2.3 is largely driven by above mentioned effect of saturation. After the peak of the event, during the falling limb (Figure 2.3; $T = 1030$ to 1050 h), the curved shape of the groundwater level indicates the movement of water into both directions (into the stream and towards the distant riparian zone), i.e., the groundwater level (saturation) in the distant domain is still rising (around $x = 20$ m) leading to additional mobilization of solutes in the distant domain. At the same time, the groundwater level is declining in the near-stream zone due to the increasing Q_{out} towards the stream.

During the falling limb, the decrease in groundwater level in the entire domain, results in a vertical downward movement of the solute mass. The higher solute mass (dark red area at $T = 1012$ to $T = 1100$ h) is moving downwards with the lowering of the 100 % saturation line indicating solute movement from the unsaturated zone to the saturated zone. At the same time solute is also moving horizontally in the unsaturated zone towards the stream with Q_{out}. The near stream area of the domain ($x < 3$ m) is free of solutes at ($T = 1030, 1050h$), therefore, no solute export occurs in the beginning of Q_{out}. The solute carrying water reaches the stream 15 h later at $T = 1080$ h (Figure 2.3) indicated by increased C_{str}. This explains the lag between starting time of Q_{out} and C_{str}.

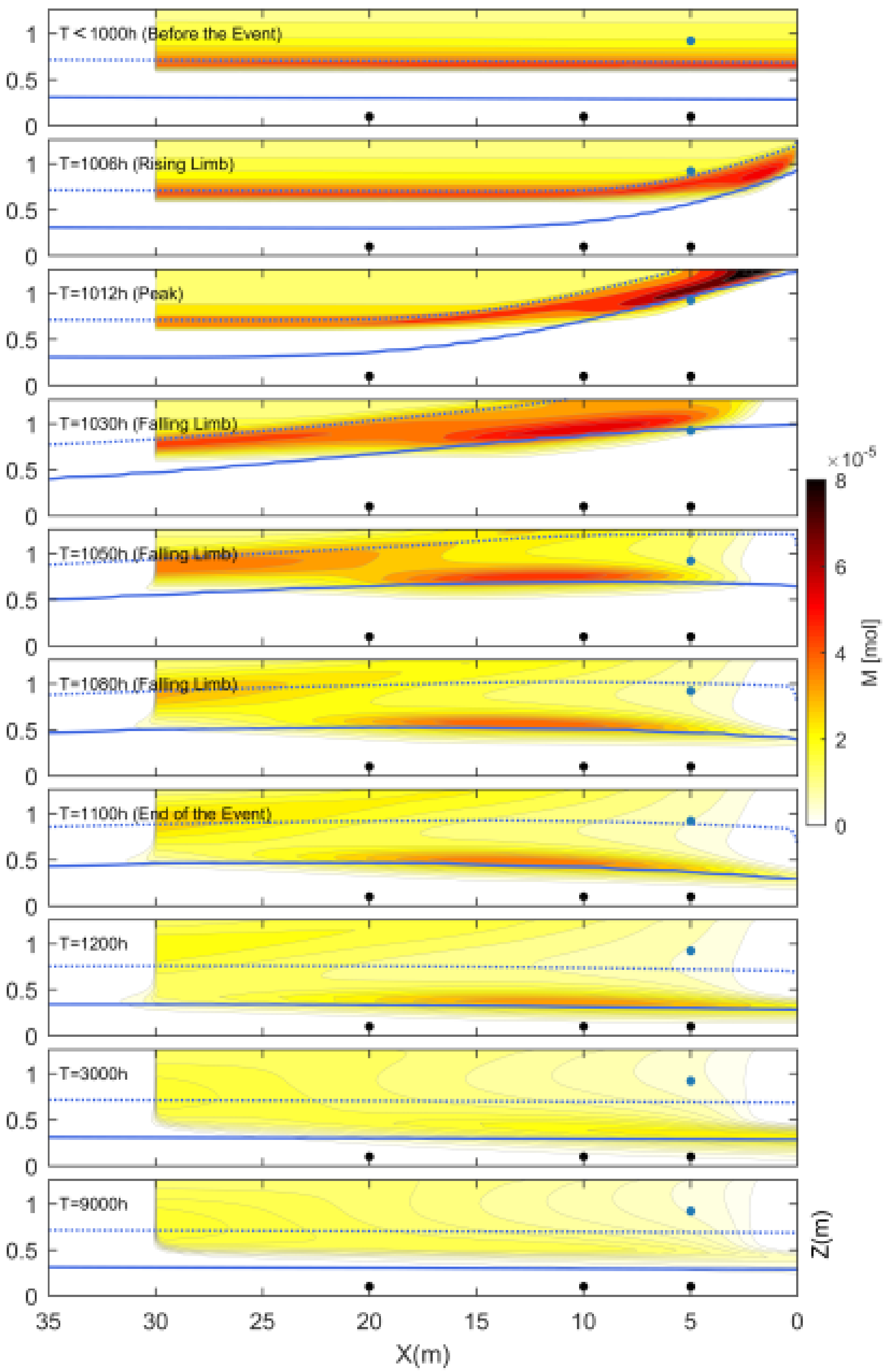

Figure 2.3: Solute mass ($M[mol]$) in the part of riparian zone at various time steps. The solid and dotted blue lines show the 100 % (water level) and 5 % water saturation respectively. The black dots indicate the locations of the observation points for groundwater heads, while the blue dot shows the location for which a detailed description of the solute mobilization process in unsaturated zone follows in the next section.

At the end of the event (T = 1100 h), groundwater levels adjacent to the stream

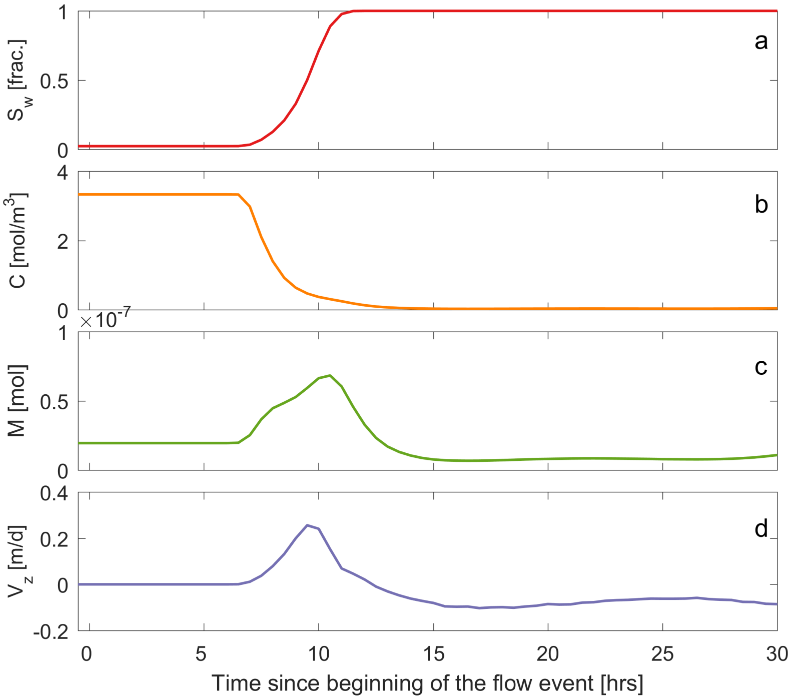

Figure 2.4: Water saturation (a), solute concentration (b), solute mass (c) and vertical velocity component (d) at one individual cell at location $x = 5$ m and $y = 0.9$ m (indicated by the blue dot in Figure 2.3.

have returned to pre-event level while in the distant riparian zone ($x > 10$ m) heads are still high indicating that a part of Q_{in} still remains in the domain. At this stage, a large portion of Q_{out} is already discharged to the stream and solute concentration C_{str} is at the maximum value (Figure 2.2f) meanwhile lowering of water table resulted in the movement of solute mass from unsaturated part to the groundwater, from where it is transported to the stream. This is visible at time 1200 h, when the groundwater level is almost back to the pre-event conditions and an increased solute mass is observed in groundwater. This increase in solute mass in the groundwater is the result of the gravity driven vertical drainage from the unsaturated zone.

At 3000 h, we would expect the groundwater to be free from solute; however solute mass is visible even after 9000 h indicating that vertical solute movement from the unsaturated to the saturated parts of the domain continues very long after the end of the flow event. This is due to the slow drainage of Q_{out} from the unsaturated zone as explained in the previous section (see section 2.3.1.1 “water exchange time scales”) and is consistent with previous studies (e.g., McCallum and Shanafield, 2016). This explains the long tailing of stream concentration C_{str} in Figure 2.2f.

The general trends explained above, hold for all simulated scenarios. Flushing of solute mass from near stream riparian zone, longer time periods of Q_{out} and C_{str}

were observed in all cases.

2.3.3. Influence of Peak Height and Event Duration on Solute Mass Export towards the Stream

In the following sections, we evaluate the effects of changes in peak height and event duration on cumulative solute export from riparian zone.

Since the cumulative mass export keeps increasing over time long after the flow event, we chose to constrain the output time to 4000 h (166 days) after the beginning of the flow event, the time when water outflow rate falls back to the pre-event flow rate for all of the simulated scenarios, i.e. when steady state flow conditions are reached again.
The solute export to the stream is a function of both event peak height and event duration (Figure 2.5a). The lines in Figure 2.5b represent the solute export for varying peaks but equal duration, e.g., a 10 h duration line means the solute export for varying peak discharge scenario for equal 10 h duration. Similarly in Figure 2.5c each peak line represents the export for varying duration with equal peak heights.

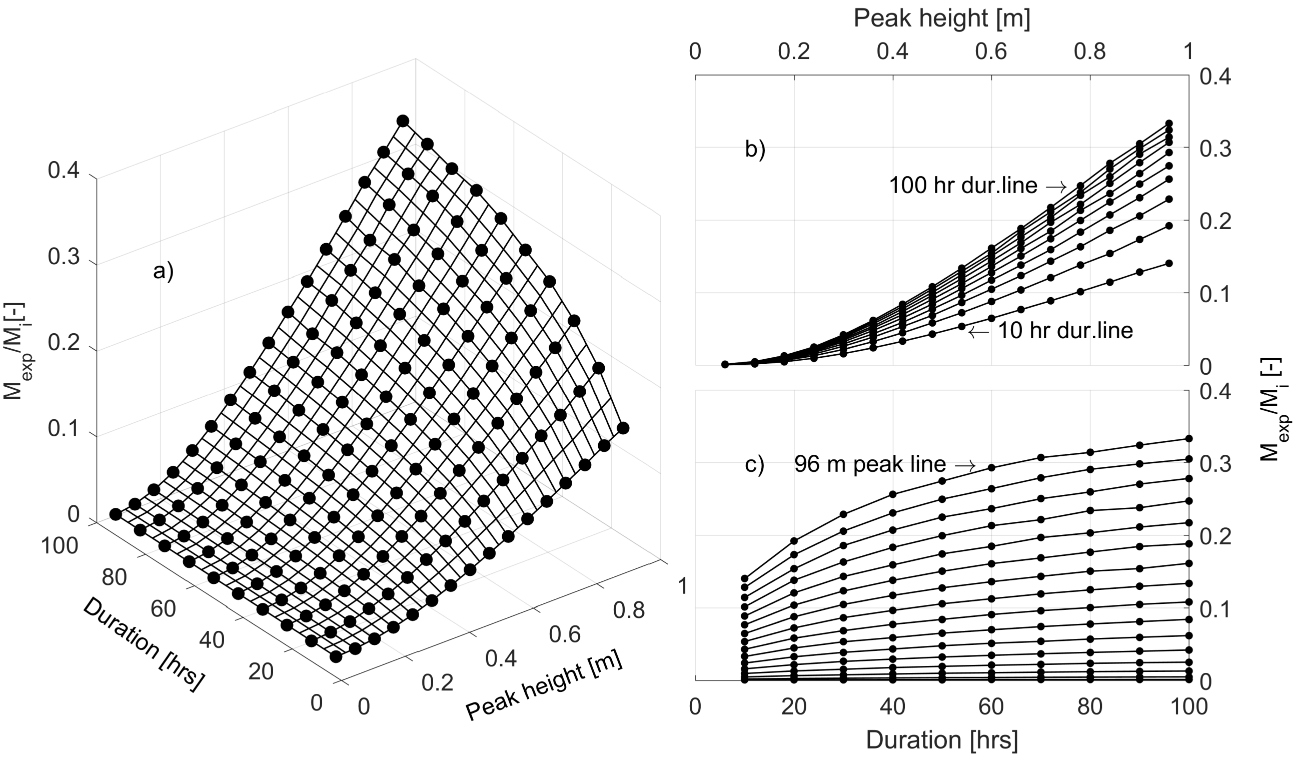

Figure 2.5: Total solute mass exported into stream in 4000 h (166 days) as a fraction of total solute mass in the domain at pre-event conditions, (a) combined effect of event peak height and duration, (b) effect of event peak height, and (c) effect of event duration.

For events with peak heights of less than 0.3 m where the infiltrated water does not reach the solute layer, the exported mass remains low and is independent of the actual event peak height (Figure 2.5b). An increase in the event peak height causes a groundwater level rise into the solute source layer, which results in an increased solute mass mobilization and consequent export. Therefore variations in event peak height have a pronounced effect on solute export. For instance, the solute export on the 100 hrs duration line (Figure 2.5b), is increased from 6 % for the minimum peak reaching the solute layer (0.36 m) to 33 % for the highest peak (0.96 m). Hence for an increment of 0.6 m in peak height, solute export is increased by 5.5 times.

The solute mass export is also positively related to the event duration. However, each line of equal peak height tends to converge to an upper value of mass export with increasing event duration (Figure 2.5c). This is due to the reason that longer durations push the mobilized solute away from stream (along x dir.), decreasing the availability of solute to be exported with initial high Q_{out} flow rates. It means, although solute mass export increases with increasing event duration, it has lower impact on solute export compared to the peak height. For instance, given the minimum peak height touching the solute layer (0.36 m), solute mass export is 0.14 % of the initial solute mass in the riparian zone for the shortest duration (10 h) while for the longest duration (100 h) of the same peak height, 0.33 % mass is exported. Hence, by an increase of 90 h event duration for the same peak height, mass export is increased by 2.35 times.

The mass export analysis suggests that events with higher peak height result in increased mobilization and therefore increased solute export while longer durations tend to delay the timing of bank outflow causing retardation in solute export. Therefore, frequent, short term stream fluctuations will be more efficient than flow event of longer duration with lower peaks in mobilization and consequent export of solute into the stream. Boutt and Fleming (2009) also demonstrated that the frequent stream fluctuations transport solute mass from the stream to the aquifer under zero net water flux by enhancing mixing process inside the aquifer. Gu et al. (2012) found that strong stream events significantly influence the chemistry of both surface water and groundwater by enhancing mixing and reaction efficiency in the near stream zone. They also observed that time frames of chemical activity within riparian zone are much longer than the hydraulic exchange time scales, which is in line with our observations (Figure 2.3A).

2.3.4. Effects of Event Hydrograph Shape on Stream Water Solute Concentration

Since solute export starts with the onset of Q_{out}, (bank outflow) a time delay between the peak in stream discharge and peak concentration of stream water was expected. Figure 2.6 depicts the stream discharge and concentration change during the stream flow event. Generally, stream concentrations start increasing during the falling limb of the flow event, reaching a maximum value near the end of the flow event. The fixed time of peak concentration at the end of discharge event for all of simulated scenarios is due to the decline in Q_{out} as shown in Figure 2.6e, which is caused by the turning point in the positive hydraulic gradient i_5 in the near stream zone (Figure 2.6d). An increase in the duration of the flow causes a damping effect on the concentration peak in the stream water (Figure 2.6a-c). However, tail concentrations are elevated with increasing duration indicating a retardation effect of event duration on stream concentration as explained in the previous sections. The time difference between the peak discharge (Q_{max}) and peak concentration ($C_{str-max}$) is increasing with increasing event duration. The increasing time lag and damping of concentration peak is related to the longer Q_{in} duration which initially pushes the mobilized solute mass horizontally away from the stream as well as delays the starting time of Q_{out} and corresponding J.

In contrast, an increase in the event peak height results in a significant increase in the peak stream concentration (Figure 2.6d-f). Higher concentration peaks for higher inflow are due to the water saturation of an increasing portion of the solute source and thus a more efficient mobilization. Therefore, higher peaks release more solute without delaying the solute release from the riparian zone. However, this does not hold for event peaks where the solute source layer is not tapped into by the rising groundwater levels. In such cases no direct solute mobilization is possible and the solute export is mainly caused by diffusion and gravitational solute movement through the unsaturated zone resulting in delayed concentration peaks.

The time lag between Q_{max} and $C_{str-max}$ is constant for scenarios of varying peaks and fixed duration, provided the peak height is high enough to reach the solute layer (2.2A-c), while it is linearly increasing with event duration for scenarios of constant peak height (2.2A-d). This is due to two reasons: a) longer durations induce longer Q_{in} resulting in later starting times for Q_{out} and b) longer Q_{in} pushes the solute mass further away from the near stream zone. As a result, the part of Q_{in} which entered the riparian zone after the solute has been pushed away from the near stream zone may drain back to the stream without having been in significant contact with the solute, causing a significant time lag between the starting times of Q_{out} and J.

Overall, higher and shorter events result in higher and earlier release of solute and increased total solute mass export resulting in higher and earlier peak $C_{str-max}$ whereas increase in duration results in retardation in release of solute mass resulting in delayed and damped peak C_{str}.

Our results are mainly in line with the concentration-discharge relations found in field studies. Especially, the significant lag between peak discharge and solute peak in stream water has been also observed by many field studies (e.g., Hangen et al., 2001; Inamdar et al., 2004; Pellerin et al., 2012; Welch et al., 2015). In line with our modeling results, they concluded that the rise in groundwater table mobilizes DOC but with a delayed maximum groundwater level compared to the maximum stream stage, leading to delayed solute concentration peak in stream water. Mei et al. (2014) concluded that the time lag is mainly controlled by event duration and hydraulic connectivity between groundwater and stream. Xie et al. (2016) also observed time lag increase with increasing event duration. These studies have suggested that bank inflows have significant effects on the chemical conditions of both stream water and groundwater. In this context, our results give detailed insights into the process of the solute mobilization and export to the stream.

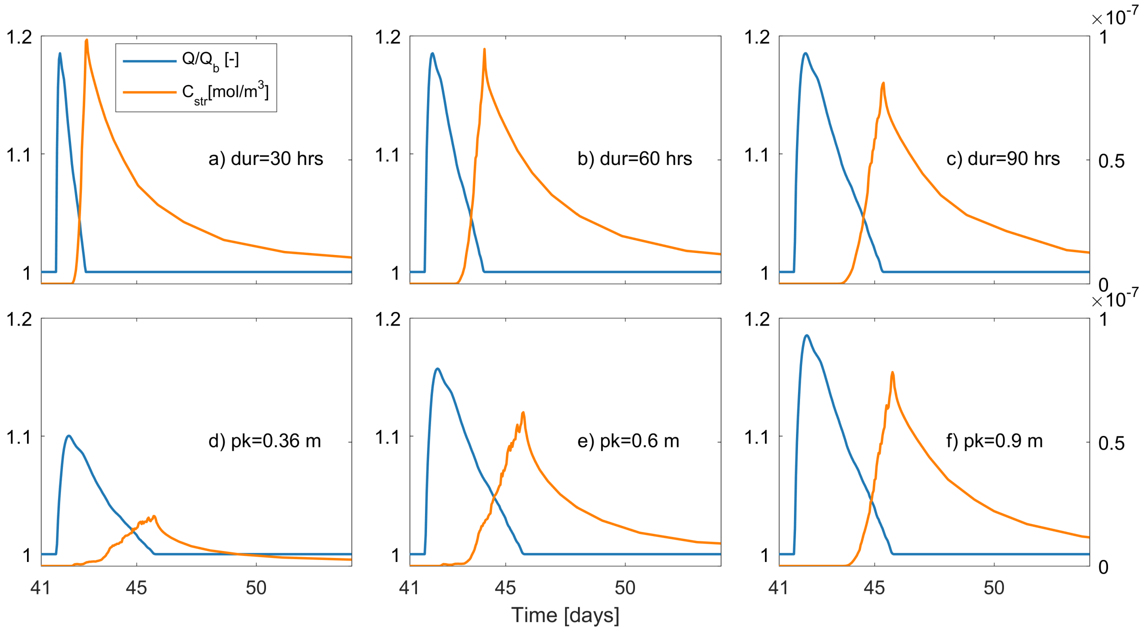

Figure 2.6: Stream discharge $Q/Q_b[-]$ versus solute concentration in stream $C_{str}[mol/m^3]$ for (a-c) increasing discharge event duration (30, 60, and 90 h, respectively) for a fixed maximum peak height (0.96 m) (d-f) increasing maximum peak height (0.18, 0.54, 0.96 m) above base flow level respectively) for a fixed event duration (100 h).

2.3.5. Model Limitations and Future Studies

Our modeling setup represents a simplified riparian zone with reduced process complexity as we exclusively study the effect of stream discharge scenarios on solute mobilization and transport processes e.g., in our model the riparian aquifer is homogeneous and isotropic in both effective porosity and hydraulic conductivity, similar to the study of McCallum et al. (2010). Therefore, we did not account for any highly conductive zones although they may facilitate fast preferential flow and transport that potentially exists in riparian aquifers (Beven and Germann, 1982). In turn, layers of lower permeability may reduce the zone of water exchange and solute removal (Chen and Chen, 2003). However, since sediment properties will hardly change during short term stream discharge events the comparative metrics derived in our study are likely the same as for the heterogeneous case.

In this study recharge by precipitation was not simulated, although it is potentially an important process for water and solute mobilization (Nielsen et al., 1986; Xie et al., 2016). Recharge can mobilize solutes during infiltration and also contributes to the rise of the water table. However to test the additional effect of recharge, we simulated a scenario with a constant recharge of 2 mm at the top surface during the entire period of the flow event and compared the total solute export with the scenario without additional recharge. We found that the overall solute export is enhanced by factor 5.6 after 300 h when a major portion of Q_{out} has been released to the stream and by factor 5.9 after 5000 h when Q_{out} reaches the pre-event level. This clearly indicates that the addition of vertical recharge will significantly increase the overall amount of solute export. However, for a thorough analysis of the effect of groundwater recharge future modeling scenarios should consider rain events with realistic timing and amount of water per time.

Furthermore, in our study solute transport is purely conservative, although in natural aquifers, sorption and reaction may alter solute export to the stream. Incorporating reactions into future modeling scenarios would highlight the effect of solute mobilization on spatial extent and efficiency of solute turn-over.

2.4. Summary and Conclusions

Infiltration and exfiltration of water into and out of the riparian soils during stream flow events may lead to solute exchange between streams and their connected riparian zones. In this study, we have investigated the effect of stream discharge events on solute mobilization in riparian zones and the subsequent export of solutes to the stream. The dynamics of riparian solute mobilization and transport were simulated for stream discharge scenarios of varying peak height and durations. Our results show that the magnitude and timing of bank inflow, outflow and therefore solute mass outflux from the riparian zone into the stream is controlled by the shape of the discharge event (i.e. event peak height and duration). The initially unsaturated conditions in parts of the riparian soils allow higher inflow rates in significantly shorter times than the subsequent bank outflows. The bank outflows typically start during the falling limb of the stream flow event, when the local hydraulic gradient reverses back to gaining conditions. A significant fraction of the infiltrated water was discharged back to the stream until the end of the flow event; however a small fraction of outflow stayed in the bank, and was discharged back to the stream over a longer period of time after the flow event. Upon infiltration of stream water, the water level in the riparian zone rises resulting in the mobilization of solutes residing in the previously unsaturated zone. The export of mobilized solutes into the stream occurs in two stages. In the first stage, the bulk of the mobilized solute is transported by the direct bank outflow from the riparian zone resulting in peak concentration at the end of flow event. Bank outflow driven export lasts for a relatively short period of up to 12 days, while during the second stage solute mass from zones of increased saturation moves vertically downward to the saturated zone under the influence of gravity. This drainage process from the unsaturated zone is very slow and is responsible for the long tailing of stream concentration (> 400 days) after the event.

Both event peak height and event duration enhance solute mass export. However, in comparison to the event duration, peak height plays a dominant role for the total solute mass exported. The timing of change in stream concentration is directly linked to the timing of the bank outflows which in turn depends on the hydraulic gradients near the stream. The time lag between peak discharge and peak concentration increases with event duration as longer durations delay the reversal of the local hydraulic gradients from negative (losing) to positive (gaining).

Our findings are consistent with previous studies (e.g., Boutt and Fleming, 2009; Gu et al., 2012; Mei et al., 2014; Sawyer et al., 2014). It also supports the idea that the export of the riparian solutes during bank outflows is dominantly controlled by the fluctuations in near stream hydraulic gradients (Welch et al., 2015). Another important finding is that presence of unsaturated zone can lead to long term solute export into the stream after the flow event. For a field based evaluation of the effects of stream flow events on river solute loads, measurement windows have to be long enough to capture the delayed response caused by solute mobilization from the unsaturated soil zone. The prolonged stays of stream water in the riparian zone provide opportunity for long term reactions and therefore have important implications for both stream and groundwater quality.

Acknowledgements

This study was funded by Higher Education Commission Pakistan and German Academic Exchange Service (Project ID: 57076459). We are thankful to the editors, Steffen Birk, Olivier Bour and one anonymous reviewer for their reviews and feedback on the manuscript.

Author Contribution Statement

M.N. Mahmood and C. Schmidt conceived the idea and jointly planned the project outline. M.N. Mahmood developed the model, performed numerical simulations, produced the results and wrote the article. N. Trauth supervised the modeling work. C. Schmidt, N. Trauth and J.H. Fleckenstein provided critical feedback and helped shape the results and manuscript. C. Schmidt was in-charge of overall direction and planning.

Appendix 2

Figure 2.1A: Selected discharge scenarios of varied peak height and duration used in simulations (shortened list). Tick marks on x and y axes indicate duration of events [h] and peak height [m] respectively.

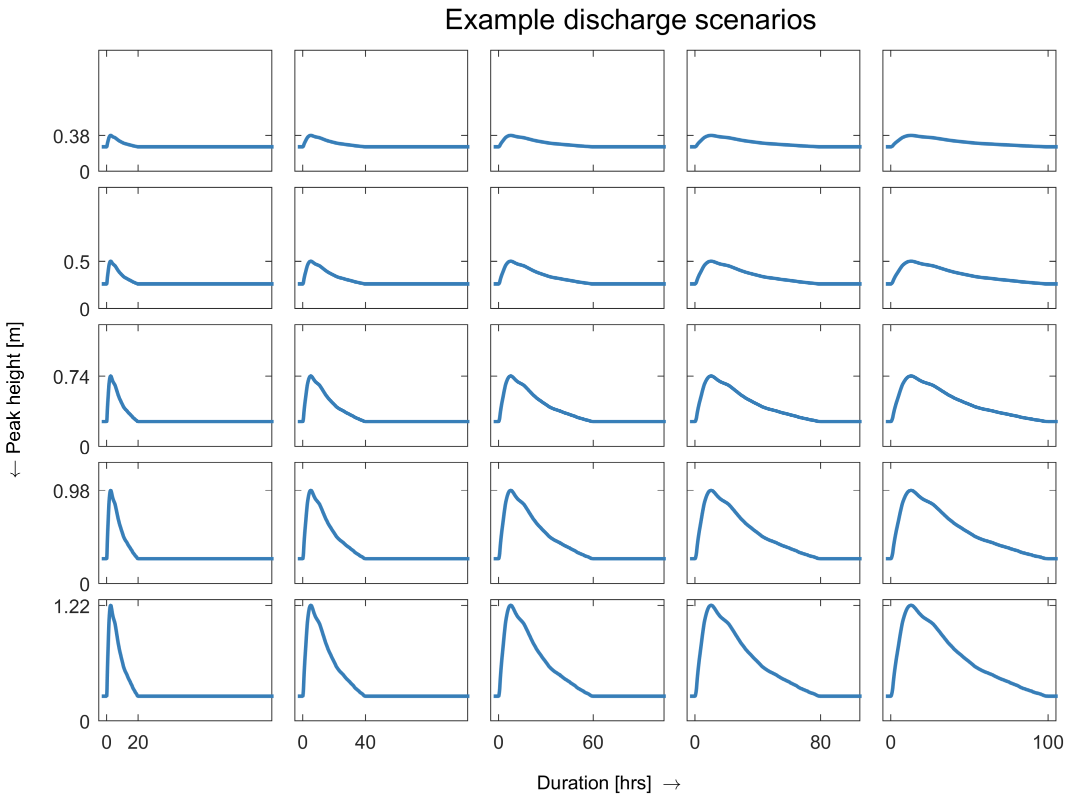

Table 2.1A: Simulated discharge Scenarios of systematically increasing event peak height and duration

		Event Peak Height [m]															
		0.06	0.12	0.18	0.24	0.3	0.36	0.42	0.48	0.54	0.6	0.66	0.72	0.78	0.84	0.9	0.96
Event duration [hr]	10	1p1	1p2	1p3	1p4	1p5	1p6	1p7	1p8	1p9	1p10	1p11	1p12	1p13	1p14	1p15	1p16
	20	2p1	2p2	2p3	2p4	2p5	2p6	2p7	2p8	2p9	2p10	2p11	2p12	2p13	2p14	2p15	2p16
	30	3p1	3p2	3p3	3p4	3p5	3p6	3p7	3p8	3p9	3p10	3p11	3p12	3p13	3p14	3p15	3p16
	40	4p1	4p2	4p3	4p4	4p5	4p6	4p7	4p8	4p9	4p10	4p11	4p12	4p13	4p14	4p15	4p16
	50	5p1	5p2	5p3	5p4	5p5	5p6	5p7	5p8	5p9	5p10	5p11	5p12	5p13	5p14	5p15	5p16
	60	6p1	6p2	6p3	6p4	6p5	6p6	6p7	6p8	6p9	6p10	6p11	6p12	6p13	6p14	6p15	6p16
	70	7p1	7p2	7p3	7p4	7p5	7p6	7p7	7p8	7p9	7p10	7p11	7p12	7p13	7p14	7p15	7p16
	80	8p1	8p2	8p3	8p4	8p5	8p6	8p7	8p8	8p9	8p10	8p11	8p12	8p13	8p14	8p15	8p16
	90	9p1	9p2	9p3	9p4	9p5	9p6	9p7	9p8	9p9	9p10	9p11	9p12	9p13	9p14	9p15	9p16
	100	10p1	10p2	10p3	10p4	10p5	10p6	10p7	10p8	10p9	10p10	10p11	10p12	10p13	10p14	10p15	10p16

Figure 2.2A: Effects of event hydrograph shape on stream water solute concentration [a, b]: Peak concentration in stream (C_{str}) with increasing peak discharge and duration [c, d]: Time lag in starting time of bank outflow (Q_{out}) and stream concentration (C_{str}) .

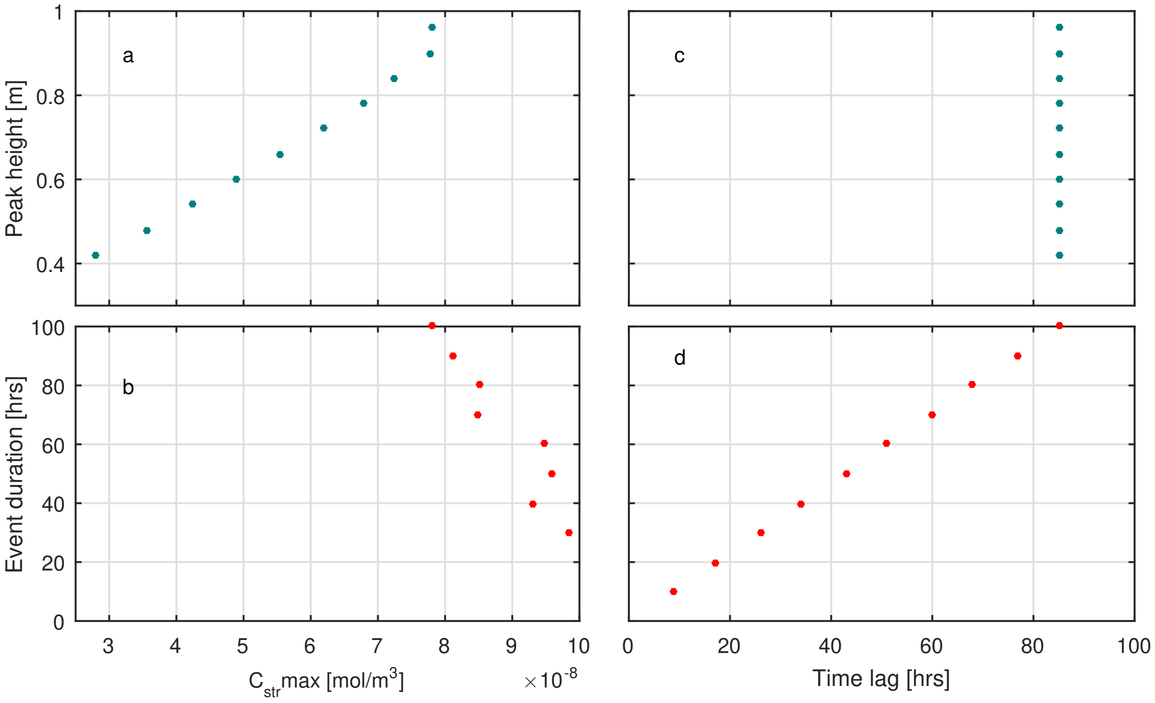

Figure 2.3A: Fraction of bank inflow water remaining in the riparian zone (green line), corresponding solute export (orange line) out of the riparian zone (top) and change in saturation within the riparian zone during and after the flow event (bottom).The vertical line indicate starting time of bank outflow, end time of flow event and time when major part of the outflow has discharged back to the stream respectively.

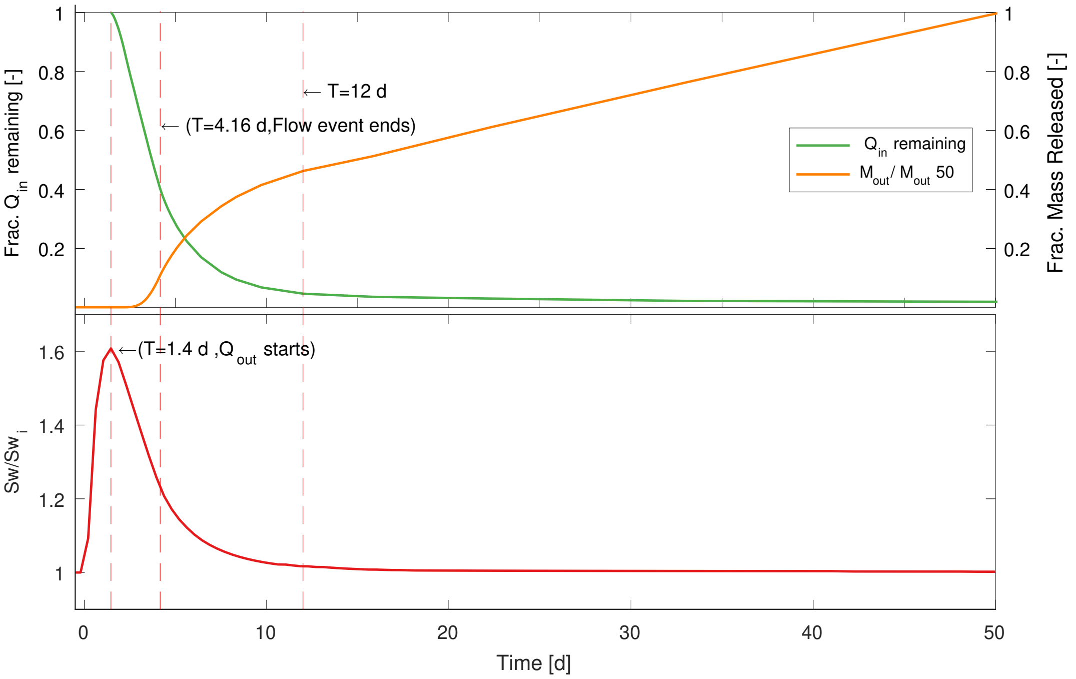

Chapter 3

Flow and Transport Dynamics within Intra-Meander Zone

3.1. Introduction

Eutrophication of freshwater due to both natural and anthropogenic activities is one of the crucial challenges for the management and the restoration of riverine ecosystem (Skogen et al., 2014). In the past few decades, a steady increase in the loads of dissolved organic carbon (DOC) has been observed in the streams (e.g., Rinke et al., 2013). Similarly anthropogenic activities have increased nitrogen (N_2) fluxes into stream systems (e.g., Aber et al., 1998; Smith et al., 2006; Mulholland et al., 2008) resulting in the deterioration of stream water quality as well as increasing the cost of water treatment in the downstream drinking water reservoirs. Large quantities of nutrient loads carried by surface and subsurface flow from upland are usually intercepted by the riparian buffers (e.g., Bishop et al., 1990; Karr and Schlosser, 1978) and therefore, near stream riparian zones serve as a temporary storage for agricultural nutrients, reducing the contaminant loads into stream (Hill, 2000; Vidon et al., 2010). However, surface water bodies and their riparian zones continuously interact in a variety of forms and scales in all types of landscape settings (Bencala, 1993; Winter, 1998) leading to dynamic exchange of waters between entirely different sources with distinct chemical signatures. The continuous dynamic exchange of water between stream and surrounding riparian zone enhances mixing and transport of contaminants across the stream-riparian interface as well as facilitates complex biogeochemical processes within the riparian zone (Stanford and Ward, 1993). Identification of the potential of stream-riparian interactions to influence water quality has drawn the attention of researchers towards the complex nutrient transformation and exchange mechanism across stream-riparian interface and associated effects on water quality of both ground and surface water. Therefore, in the last two decades, the role of stream-riparian exchange in attenuation and transformation of nutrients within riparian zone as well as regulating contaminant fluxes into streams has been extensively studied (e.g., Stanford and Ward, 1993; Bencala, 1993; Hill, 1996; Brunke and Gonser, 1997; Boulton et al., 1998; Woessner, 2000; Vidon and Hill, 2004b,a; Fleckenstein et al., 2010).

One of the most important stream-riparian exchange processes is hyporheic exchange flow (HEF) which is defined as the continuous entry of stream water into surrounding sediments and re-entry back to the stream after some time (Harvey et al., 1996; Winter, 1998; Harvey, 2000; Storey et al., 2003; Bencala, 2005). Due to unique flow paths, HEF provides opportunity of nutrient exchange across stream-riparian interface as well as facilitates biogeochemical transformations within riparian zone. These biogeochmical transformations within the hyporheic zone may result in degradation of contaminants and therefore HEF zone is also seen as a self cleaning mechanism of riverine ecosystem. For example, a major portion of stream respiration, a process responsible for removal of carbon in the form of CO_2, occurs mostly within the hyporheic zone (e.g., Kaplan and Newbold, 2000). Furthermore, denitrifcation, i.e. reduction of NO_3^- to gaseous N_2 is also exclusively attributed to the processing within hyporheic zone (Laursen and Seitzinger, 2002; Lansdown et al., 2012). Due to the above mentioned functionality, hyporheic exchange processes are key to the ecology and water quality of riverine ecosystem and therefore it is important to improve our understanding of nutrient cycling mechanism at hyporheic exchange zone (e.g., Fisher et al., 1998; Mulholland et al., 2000; Krause et al., 2009; Fleckenstein et al., 2010; Trauth et al., 2014; Boano et al., 2014; Trauth et al., 2015, etc.)

Hyporheic exchange flow (HEF) occurs at a variety of scales (e.g., Stonedahl et al., 2010), beginning from as small as the scale of centimeters e.g., due to pressure variation on individual bedforms (Elliott and Brooks, 1997; Storey et al., 2003) to a much larger scale between meters and 10 of meters due to large morphological features such as pool riffle effect (e.g., Trauth et al., 2014) and gravel bars (e.g., Shope et al., 2012). The HEF further extends to channel scale such as lateral exchanges through stream banks (Harvey and Bencala, 1993; Kiel and Cardenas, 2014; Wroblicky et al., 1998; Cardenas, 2009) and meander bends (Boano et al., 2006; Revelli et al., 2008; Gomez et al., 2012; Cardenas, 2009). The mechanism of HEF differs depending upon the type and extent of morphological features as well as other factors such as varying hydrological conditions. For example, large scale lateral HEF is induced by the hydraulic head difference across morphological features i.e. water enters the bed at locations of higher water level (upstream) and exits at the lower water level (downstream). This type of hydrostatic head driven hyporheic flow occurs under all conditions throughout the river reaches (e.g., Stonedahl et al., 2010; Kiel and Cardenas, 2014; Boano et al., 2014). The spatial extent and residence time for hyporheic flow are key variables for hyporheic zone functionality as they control the amount and timing of biogeochemical transformations of contaminants (Boano et al., 2014). Since hydrostatic hyporheic exchanges are much larger in terms of magnitude as well as spatial and temporal extent as compared to the small scale exchanges, they may transport large quantities of solute to and from the stream into the riparian sediments and provide opportunity of mixing and biogechemical transformation for longer period of times. Especially channel sinuosity driven hyporheic exchanges are one of the largest in spatial (ranging from meters to 10 of meters) as well as temporal (from days to years) extent (Revelli et al., 2008; Cardenas, 2008; Boano et al., 2006; Gomez et al., 2012). Furthermore, hydrostatically driven exchange flows are dominant in non-submerged morphological features (Harvey and Bencala, 1993; Woessner, 2000; Cardenas, 2008) and therefore are likely to be influenced by the variability in hydrologic conditions e.g. rise in water level due to a flow event.

Due to the complex nature of hyporheic flow and involvement of diverse processes such as hydrological and chemical dynamics (Böhlke et al., 2009), temporal and spatial variability (Boano et al., 2014; Trauth and Fleckenstein, 2017) as well as methodological constraints, numerical modeling approaches are often required to improve the understanding of complex exchange processes (Fleckenstein et al., 2010). Past research has mainly focused on small scale hyporheic exchange flow (HEF) driven by fully submerged features like dunes (Cardenas and Wilson, 2007; Elliott and Brooks, 1997), pool and riffles (Trauth et al., 2014) etc. Whereas, large scale hyporheic exchange processes and resulting solute transformations in partially submerged features are rarely studied, although these features occur frequently throughout natural river systems and have pronounced implications for nutrient transformations and transport (e.g., Shope et al., 2012; Boano et al., 2014; Trauth et al., 2015). Shope et al. (2012) investigated the influence of stream bar on hyporheic exchange during the variable hydrologic conditions, using field data and heat transport simulations. Trauth et al. (2015) simulated the biogeochemical transformations in a partially submerged in-stream gravel bar under varying hydrologic conditions. Similarly a few attempts have been made to explore the intra-meander flow and exchange process with the help of field and laboratory studies (e.g., Han and Endreny, 2014; Konsoer et al., 2016). These studies include theoretical models focused on predicting meander evolution time scales and estimation of intra-meander residence times based on the particle tracking techniques (Boano et al., 2006; Revelli et al., 2008), influence on reactions under steady state conditions in the saturated zone (Boano et al., 2010) and influence of ambient groundwater on intra-meander flow paths (Gomez et al., 2012). However, some key aspects of intra-meander flow still need more insight, for example, in past intra-meander flow has been represented as two dimensional process due to dominant lateral extent of intra-meander HEF. However, biogeochemical transformation are very sensitive to the vertical extent of the hyporheic flow paths (e.g., Storey et al., 2003). In addition to that, majority of the available studies have considered hyporheic flow under steady state conditions. Furthermore, intra-meander HEF studies are often limited to the fully saturated intra-meander zone below water table and do not address the variably saturated intra-meander zone above the water table. Gomez-Velez et al. (2017) recently attempted to model the impact of stream discharge on sinuosity and bank storage driven exchanges. In their study using the 2D modeling concept of Cardenas (2009), they simulated the impact of single discharge event on bank storage and sinuosity driven flow. However, mobilization and biogechemical transformation of riparian solutes initially residing in the non-submerged unsaturated zone was ignored. Since the intra-meander hyporheic exchange is induced by the head difference across the intra-meander zone, variation in stream stage can significantly influence the intra-meander flow field by altering the degree of submergence and therefore may mobilize and transform solutes present within initially unsaturated intra-meander zone (Trauth et al., 2015).

Hence, nutrient loads accumulated in the initially unsaturated riparian zone (e.g., Bishop et al., 1990, 1994; Grabs et al., 2012), can be mobilized and exported to the stream due to the variation in near stream water table (e.g., Creed et al., 1996; Hill, 2000). However, little is known about the effect of changing hydrological conditions on intra-meander hyporheic exchange flow and resulting chemical transformations. In particular, it is not known how significant is the impact of a stream flow event on the mobilization of solute residing in the previously non-submerged intra-meander zone. For example, intra-meander hyporheic flow during a flow event, may enhance solute transport towards the stream by infiltrating into solute deposits residing in the unsaturated intra-meander zone and ultimately exporting it towards the stream. On the other hand, there is also a possibility that the solutes present in the stream water are filtered by entrapment in the intra-meander region i.e. intra-meander zone may either act as a source or sink of nutrients. Recently, in a 2D modeling study of a single intermediate stage meander, Dwivedi et al. (2018), showed that stream discharge event can deposit as well transport carbon to and from intra-meander zone. Moreover, long intra-meander residence times facilitate biogeochemcial transformation within the intra-meander zone which may result in complete removal of solute species. Hence, identification of the important factors affecting the intra-meander HEF and associated transformation and export of solutes from or to the stream is important for the better management of the stream water quality.

This chapter aims at investigating the role of stream sinuosity on the intra-meander HEF and the influence of stream discharge event on solute (DOC) mobilization/ transformation within the intra-meander zone and export to the stream. For this purpose, a three dimensional groundwater reactive transport model of variably saturated flow has been developed. The influence of different meander shapes on intra-meander flow field under base flow conditions as well as during stream discharge event on solute mobilization and reactive transport from the unsaturated zone is investigated by the application of varying morphological, hydrologic and reaction scenarios. In the first part, three dimensional steady flow has been simulated for a set of meander shape scenarios with varying degree of sinuosity. The steady state flow analysis allows to predict the influence of meander sinuosity on intra-meander residence times. In the second part, using the flow distribution of steady state flow simulations as the initial conditions, we investigate the influence of stream discharge event on mobilization and conservative transport of solute (DOC) initially stored in the non-submerged portion (unsaturated zone) of intra-meander region. In the third and final part, we investigate the influence of stream discharge event on biogechemical transformation within the intra-meander zone. For this purpose, we simulated aerobic respiration (AR) and denitrification (DEN) of intra-meander solutes for varying chemical scenarios.

3.2. Methods

Hyporheic exchange flow is often characterized on the basis of residence time and spatial extent (Boano et al., 2014), as residence time provides a direct measure of timescales of transport processes whereas spatial extent of HEF defines the amount of solute and water exchange. In order to investigate the influence of meander sinuosity, hydrologic and chemical conditions on intra-meander hyporheic exchange, this study is divided into three phases. In the first phase, we simulate intra-meander flow and residence times for various meander shape scenarios with a systematically varying degree of sinuosity under fully saturated steady state flow conditions. In the second phase, using the flow field distribution obtained from the steady state analysis as initial conditions, we simulate hyporheic exchange under transient flow conditions caused by the streams stage fluctuations. In order to investigate the effect of a stream flow event on conservative solute transport within the intra-meander zone, a solute (DOC) layer within the unsaturated intra-meander zone is introduced which may come in contact with the stream water during the flow events. In the third phase, we further extend the model by simulating removal of intra-meander solute (DOC) through aerobic respiration (AR) and denitrification (DEN) during stream flow event.

3.2.1. Meander Shape Scenarios

Natural river bends occur in a variety of shapes and sizes. During meander evolution process, the shape of meander bends changes in a well known pattern. Initial stage meanders are characterized by smaller curvature near the apex which is usually estimated by the measurement of radius of curvature (R_c) and longer wavelength (λ) as shown in Figure 3.1 i.e. longer distance at the opposite corners of the meander. Under the influence of stream hydrodynamics i.e. continuous erosion of outer bank and sediment deposition at inner bank, the meander form continuously evolves over the time. One of the most common feature of the evolution process is the narrowing of distance at the steepest head difference within the meander bend which occurs usually near the opposite corners of the meander, i.e. λ starts decreasing with meander evolution, whereas R_c tends to increase. The phenomenon of decrease in length around the point of steepest head difference is termed as neck formation. This process of narrowing meander neck continues until the meander is cut off.

In the past, various analytical methods have been developed to predict meander evolution and river migration (e.g., Ikeda et al., 1981; Johannesson and Parker, 1989; Camporeale et al., 2005). The analytical model proposed by Zolezzi and Seminara (2001) has been utilized by Boano et al. (2006) and Cardenas (2009) to predict the evolution of meanders and intra-meander flow patterns. In this study,

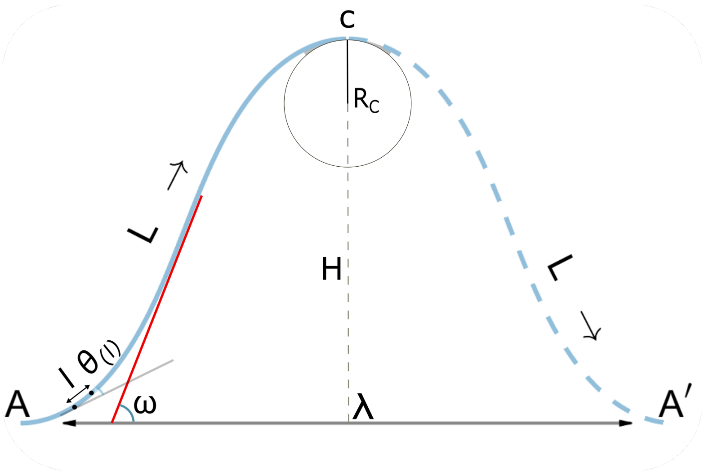

Figure 3.1: Basic form parameters of a meander, wavelength (λ), height or amplitude (H), radius of curvature (R_c) and meander length (L).

we are focusing on the effect of meander shapes on the intra-meander HEF and associated solute fluxes instead of mechanism involved in the evolution and migration of meander under various morphodynamic factors. Therefore, we opt for a simple way to obtain unique curves representing various meander evolution stages ranging from the initial to the cut off stage. This has been conveniently achieved by a sine generated curve based on a simple approach known as the minimum variance approach. The minimum variance approach was first proposed by Langbein and Leopold (1966). Using this approach the unique curvatures representing meander sinuosity of varying degrees can be generated by specifying a single variable known as direction angle using following equation.

$$\theta(l) = \omega sin(\frac{2\pi l}{L}) \tag{3.1}$$

where;

$\theta(l)$ [°] is the channel direction angle along the curvature of the meander

ω [°] is the maximum angle which the curve makes with horizontal (direction angle)

l [m] is the small incremental segment of the meander length (L) where θ and ω are defined

L [m] is the path length along the arc from trough to trough i.e from point A to A'

In equation 3.1 channel direction angle $\theta(l)$ [°] varies in a sinusoidal way along the path of the curve. The ω specifies the shape of the curve, therefore we refer to ω as the shape angle in the following text. Using the equation 3.1, twenty two (22) meander shape scenarios representing systematically increasing degree of meander sinuosity from initial to near cut off stage are generated. These scenario are named

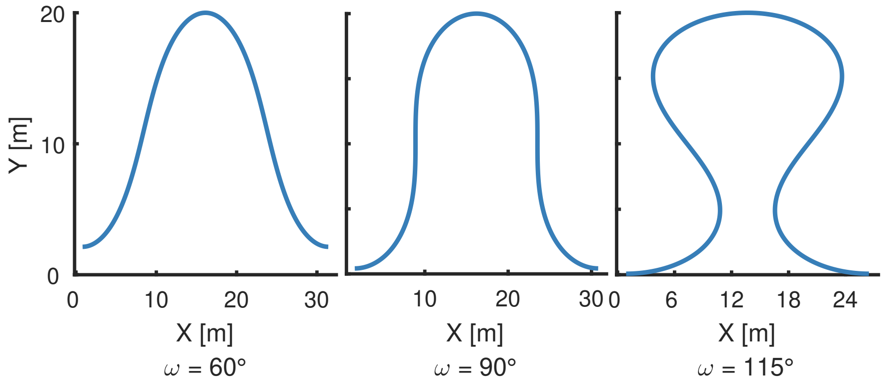

Figure 3.2: Three of the meander shape scenarios developed using different values of ω. The sinuosity increases with increasing value of ω.

after so called shape angle (ω) ranging from $\omega = 15°$ (initial stage bend) to the $\omega = 120°$ (near cut off bend). The degree of sinuosity of meander bend is represented by the value of ω i.e. higher value of ω means higher degree of sinuosity. Three representative shape types defined by the ω value of 60°, 90° and 115° are shown in Figure 3.2. The scenarios with the shape angle $\omega \leq 60°$ represent meanders of low sinuosity or initial stage meanders, the scenarios with the shape angle around 90° represent middle stage meanders, whereas the scenarios with the shape angle $\omega \geq 105°$ represent highly sinuous advanced stage meanders. A maximum amplitude (H) of 20 m and wavelength (λ) of 30 m is set for individual meander scenarios. Once these shape curves were obtained using equation 3.1, they were transformed into Cartesian for the representation of stream cells in the surface and groundwater models (Code 3.1A).

3.2.2. Surface Water Simulations

The influence of event peak and duration on solute mobilization has been investigated in chapter 2 in details by simulating systematically varying peak height and duration of the flow event. In this chapter, we use a stream discharge event with maximum peak height (0.96 m above base flow level) and the longest duration (120 h) from the scenarios used in chapter 2 to three representative meander shape scenarios to investigate the response of meander shapes on solute mobilization during the stream flow event. In order to simulate the effect of stream stage variation on intra-meander HEF, a variable stream head boundary is required at the cells in top layer of the groundwater model representing stream i.e. outer boundary of intra-meander zone where heads at boundary cells respond to a stream flow event. To obtain realistic transient heads at the meandering boundary, we simulated stream flow using unsteady flow simulation package of 1 D HEC-RAS 4.1.0 for three meandering streams scenarios i.e. ω 60, ω 90, ω 115. 1 D HEC RAS solves Saint-Venant equations that describe one dimensional unsteady flow in open channels. The Saint Venant equations are a simplified solution of Navier-Stokes equations which solve continuity and momentum equation combined. The solution of these equations defines the propagation of a flood wave with respect to distance along the channel and time.

The stream geometry in HEC RAS is defined by specifying the orientation of a cross section with respect to the next cross section. The meandering stream shapes obtained from the section 3.2.1 were transformed into cross sections to be implemented as stream geometry in HEC RAS. To preserve the stream geometry intra cross section distance (reach lengths) of less than 1 m was adopted, resulting in total 272 to 290 cross sections depending upon the degree of meander bends. A triangular stream cross section of 0.75 m width and 1.5 m depth was chosen for all the simulation scenarios. In the first step steady state flow was simulated by specifying upstream stage height of 8.95 m (i.e. 0.45 m above the streambed), average river bed slope ($S_o = 0.01$), Manning's roughness coefficient ($n = 0.04$) as well as other parameters such as contraction and expansion coefficients. The results of the steady flow simulations were then used as initial conditions for unsteady flow simulations. The unsteady flow simulation package in 1D HEC RAS requires two key boundary conditions for the simulations of surface water profiles (i.e. time variant stream elevations) of a stream reach. At the channel head it requires a stage or discharge hydrograph with uniform time steps and a downstream parameter e.g. normal or critical depth. For unsteady flow analysis, a discharge value of 0.042 m^3/s (obtained from steady state simulation) was applied as initial flow corresponding the stage of 0.45 m above streambed. At the upstream boundary, a stage hydrograph of 120 h duration with peak height of 1 m above base flow was applied. Other hydraulic parameters used for the unsteady HEC-RAS simulation are given in the table 3.1. The peak discharge of 1.4 m^3/s was computed corresponding to the height of 9.95 m (stage height of 1.45 m). The computed time variant water surface elevations (hydraulic heads) obtained from surface water model were then applied as transient (time variant) head boundary conditions to the top of the groundwater model i.e. to the stream cells.

Parameter	**Value**	**Units**
Stream depth from surface	1.5	[m]
Stream bed slope (S_o)	0.045	[m/m]
Manning's (n)	0.04	[m/m]
Base flow	0.01	[m^3/s]
Peak Flow	1.5	[m^3/s]
Max. channel elevation	9.99	[m]
Boundary Conditions [Unsteady Flow]		
Upstream boundary condition	Stage hydrograph	
Downstream boundary conditions	Normal Depth	

Table 3.1: Hydraulic parameters for surface water model [HEC RAS].

3.2.3. 3D Groundwater Flow Simulations with Modeling Code MIN3P

A three dimensional groundwater model was set up with the groundwater modeling code MIN3P, which is capable of simulating flow and reactive transport in a variably saturated medium (Mayer et al., 2002). As shown in Figure 3.3, the model domain extends 100 m in horizontal direction 'X', 30 m in lateral direction 'Y' and 10 m in vertical direction 'Z'. After the meandering stream co-ordinates were obtained, the cells in the top layer of groundwater model with same co-ordinates were located and adjusted to the streambed elevation by deforming the mesh using a mesh deformation algorithm (Code 3.2A). It not only enables incised channel in the top layer of the model but also deforms the mesh in the vertical direction (z-direction) to adjust the valley slope (topography) to the streambed slope. The incised channel depth was set to 1.5 m from the top surface of the model domain.

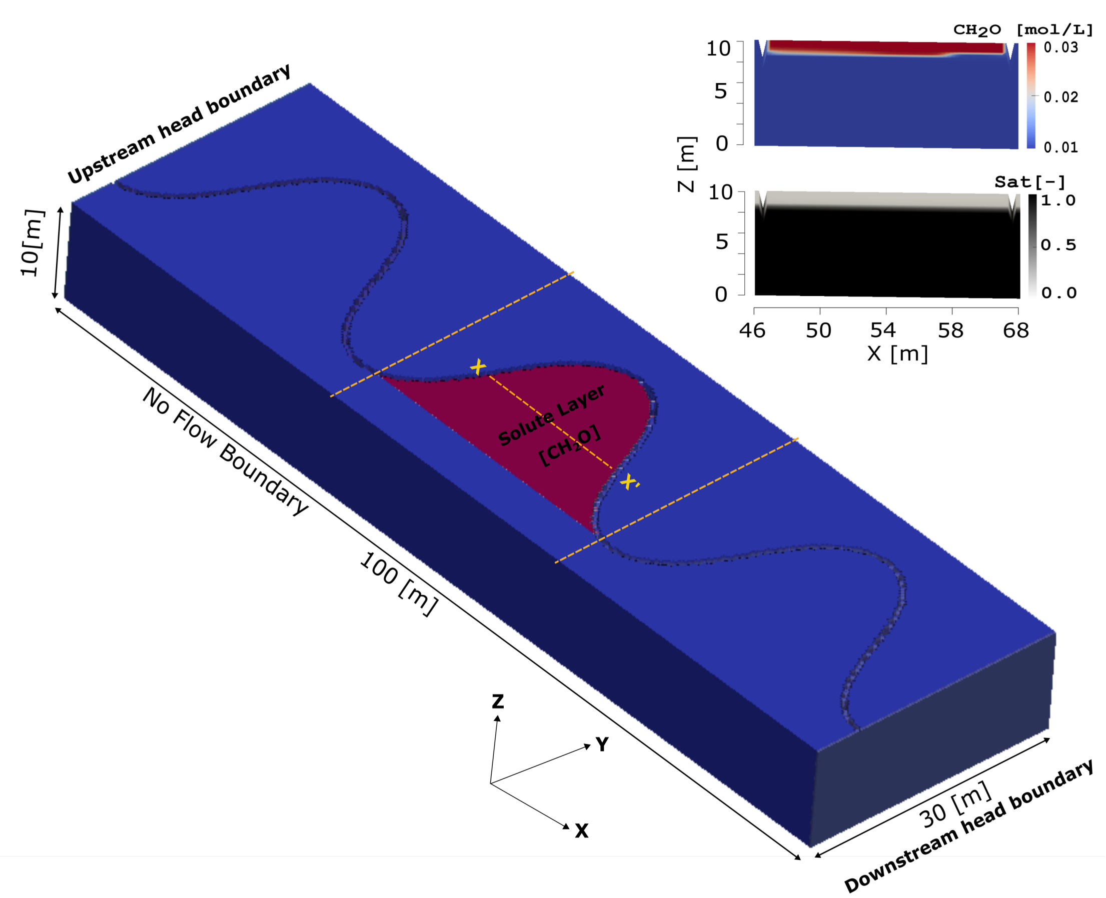
Upstream head boundary
10[m]
No Flow Boundary
100 [m]
Solute Layer
[CH$_2$O]
X
X'
Z
Y
X
30 [m]
Downstream head boundary
CH$_2$O [mol/L]
0.03
0.02
0.01
Sat[-]
1.0
0.5
0.0
Z [m]
10
5
0
10
5
0
46
50
54
58
68
X [m]

Figure 3.3: Model set-up showing the extent of modeling domain with incised meandering channel and location of solute source. The domain area between two dotted lines parallel to Y direction is used for results evaluation. Two (XZ) cross sections on the right side show vertical profile of simulated water saturation (bottom) and solute concentration (top) under steady state conditions at the section XX' (marked in yellow).

Type	No.	Name of Meander Shape Scenarios (ω[°])
Steady flow	22	15 20... 115 120
Transient Flow	3	60 90 115

Table 3.2: Meander shape scenarios for steady and unsteady flow simulations.

A constant head of 0.45 m above the channel bed was assigned to stream cells (free water surface elevations) with a streambed slope (S_o) of 0.01 m/m. Hence, an initial fixed head of 8.95 m at upstream head boundary (see Figure 3.3), whereas at the downstream boundary the initial head was varied from 7.45 to 6.8 m depending upon the length of meandering stream. A uniform mesh grid of 0.25 m was set along the x and y direction throughout the model, whereas the vertical extent (z axis) was divided into three sub regions. Up to 3.5 m depth from the surface of the model, a finer grid of 0.125 m while from 3.5 to 5 m a grid size of 0.25 m was applied. The grid size from 5 to 10 m was gradually increased from 0.25 m to 1 m. Depending upon the shape of the stream the total number of cells varied from 1399920 to 1587222. The finer mesh in the top layers of the model containing stream and variably saturated intra-meander region ensures better representation of intra-meander flow field as solute mobilization and reactions.

No flow boundaries were assigned along the upstream, downstream as well along the lateral directions i.e. no groundwater inflow and outflow was considered (for steady state simulation). Similarly bottom of the model as well on the top (except the stream cells) were also assigned no flow boundaries i.e. no recharge from the top boundary was simulated. In order to eliminate any boundary effects on intra-meander flow, we extended the modeling domain up to 5 m out of stream bank in lateral direction. In order to minimize the effect of no flow boundary at upstream and downstream head boundaries along the stream flow direction, the modeling domain was extended up to three meander bends, however, only the results from the central meander were considered for evaluation purpose.

3.2.3.1. Steady Flow Simulations

Steady flow was simulated for twenty two (22) meander shape scenarios ranging from ω 15 to ω 120 (see Table 3.2). The flow field obtained through steady simulation was utilized for the estimation of intra-meander residence times. In order to investigate the flow velocities and residence times across the intra-meander area, forward advective particle tracking was conducted using the open source visualization software ParaView (version 5.1.2). Steady state pore water velocity field was generated using fourth-fifth order Runge-Kutta integration technique. A number of particles (two particle per mesh cell) were released at the depth 0.2 m below the streambed along the upstream segment (segment AC in Figure 3.1) of the meander. The particles were traced by forward particle tracking until they reach the downstream end of the meander i.e. travel time for each particle was computed from release point at upstream section until the time, they exit in or pass under the downstream segment (i.e. segment CA' in Figure 3.1).

The lateral extent of intra-meander flow is considerably greater compared with the vertical direction and therefore generally vertical flow has been ignored in the past studies (e.g., Boano et al., 2006; Revelli et al., 2008) etc. However, the vertical extent of hyporheic zone is important and more relevant when investigating the chemical transformations within the zone as it controls the extent of solute mobilization, transformation and transport from the dominant solute layer (Storey et al., 2003). Using 3D modeling setup, it is possible to simulate the vertical extent of intra-meander flow paths. The maximum penetration depth of the intra-meander flow paths (D_{max}) for each flow path has been calculated in order to explore the effect of meander sinuosity (ω) on vertical extent of flow paths and intra-meander residence times (RT). Furthermore, relationship of intra-meander residence times (RT) with intra-meander area (A) and average intra-meander hydraulic gradient was also analyzed. Although groundwater flow direction may influence the intra-meander flow field (e.g., Cardenas, 2009; Gomez et al., 2012), in this study no flow boundary conditions on lateral (Y direction) as well as along valley (X direction) are applied for steady flow simulations. This setup allows to investigate the sole effect of meander shape on the intra-meander flow dynamics.

3.2.3.2. Stream Flow Event and Solute Mobilization Set-Up

In order to simulate the stream flow event in the groundwater model, transient stream heads obtained from the surface water model were applied as transient boundary conditions to stream stream cells in the top layer of groundwater model. For the simulation of the mobilization and transport of the solute from the unsaturated intra-meander zone we apply a uniform concentration of solute layer in the non-submerged (unsaturated) intra-meander region which is tapped by the rise in groundwater level. A uniform layer of carbon source (CH_2O) having concentration of 3.3 mmol/L (100 mg/L) is applied in the upper unsaturated part of the meander. The vertical extent of solute layer is restricted only to the upper 1.0 m (the non-submerged part) of intra-meander depth (see Figure 3.3).

In the subsequent analysis, the influence of stream discharge event on intra-meander solute mobilization and conservative transport has been simulated and analyzed for three meander shapes.

For transient simulations, the same modeling setup is used as in steady flow analysis. Similar flow boundary conditions are applied except constant head boundaries (Dirichlet boundary) at the inflow (upstream) and outflow (downstream) locations (see Figure 3.3). The groundwater head is set equal to the bed level at both upstream and downstream locations. The constant head boundaries at upstream and downstream locations and no flow boundary on lateral sides enable average groundwater flow direction parallel to the overall direction of the stream i.e. along the down-valley axis. This setup maintains groundwater level along the down-valley axis near the channel bed and prevents any backwater effect at downstream boundary during the simulation of stream flow event.

3.2.4. Reactive Transport

As stated in the section 3.1 important chemical transformations occur in the hyporheic zone (HZ). These reactions include aerobic respiration (AR) i.e. decomposition of organic carbon in presence of oxygen (O_2) and denitrification (DEN), a process responsible for transformation of nitrates (NO_3) into gaseous N_2 (Bencala, 2000).

A large amount of carbon is deposited in the riparian wetlands including in the intra-meander zone which is available for mobilization and transport in the form of DOC under suitable hydrologic conditions (e.g., Bishop et al., 1990). Stream water is usually enriched with oxygen (O_2) (e.g., Battin et al., 2003; Diem et al., 2013) whereas, a very small to no amount of O_2 is found in the groundwater (e.g., Kaplan and Bott, 1982). During hyporheic flow, oxygen rich stream water enters into subsurface, resulting in consumption of DOC through aerobic respiration (e.g., Trauth et al., 2015). Furthermore, due to use of fertilizers in the agricultural lands, nitrogen is increasing in the surface water as well as in groundwater in the form of nitrates (e.g., Peterson et al., 2008) i.e. nitrates may originate either from surface water ($S-NO_3$) or from the groundwater ($G-NO_3$).

Considering above mentioned possibilities of biogeochemical processes of aerobic respiration and denitrification, following chemical reaction scenarios are most likely to occur within riparian zone.

$$\text{Aerobic respiration: } \mathrm{CH_2O + O_2 \longrightarrow CO_2 + H_2O}$$

$$\text{Denitrification: } \mathrm{5\,CH_2O + 4\,NO_3{}^- + 4\,H^+ \longrightarrow 5\,CO_2 + 2\,N_2 + 7\,H_2O}$$

According to above equations, there are three possibilities of chemical interactions with DOC source (CH_2O), 1) aerobic respiration (AR) upon coming in contact with surface water, dentrification (DEN) with 2) stream originated nitrates ($S-NO_3$) and 3) groundwater originated nitrates ($G-NO_3$). Our chemical scenario is inspired by the measured data at a field site at Selke river in central Germany (Trauth et al., 2015).

Constant concentration of 10 mg/L (0.31 mmol/L) for stream oxygen (O_2) and 10 mg/L (0.16 mmol/L) for stream nitrates ($S-NO_3$) is assigned as top chemical boundary conditions (stream cells). We assume that stream water is free of DOC, i.e. zero DOC concentration is assigned to the top boundary (stream cells). Similarly a constant concentration of 10 mg/L (0.16 mmol/L) of groundwater nitrate ($G-NO_3$) is assigned at upstream inflow boundary, whereas zero concentration of DOC and O_2 is assigned to the upstream inflow boundary. Hence groundwater is assumed as free of DOC as well as O_2. This setup allows us to evaluate the influence of surface and subsurface nitrates and surface oxygen on the consumption of intra-meander DOC during a flow event.

Parameter	**Value**	**Units**
Water flow (saturated zone)		
Aquifer depth	10	$[m]$
Porosity	0.3	[-]
Sat. Hydraulic Conductivity $[K_x, K_y, K_z]$	0.001	$[m/s]$
Specific storage $[S_s]$	0.00001	$[m^{-1}]$
Water flow (unsaturated zone)		
Residual Saturation [ϑr]	0.01	[-]
Van Genuchten [α]	8.5	$[m^{-1}]$
Van Genuchten [n]	3.5	[-]
Solute Transport		
Longitudinal dispersivity	0.01	$[m]$
Horizontal transverse dispersivity	0.001	$[m]$
Vertical transverse dispersivity	0.0001	$[m]$
Diffusion coefficient (aqueous phase)	1.0×10^{-09}	$[m^2/s]$
Diffusion coefficient (gaseous phase)	1.0×10^{-05}	$[m^2/s]$
Parameterization of Monod kinetics for solute reactions		
Half-saturation constant K_{O_2}	6.25×10^{-06}	$[mol/L]$
Half-saturation constant K_{DOC}	1×10^{-04}	$[mol/L]$
Half-saturation constant K_{NO_3}	3.2258×10^{-05}	$[mol/L]$
Inhibition constant for denitrification K_I	3.13×10^{-05}	$O_2[mol/L]$
Maximum reaction rate $AR(\mu_{max,AR})$	4.75×10^{-01}	$[mmol/L/d]$
Maximum reaction rate $DEN(\mu_{max,DEN})$	8.64×10^{-02}	$[mmol/L/d]$

Table 3.3: Flow and transport parameters for the groundwater model [MIN3P].

MIN3P uses a general framework for kinetically controlled intra aqueous reactions. Related reaction and rate parameters can be incorporated into the model through an accompanying database. For microbially mediated reactions, MIN3P uses Monod approach. The general form of Monod kinetics is as following:

$$R = \mu_{max} l(\frac{C_d}{K_d + C_d})(\frac{C_a}{K_a + C_a}) \tag{3.2}$$

Where R is the reaction rate, μ_{max} is the maximum reaction rate , C_d and C_a are the concentrations of the electron donors and acceptors and K_d, K_a are the half saturation constants for electron donors and acceptors, respectively. In this model, reactions are simulated considering CH_20 as electron donor while O_2 and NO_3 as electron acceptors. Since O_2 acts as electron acceptor in case of organic matter decomposition (Hedin et al., 1998), the reaction rate of denitrification (DEN) is limited by the presence of O_2, therefore following inhibition factor 'l' is used for simulation of the DEN kinetic.

$$l = \frac{K_l}{K_l + C_{O_2}} \tag{3.3}$$

where K_l is the inhibition constant and C_{O_2} is the O_2 concentration.

The Monod kinetics parameters used in simulation are given in the table 3.3. The maximum reaction rate of AR used in the simulations ($\mu_{max,AR} = 0.475 mmol/L/d$) is calculated by field measurements at Selke river (Schmidt et al., 2012) whereas the half saturation constants K_{O_2}, K_{NO_3}, K_{DOC} and maximum reaction rate of denitrification $DEN(\mu_{max,DEN})$ are based on literature values from previous studies (Trauth et al., 2014).

In order to simulate controlled scenarios, a few assumptions are made which are usually necessary for this kind of exploratory modeling studies. We assume that the porous medium is homogeneous and isotropic i.e. uniform hydraulic conductivity along all x, y and z directions is assumed. The soil parameters used in the groundwater model (see Table: 3.3) closely resemble with sand. Groundwater flow direction is assumed in parallel to the general direction of valley slope in the transient simulations. No ambient groundwater flow, from the lateral sides of the model domain as well as no recharge on the top of the model has been incorporated.

3.3. Results and Discussion

3.3.1. Groundwater Heads and Flow Paths in the Saturated Intra-Meander Zone

In this section we present simulated groundwater flow patterns in the intra-meander region under steady flow conditions. Steady state flow and residence time simulations of all 22 scenarios show that meander shape scenarios (ω) can be broadly categorized in three geometric types. The scenarios with shape angle $\omega \leq 60°$, representing initial stage meander bends, the scenarios with shape angle value around 90°, representing middle stage meander bends and the scenarios with shape angle $\omega \geq 105°$, representing advance stage meanders. The scenarios within each group show similar patterns of groundwater flow and residence times. Therefore for simplicity, results from three scenarios i.e. $\omega = 60°$, 90° and 115° are compared in the following sub-sections.

3.3.1.1. Groundwater Heads

The 2D planes (XY) of the 3D intra-meander steady flow field generated by linearly decreasing stream heads at a depth of 0.25 m below streambed are shown in the Figure 3.4 (a1, b1, c1). This depth was selected to ensure fully saturated conditions. Head contours are plotted at a constant interval of 0.02 m. Head difference across the intra-meander area ranges from 0.1 m for the scenario ω 60 to 0.11 m up to the ω 90, whereas a substantial increase up to 0.15 m is observed for scenario ω 115. The substantial increase in head difference in advanced stage meanders is because of two reasons. Firstly, this is due to the formation of meander neck (e.g. in ω 115) which induces the steepest gradient at neck area. Secondly, meander length (L) is also increased in advanced stage meanders, which further increases the head difference across meander due to linearly decreasing bed slope. Hence, the shape of meander is a controlling factor for the intra-meander groundwater flow patterns.

3.3.1.2. Flow Paths and Isochrones

Intra-meander flow paths and isochrones obtained through forward particle tracking for three meanders are shown in sub-figures a2, b2 and c2 of the Figure 3.4. The particles were released throughout the length of upstream segment of meander at a depth of 0.25 m below the streambed. The blue lines are flow paths of the particles leaving from the upstream segment of the meander while the gray lines perpendicular to the blue lines are 10 h isochrones representing the location of particles after every 10 hours. The flow paths in the scenario ω 60 and ω 90 follow almost straight paths along the XY-plane (Figure 3.4 a2, b2) within the major portion of the meander indicating that the flow direction does not change along the XY-plane except at the top and bottom end of the meander where the

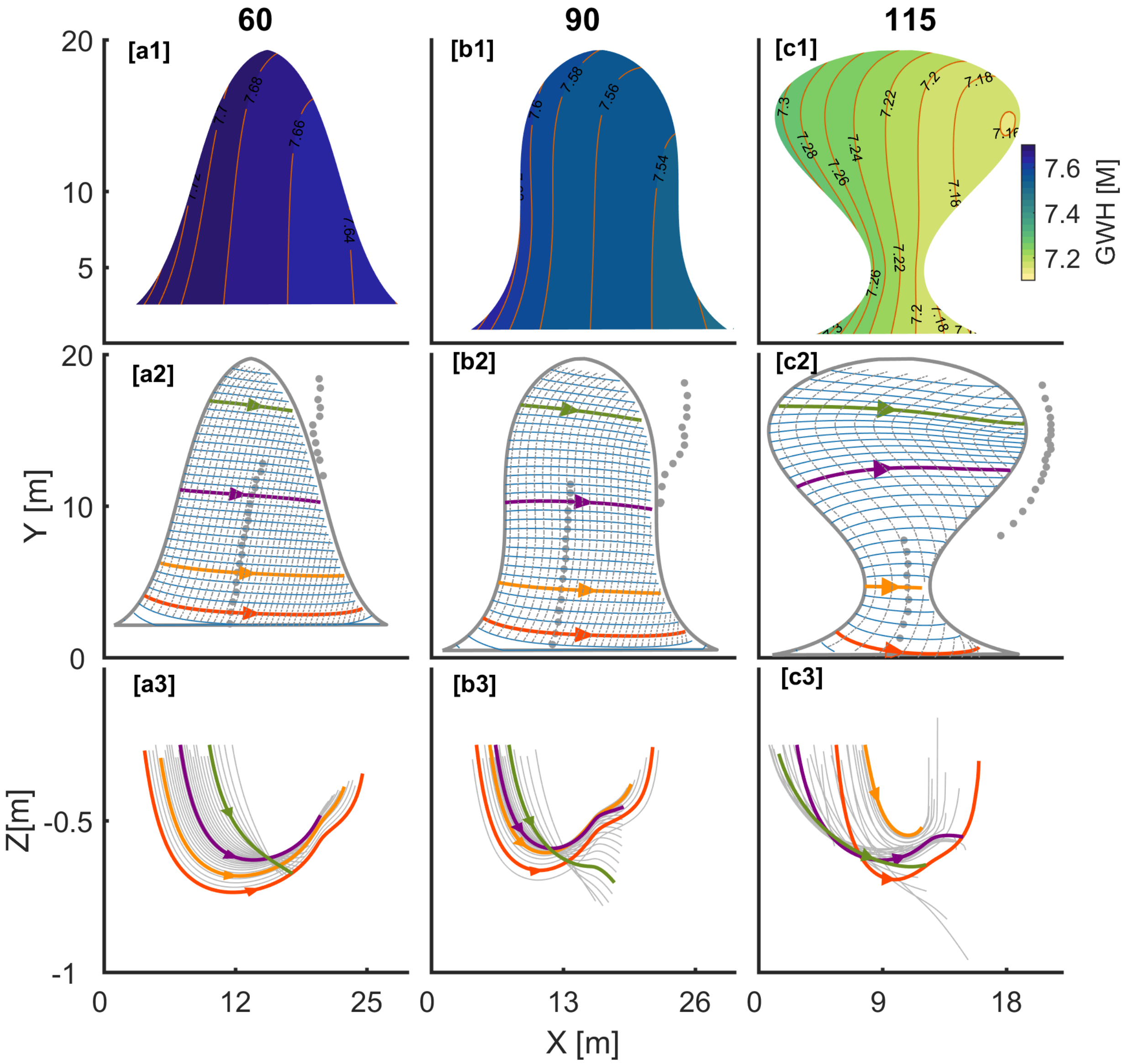

Figure 3.4: Groundwater heads (GWH) distribution at a depth 0.25 m below the streambed for the scenarios $\omega = 60°$, $\omega = 90°$ and $\omega = 115°$ respectively (first row, sub-figures a1, b1, c1). Flow paths of the particles released from the upstream segment (segment AC in Figure 3.1) of the meander at the same depth are shown in second row (sub-figures a2, b2, c2). The blue lines show the particle paths in [XY] plane. Vertical extent of flow paths with colored lines are also shown in [XZ] plane (row 3, sub-figure a3, b3, c3). The arrows show the direction of flow paths. The dotted line perpendicular to flow paths in the second row represents 10 h isochrones while the gray dots show the locations of deepest points of flow path.

flow paths are slightly curved. Whereas, in the scenario ω 115 flow paths at the meander neck are straight, however when moving away from the neck, the particles tend to follow curved path at either side of the meander neck. This is due to the presence of meander neck in the advanced stage of meander. The strongest head difference at neck area forces the particles to travel in straight lines. The head difference gradually decreases when moving away from the meander neck resulting in curvature of flow paths.

The 10 h isochrones clearly show that with increase in meander sinuosity, distance between isochrones increases. For example the isochrones in scenario ω 60 are densely spaced compared to the scenario ω 90 and ω 115, whereas they are gradually widening apart in ω 90 and ω 115 resulting in less number of isochrones in ω 115. Furthermore, isochrones in the scenarios ω 60 and ω 90 are straight lines except near the apex where they tend to slightly bend towards the downstream segment, indicating the relatively uniform flow velocities except near the apex region. In the scenario ω 115, as stated before, the head difference across the intra-meander area is substantially large compared to the rest of scenarios resulting in faster overall flow velocities. Moreover, scenario ω 115 exhibits different zones of flow velocities e.g. larger spacing between isochrones passing through meander neck indicates the quickest flow through the meander neck due to the strongest head difference. When moving away from the neck, the curvature of isochrones indicates slower flow in the apex area. The concentrated isochrones in the upper second half indicate slow flow velocities through those areas, caused by lower head difference. This formation of zones of high and low flow velocities in advanced stage meander (with neck feature) has also been reported in many previous studies (e.g., Boano et al., 2006, 2010).

3.3.1.3. Vertical Extent of Flow Paths

The flow trajectories in YZ plane for four sample flow paths (colored lines) are shown in the third row of the Figure 3.4 (a3, b3, c3). The locations of the deepest point of the flow path D_{max} are also marked as gray dots in XY-plane. Generally, it is expected that the particle released from upstream part of meander should ex-filtrate at downstream part of meander. However, from Figure 3.4 (a3, b3, c3), it is evident that not all of the stream particle exfiltrate in the stream at the downstream segment of the meander. The particles introduced in the upper portion (in the apex area) of the meanders in most of the scenarios do not exfiltrate in the stream at downstream part of meander, instead they continue to go deeper in the downward direction. As a result, their deepest point occurs beyond intra-meander zone. In the scenario ω 60 (Figure 3.4, a3) particles follow semicircular paths in vertical direction. Maximum penetration depth ranges from 0.62 to 0.74 m below streambed. In the scenario ω 90, the maximum penetrating depth ranges from 0.6 to 0.66 m, whereas for ω 115 the maximum penetration depth ranges from 0.55 m for the flow path passing through meander neck to 0.7 m for the flow path passing through apex region.

Generally, in scenarios without neck feature, the deepest point of flow paths for the particle ex-filtrating in the stream at downstream end, occur either at the center or just before the center of intra-meander zone. However as the length of flow path decreases, the location of the deepest point shifts slightly towards the downstream end, while for the flow paths passing near the apex, the deepest point occurs outside of meander. In all of the flow paths ex-filtrating in the stream, the penetrating depth is positively related to the length of flow path i.e. the longer the flow path, the deeper it penetrates, e.g. the longer flow paths in the Figure 3.4 (a2, a3, b2, b3) penetrate deeper.

In the scenario ω 115, maximum depth occurs after the center for the flow path passing through the neck region whereas for the rest of flow paths maximum depth occurs before the center of flow path. The shape of flow paths ex-filtrating in stream is semicircular but with shallower penetration. For example, the flow path passing through meander neck penetrate only up to 0.55 m below streambed.

The simulation results indicate that the flow path length and hydraulic gradient at various zones of the meander are controlling factors for the velocities, maximum penetration depth as well as ex-filtration points of the flow paths. For example, in flow paths that ex-filtrate at downstream, penetration depth is positively related to the 2D (XY-plane) length of flow path. Moreover, strong gradient results in shallower flow paths and shorter residence time (e.g. in meander neck area). Furthermore, we found that there is a certain threshold hydraulic gradient value required for the flow path to exfiltrate at the downstream end. This threshold hydraulic gradient for meander scenario ω 60 and ω 90 was observed as 0.014, whereas for ω 115 it was 0.018. We found that if the hydraulic gradient at a meander location is lower than threshold value, the particle will not exfiltrate in downstream end of the stream.

3.3.2. Intra-Meander Residence Time Distribution

Residence time distributions of the particles released from the upstream segment of the selected scenarios are shown in Figure 3.5. The mean residence times (MRTs) vary from 18.5 days for an advanced stage meander to 60.4 days for an initial stage meander indicating a tendency of decreasing MRTs with increasing sinuosity. The histograms for scenarios $\omega \leq 60°$ (Figure 3.5 [a-d]) have wide base and shorter frequency range, indicating longer and more spatially scattered residence times. For the scenarios ω 75 to ω 100 (Figure 3.5 [e-i]), residence time histograms have considerably higher frequencies in the bin widths around the median value,

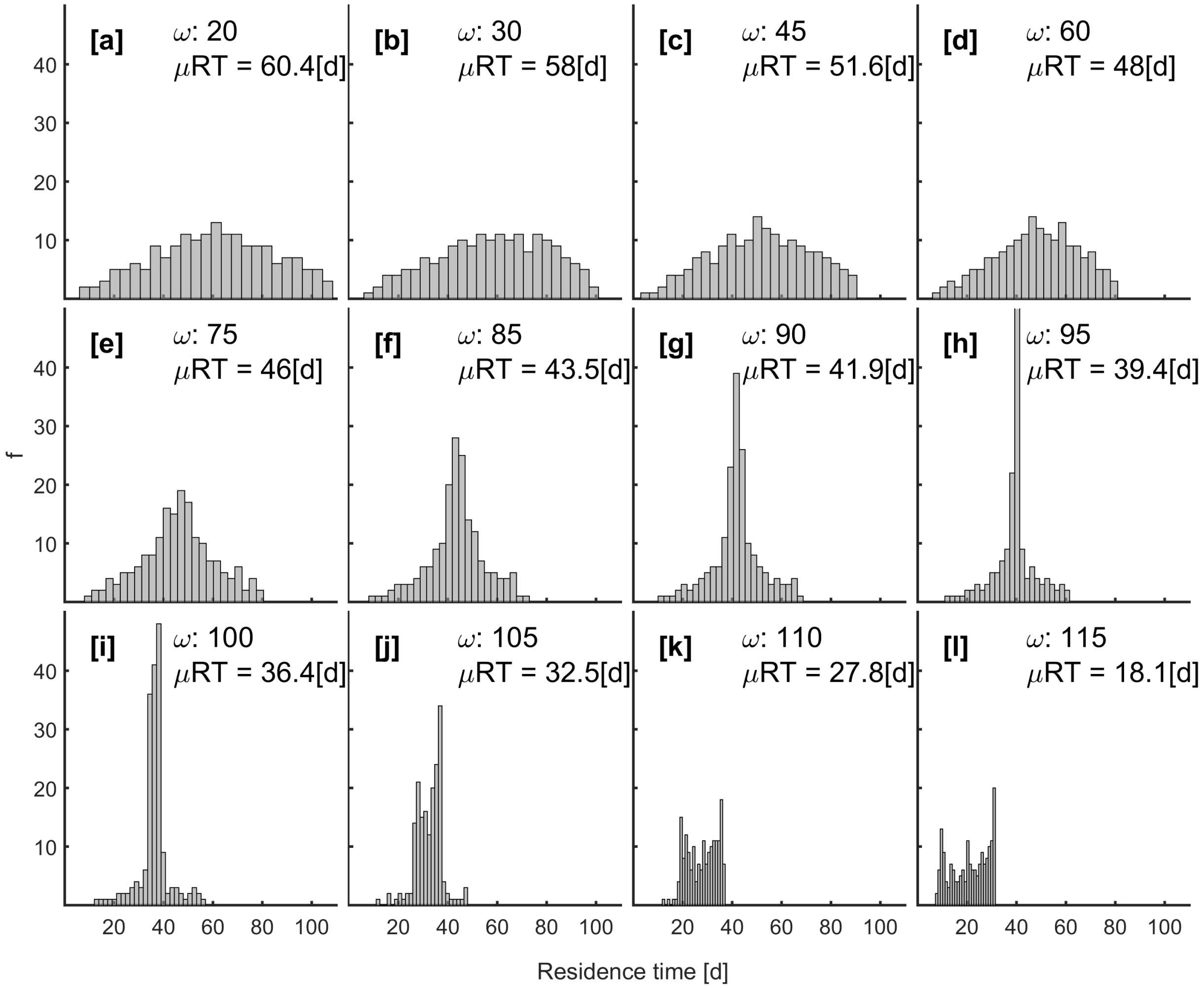

Figure 3.5: Residence time distributions (obtained through forward advective particle tracking) of the particle released from upstream segment of the meander for initial stage (a - d), middle stage (e - i) and advanced stage (j - l) meander scenarios.

indicating that most of the intra-meander residence times have similar value. The scenarios ω 105 to ω 115 in the Figure 3.5 [j-l] exhibit two peaks, before and after the median value. Hence the residence time distributions exhibit different characteristics depending on type of meander. The initial stage meandering scenarios i.e. $\omega \leq 60°$, have longer base with relatively shorter frequency range, the middle stage meandering scenario i.e. $\omega \geq 60°$ and $\leq 100°$ indicate more uniform residence times whereas advanced stage meander scenario i.e. $\omega \geq 100°$ exhibit bi-modal distribution.

In the middle stage scenarios, length of intra-meander flow paths are nearly similar in the major portion of the intra-meander area due to uniform distance between the opposite sides of meander for the major portion of the intra-meander area. Keeping in view the results from previous section (3.3.1) uniform flow paths generate uniform residence times, which is evident from histogram as well (Figure 3.5). In early stage scenarios, with narrow apex area and longer wavelength (λ),

ω	μ	σ	σ^2	Skewness	Kurtosis	Excess	Q1	Median	Q3
15	64.6	25.1	629.7	-0.1	2.3	-0.7	43.7	60.5	81.5
20	60.4	23.8	568.5	-0.1	2.3	-0.7	40.9	57.3	73.7
25	59.9	23.3	540.8	-0.2	2.2	-0.8	38.3	57.3	76.3
30	58	22.1	489.7	-0.2	2.2	-0.8	38.3	57.3	72.5
35	54.7	20.8	434.6	-0.2	2.3	-0.7	36.6	51	65.4
40	53.5	21	440.7	-0.1	2.2	-0.8	35.8	49.8	67.3
45	51.6	19.8	392.3	-0.1	2.2	-0.8	32.8	46.8	64.3
50	51.2	19.2	368.8	-0.1	2.2	-0.8	34.1	47.3	63.8
55	50.1	18.2	329.9	-0.1	2.4	-0.6	34.1	47.3	60.5
60	48	16.7	278.9	-0.2	2.4	-0.6	34.5	46.5	58.5
65	47.8	16.4	267.4	-0.2	2.5	-0.5	34.5	43.5	55.5
70	47	15.1	227.6	-0.1	2.7	-0.3	35.6	44.3	53
75	46	14.7	215.1	-0.1	2.8	-0.2	35.6	44.3	53
80	44.7	12.9	165.8	-0.2	3	0	36.4	41.8	49.9
85	43.5	11.3	128.7	-0.3	3.6	0.6	35.3	40.5	45.7
90	41.9	10	99.9	-0.1	4	1	37	39.4	44.1
95	39.4	7.9	62.7	-0.4	5.1	2.1	36.3	38.3	38.3
100	36.4	6.3	39.2	-0.3	6.5	3.5	32.7	34.5	36.3
105	32.5	5.4	28.9	-0.4	4.6	1.6	26.5	32.5	35.4
110	27.8	6.1	36.7	-0.2	1.8	-1.2	21.4	27.5	32.6
115	18.1	14	196.2	0.4	1.6	-1.4	3.8	11.5	30
120	14.7	9	80.4	-0.2	1.7	-1.3	5	15	21.6

Table 3.4: Parameters of fitted probability density functions (pdf) to the residence time distributions for meander shape scenarios.

flow paths in the lower portion are longer whereas they tend to be shorter towards apex. This results in wider base and shorter frequency range in histograms. Advanced stage meanders are characterized by the strong head difference at the neck area, which causes a lot of particle pass quickly through meander neck area, whereas another set of particles passing through meander apex with relatively smaller hydraulic gradient. Bi-modal histograms of residence times for advanced stage meander indicate two set of residence times corresponding to the dominant flow zones.

Cumulative density functions (CDF) and fitted probability density functions (PDF) of the residence times distribution of the meander scenarios are presented in Figure 3.6. From the histograms shown in Figure 3.5, it is evident that except advanced stage meanders, residence times for the rest of the scenarios follow a Gaussian distribution, therefore we fitted Gaussian functions (except advanced stage meanders) to the residence time for more clear interpretation. The probability density function (pdf) for residence times of the initial stage meanders i.e. $\omega \leq 60^\circ$ are flatter with longer base (green curves in Figure 3.6 (b)). For middle stage meanders, peaks of pdf's are increasing and base is shrinking. The detailed parameters of the fitted pdf functions are given in the table 3.4. Generally, the mean (µ), median, and variance (σ) show a decreasing trend with increasing sinuosity. Similarly , the CDF function of the residence time distribution shows that the slope of CDF function is increasing with increasing sinuosity, i.e. the CDF's of initial stage meander have relatively flatter slopes, while the CDF's of advanced stage meanders exhibit the steeper slopes.

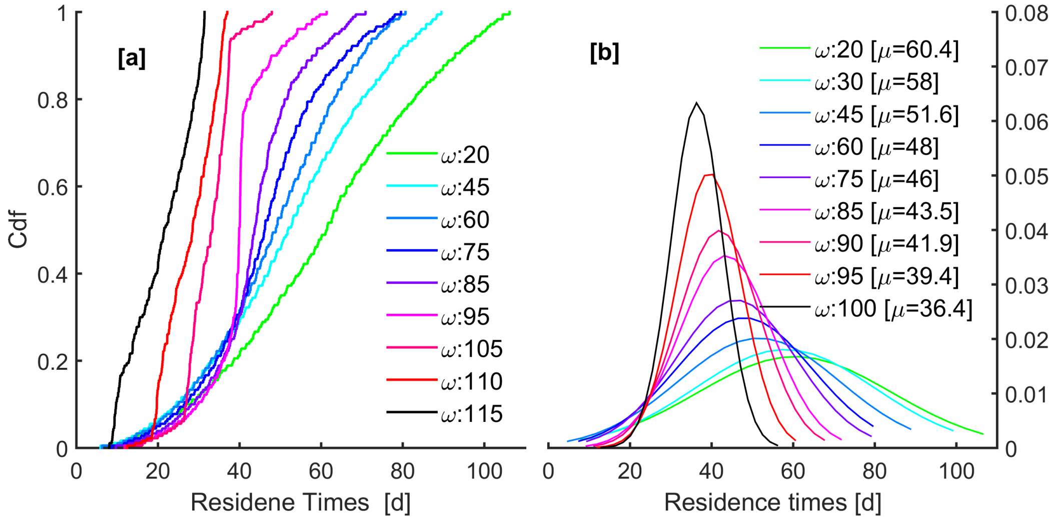

Figure 3.6: (a) Cumulative distribution functions (CDF) for selected scenarios (early, middle and advanced stage meanders). (b) Probability distribution functions (PDF) of the residence times for early and middle stage meander scenarios.

3.3.3. Factors Affecting Intra-Meander Flow and Residence Times

As discussed in previous section (3.3.1), changes in meander geometry affect flow characteristics such as flow trajectories and velocities within the intra-meander region. The length and maximum depth of flow path define the hyporheic exchange extent in horizontal and vertical direction. Residence time is also an important metric since it controls the time of contact between surface water and intra-meander solute species, thus controlling the fate of chemical reactions within the zone. In this section, we evaluate the influence of meander sinuosity and intra-meander area on intra-meander residence times and vertical extent of intra-meander flow paths.

3.3.3.1. Intra-Meander Hydraulic Gradient

Intra-meander hydraulic gradient is generated by the head difference along the inner bank of meander due to the decrease in head gradient along the meander length (L). This head difference varies with the change in the shape of meander. The average hydraulic gradient across all meanders has been compared against the meander shape scenarios (ω) in Figure 3.7 (a). The hydraulic gradient is increasing with increasing sinuosity. For the initial stage meanders i.e. $\omega \leq 60°$, the hydraulic gradient increases from 0.012 to 0.015 whereas for the middle stage meanders i.e. meander with $\omega \geq 60°$ and $\leq 95°$ the hydraulic gradient range is between 0.015 and 0.02. The most steep gradient increase occurs in advanced stage meanders ($\omega \geq 95°$) where the gradient ranges from 0.02 to 0.038.

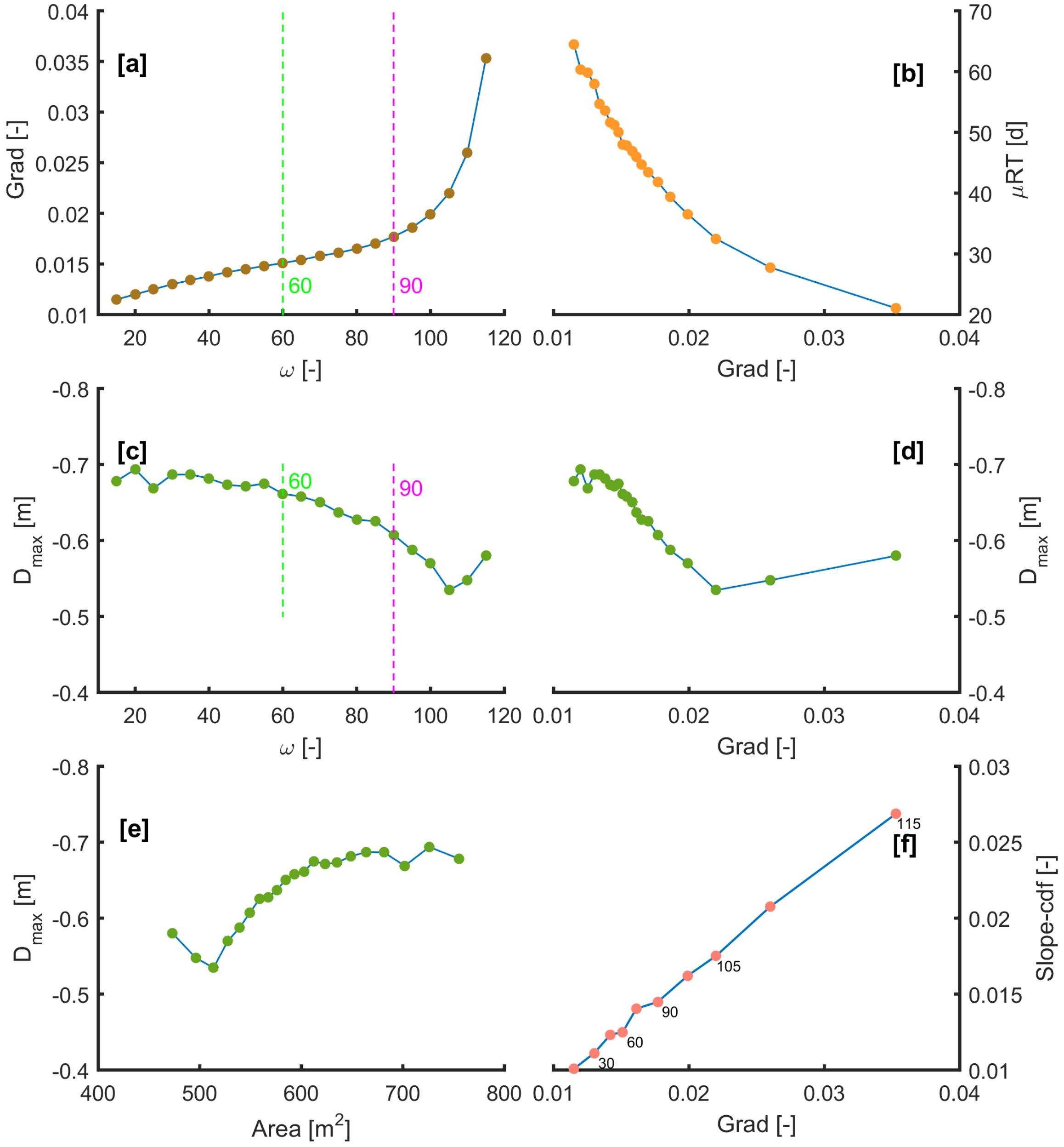

Figure 3.7: Effect of meander sinuosity ($\omega[-]$), intra-meander area ($A[m^2]$) and hydraulic gradient ($Grad[-]$), on mean intra-meander residence times ($\mu RT[d]$) and maximum depth of flow paths ($D_{max}[m]$).

Until the middle stage meander scenarios, the hydraulic gradient is increasing linearly at nearly constant rate. The steep gradient for advanced stage meander scenarios is due to the formation of neck where the largest head difference occurs at the smallest distance across inner banks of meander. These findings are in line with previous studies of intra-meander flow (e.g., Boano et al., 2006; Revelli et al., 2008).

Mean residence times (µRT) for all of the scenarios are plotted against the hydraulic gradient in Figure 3.7 (b). Clearly µRT are decreasing with increasing hydraulic gradient. The graph of µRT and intra-meander hydraulic gradient (grad) shows that µRT decreases exponentially with increasing intra-meander hydraulic gradient (grad). Furthermore, the average slope of residence times obtained from CDF (see Figure 3.6) are also plotted against the hydraulic gradient (see Figure 3.7 (f)) which shows a linear relationship. The increase in CDF slope represents the decrease in mean residence times (µRT).

3.3.3.2. Maximum Penetration Depth

The observed range of maximum penetration depth of the flow paths (D_{max}) varies from - 0.55 to - 0.7 meters below the bed level of the stream. Hence changes in geometry of meanders have no significant influence on the vertical extent of intra-meander flow paths. However, a comparison of average maximum penetration depth of the flow paths (D_{max}) with meander sinuosity shows that D_{max} is decreasing with increasing sinuosity (Figure 3.7 [*c*]) except for the advanced stage meanders. This is further confirmed in Figure 3.7 [*d*], where D_{max} shows a quick drop with increasing hydraulic gradient for grad ≤ 0.22, except for the hydraulic gradients of advanced stage menders. However, D_{max} shows an increasing trend with increasing intra-meander area (A) (Figure 3.7 [*e*]), except for the area (A) corresponding to advanced stage meanders. It means D_{max} is positively related to the length of intra-meander flow paths, whereas it is negatively related to the increasing sinuosity of the meander.

3.3.3.3. Meander Sinuosity

Figure 3.8 shows a general decrease in µRT with increasing sinuosity. In the primary stage meanders, i.e. $\omega \leq 60$, the slope of decreasing curve is small whereas for middle and advanced stage meanders, i.e. $\omega \geq 80$, the slope is relatively steeper. It implies that for primary stage meanders, there is a little influence of stream geometry on the average hydraulic gradient while in higher stages this effect becomes pronounced. The relatively low influence of meander geometry in early stage meanders is due to the fact that there is no substantial change in the shape of meander in early stage scenarios. Hence a very small increase in average hydraulic gradient is observed in scenarios $\omega \leq 60$. However, a gradual increase in the average hydraulic gradient is observed with increasing sinuosity (Figure 3.7 [a]), which results a gradual decrease in µRT. In advanced stage meanders characterized by the presence of neck, zones of strong and weak hydraulic gradient are formed as discussed in section (3.3.2) leading to a sharp decrease in µRT.

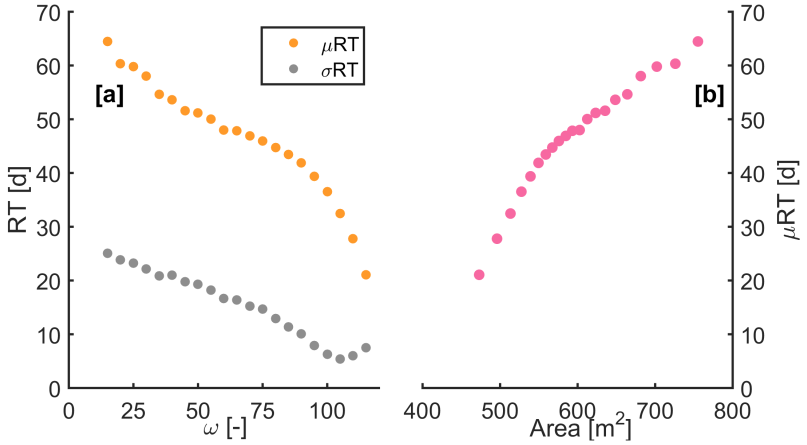

Figure 3.8: Effect of meander sinuosity ($\omega[-]$) and intra-meander area ($A[m^2]$) on intra-meander residence times ($\mu RT[d]$). Figure (a) shows relation between meander sinuosity ($\omega[-]$) and mean residence times ($\mu RT[d]$), Figure (b) shows relation between intra-meander area ($A[m^2]$) and mean residence time ($\mu RT[d]$).

3.3.3.4. Intra-Meander Area (A)

Besides meander sinuosity, another important metric for hyporheic flow exchange is the distance covered by intra-meander hyporheic flow paths. The µRTis plotted against intra-meander area (A) for various meander shape scenarios (ω) in the Figure 3.8 [b]. It is clear that regardless of the shape of meander, the mean residence time increases with increasing intra-meander area. For the given set of hydraulic parameters in table 3.3 the µRT increases from 20.4 days for intra-meander area 480 m^2 to 65 days for intra-meander area of 780 m^2. This is the simple yet useful finding that µRT is positively related to intra-meander area (A).

3.3.4. Influence of Discharge Event on Intra-Meander Flow and Solute Transport

In the previous section, we examined the influence of meander shape on intra-meander flow paths and residence times under steady conditions. The steady state simulations are helpful for predicting general behaviour of intra-meander hyporheic flow paths and their residence times as well as parameter sensitivities. However, intra-meander flow field is often altered by variable hydrologic conditions such as stream discharge events. These variable hydrologic conditions induce changes in the intra-meander flow fields which in turn may affect the water and chemical exchange processes. For example, during a discharge event, stream stage may rise substantially, increasing the intra-meander flow. As a result, the intra-meander water table may rise to the non-submerged portion, providing an opportunity to mobilize the solute residing therein, which was not in contact with groundwater at pre-event conditions.

Influence of stream discharge events on solute mobilization and consequent transport from the stream bank has been explored in chapter 2 under varying peak and duration scenarios. In this section, we evaluate the response of various meander shapes on mobilization and conservative transport of the solute residing in the previously unsaturated portion of intra-meander region during a stream discharge event. For this purpose, intra-meander flow and solute mobilization induced by a stream discharge event are simulated for three representative meander shape scenarios i.e. ω 60, ω 90 and ω 115. A layer of DOC source (CH_2O) with uniform concentration of 100 mg/L and constant thickness of 1 m is applied in the non-submerged unsaturated portion (top layers) of intra-meander zone. The stream discharge event of 120 h duration and bank full height was simulated using HEC-RAS 4.1.1. The simulated free surface heads were applied as time variable top boundary conditions to the stream cells in groundwater model.

3.3.4.1. Spatial Distribution of Groundwater Head and Solute Concentration

In the Figure 3.9, [XY] cross sections at a depth 0.75 m below the surface (row1, row2) and [XZ] cross section at Y = 20 m (marked in dotted white line in [XY] section) show intra-meander groundwater head distribution and solute concentration for scenario ω 60 at various stages of the stream flow event.

Prior to the start of flow event, the solute concentration is uniform throughout the intra-meander region because the solute lies within the unsaturated portion, which is not in contact with the steady state water table. On the commencement of the discharge event, groundwater rises near the stream at the upstream section of the meander (Figure 3.9, row 1, rising limb).

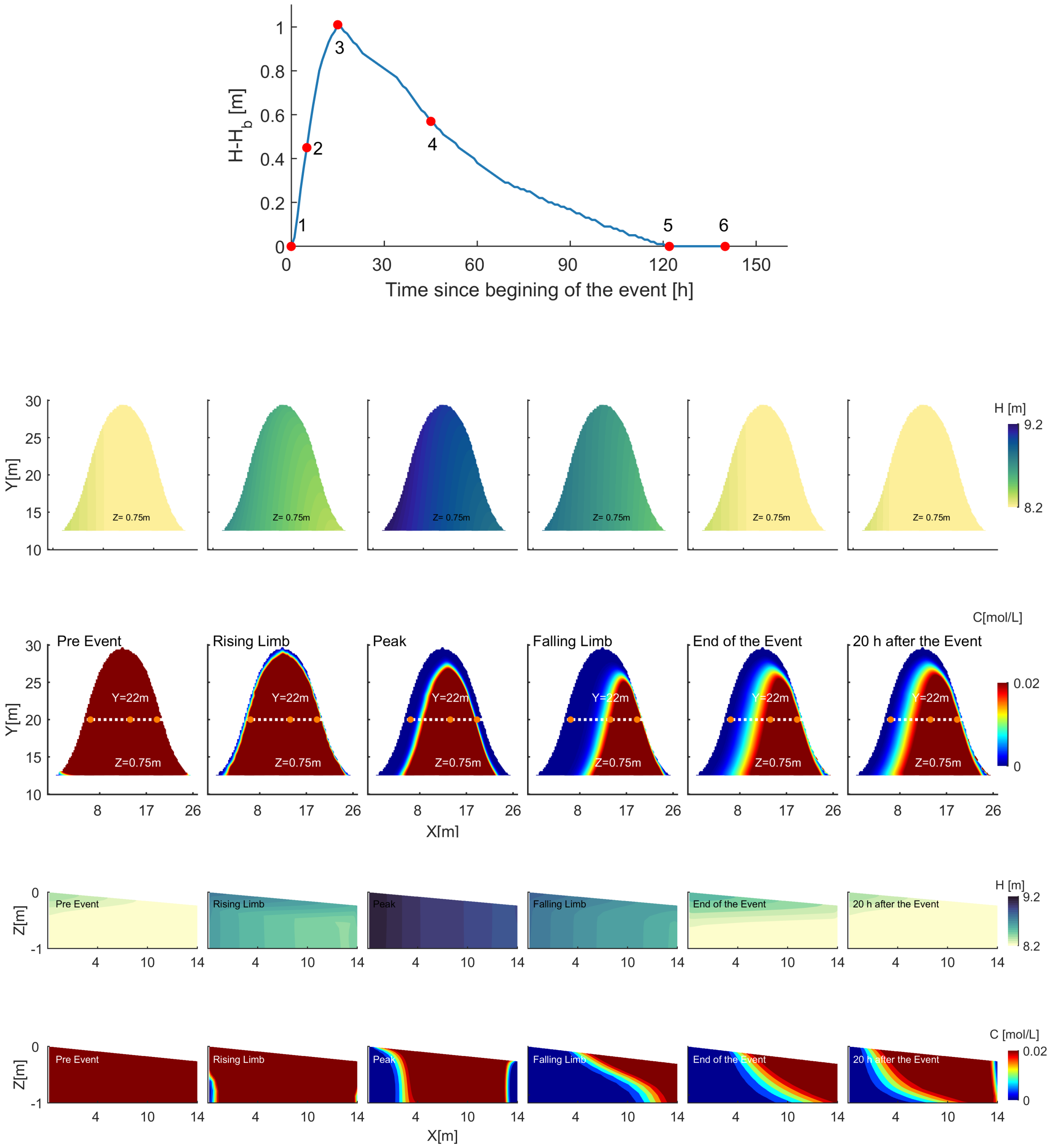

Figure 3.9: Influence of discharge event on intra-meander flow and solute mobilization (scenario ω 60). Horizontal [XY] cross sections show groundwater head distribution (row 1) and solute mobilization (row 2) at a depth of 0.75 m below surface. The vertical [XZ] section of groundwater heads (row 3) and solute mobilization (row 4) are also shown at Y = 20 m (indicated by white lines in [XY] section (row 2)).

Increase in groundwater level results in the water infiltration into the unsaturated zone, mobilizing the solute mass towards the downstream section. At the XZ section, it can be seen that on the rising limb, the mobilization of solute from the upstream side has already started towards downstream section (Figure 3.9, rows 2 & 4, rising limb). At peak stream flow, groundwater heads rise to the maximum level. As a result, a large portion of solute from the upstream half of intra-meander area has been mobilized and transported towards the downstream end of the meander. The XZ section (Figure 3.9, rows 2 & 4, peak) indicates that first 4 m length of the section is free from solute until the peak of flow event i.e. solute has been mobilized and transported towards downstream end of the meander. On the falling limb, the groundwater levels are receding, while the first 9 m of the XZ section is free of solute, i.e. more than half of the solute has been transported to the stream by now. On the downstream half of the meander section, there is still high solute concentration because the groundwater has not tapped into the solute layer in this region. At the end of the stream flow event, the groundwater level falls back to the pre-event level (Figure 3.9, rows 1 & 3, end of the flow event). The amount of solute remains nearly the same as it was at falling limb, but due to the slow water drainage, the solute is moving vertically downward with water. This results in downward spread of solute front. To confirm this behaviour, we also observed the groundwater heads and solute mobilization 20 h after the end of flow event. 20 h after the end of flow event, when the groundwater table is back to the pre-event conditions, the solute concentration area has increased when compared to the time at end of the flow event (Figure 3.9, row 4, 20 h after the flow event). This confirms the slow movement of solute under the effect of gravity, i.e. water moves vertically downward initially under gravity and then towards right (towards downstream) under the influence of intra-meander hydraulic gradient.

Flow and solute mobilization for the scenario ω 90 responded similar to the scenario ω 60. The solute mobilization begins at the upstream section (XZ view) with the increase in groundwater heads on the rising limb of the hydrograph (Figure 3.10, rising limb). At the rising limb, the first 5 m of the domain at XZ section is free from solute. At the peak flow, nearly half of the solute has already been transported towards the downstream end of meander. On the falling limb, first 10 m of the domain are free from solute (Figure 3.10, falling limb) i.e. major portion of solute has been transported to the stream. At the end of the flow event, the concentration area is once again expanding due to the downward movement of solute with water from upper unsaturated zone as described for the scenario ω 60. The increase in the solute area at [XY] section (see 3.10, falling limb) is due to movement of solute from the areas higher than the cross section level which is located 0.75 m below the surface. 20 h after the end of flow event, this trend is still observable due to the post-event slow water drainage from the unsaturated zone.

Flow head distribution and resulting solute mobilization behave in similar way for both ω 60 and ω 90, however in ω 90 substantially larger portion of solute has been transported as compared to the ω 60 during the flow event.

Figure 3.11 presents groundwater head distribution and solute concentration for scenario ω 115. As found in the steady state analysis (section 3.3.1), the sharpest hydraulic gradient is formed in the neck region for advanced stage meanders

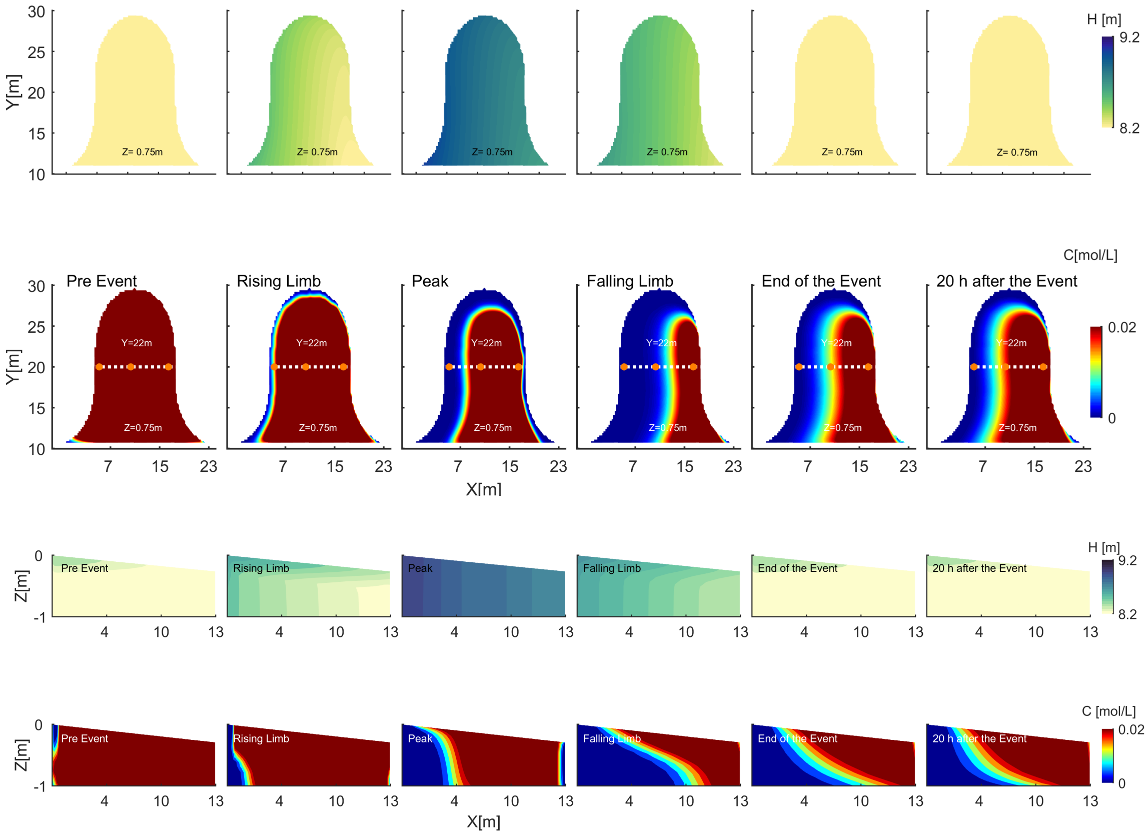

Figure 3.10: Influence of discharge event on intra-meander flow and solute mobilization (scenario ω 90). Horizontal [XY] cross sections show groundwater head distribution (row 1) and solute mobilization (row 2) at a depth of 0.75 m below surface. The vertical [XZ] section of groundwater heads (row 3) and solute mobilization (row 4) are also shown at Y = 20 m (indicated by white lines in row 2).

leading to quick flow through this area. On the rising limb of the flow event, faster flow through the meander neck leads to quick transport through the meander neck area. As a result, until peak flow, all the solute near the meander neck area is transported to the stream towards the downstream end of meander (Figure 3.11, row2). The flow velocities at the lower end (below neck) and in the apex area are considerably smaller compared with the velocities at the meander neck resulting in relatively slower solute mobilization and transport through these regions. That´s why until the peak flow, intra-meander area at the meander neck is free of the solute. Overall, a large portion of the solute has been transported into stream, i.e. complete transport from the areas near the meander neck. Similarly at the location of XZ section, almost two third portion is free from solute. At the falling limb of stream event, most of the intra-meander area is free from solute. The XZ section (Figure 3.11, row 4, falling limb), shows that the solute from entire section has been transported to the stream except a small area to top right corner. Similarly [XY] section is free from solute in the major portion of intra-meander region.

After the falling limb, remaining solute begins to move downward from the unsaturated zone with water, resulting in increase of the solute area both horizontally [XY section] and vertically [XZ section]. 20 h after the end of the event, the concentration area of the solute has substantially increased due to the slow downward movement of solute with downward moving water. Overall, the solute transport is quicker through scenario ω 115 as compared to ω 60 and ω 90 due to the higher mean velocities induced by strong hydraulic gradient.

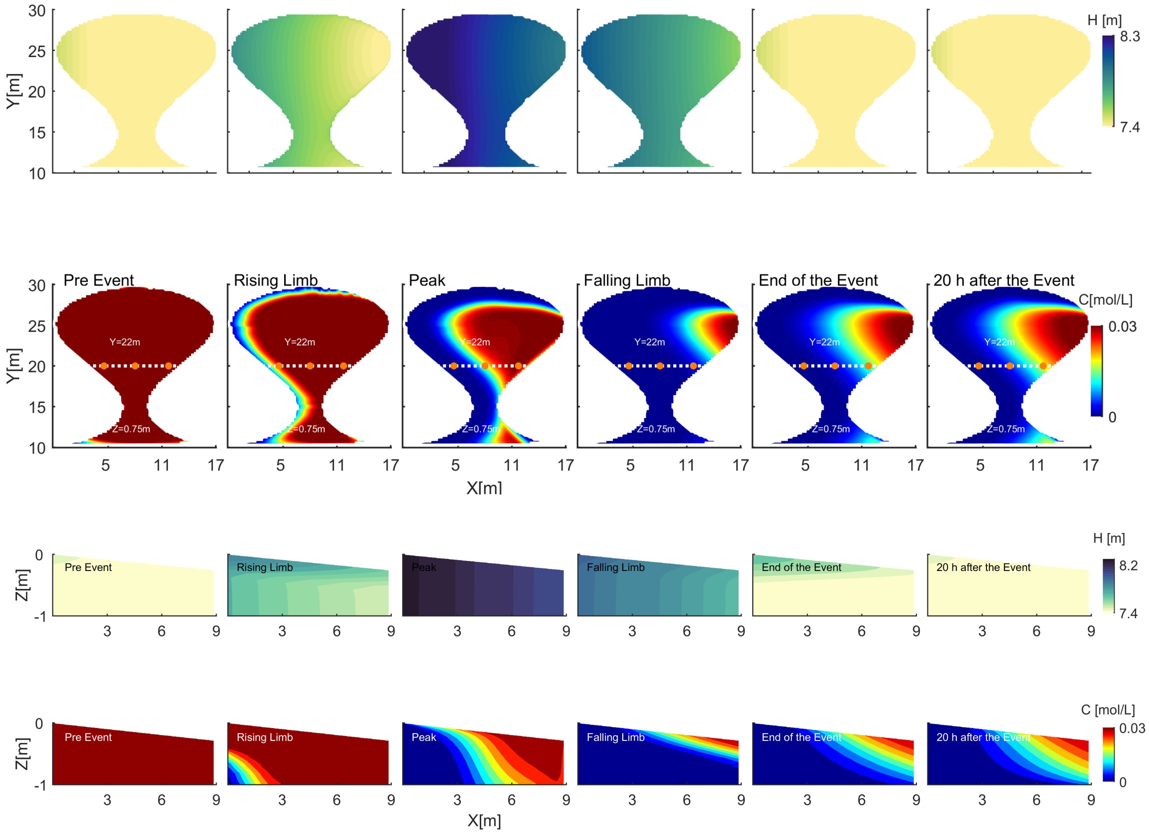

Figure 3.11: Influence of discharge event on intra-meander flow and solute mobilization (scenario ω 115). Horizontal [XY] cross sections show groundwater head distribution (row 1) and solute mobilization (row 2) at a depth of 0.75 m below surface. The vertical [XZ] section of groundwater heads (row 3) and solute mobilization (row 4) are also shown at Y = 20 m (indicated by white lines in row 2).

3.3.4.2. Time Scales of Intra-Meander Groundwater Heads and Solute Transport

Figure 3.12 presents stream water stage above the base flow at the starting point of meander (row 1), groundwater heads rise during the flow event (row 2) and resulting changes in solute concentration (row 3) at three locations shown as orange dot in the Figures 3.9, 3.10 and 3.11. The observation points are located below the solute layer within the saturated zone (at the level of streambed). For ease, we denote observation point near the upsteam section as left (L), near the middle of the intra-meander area as middle (M) and near the downstream section as right (R).

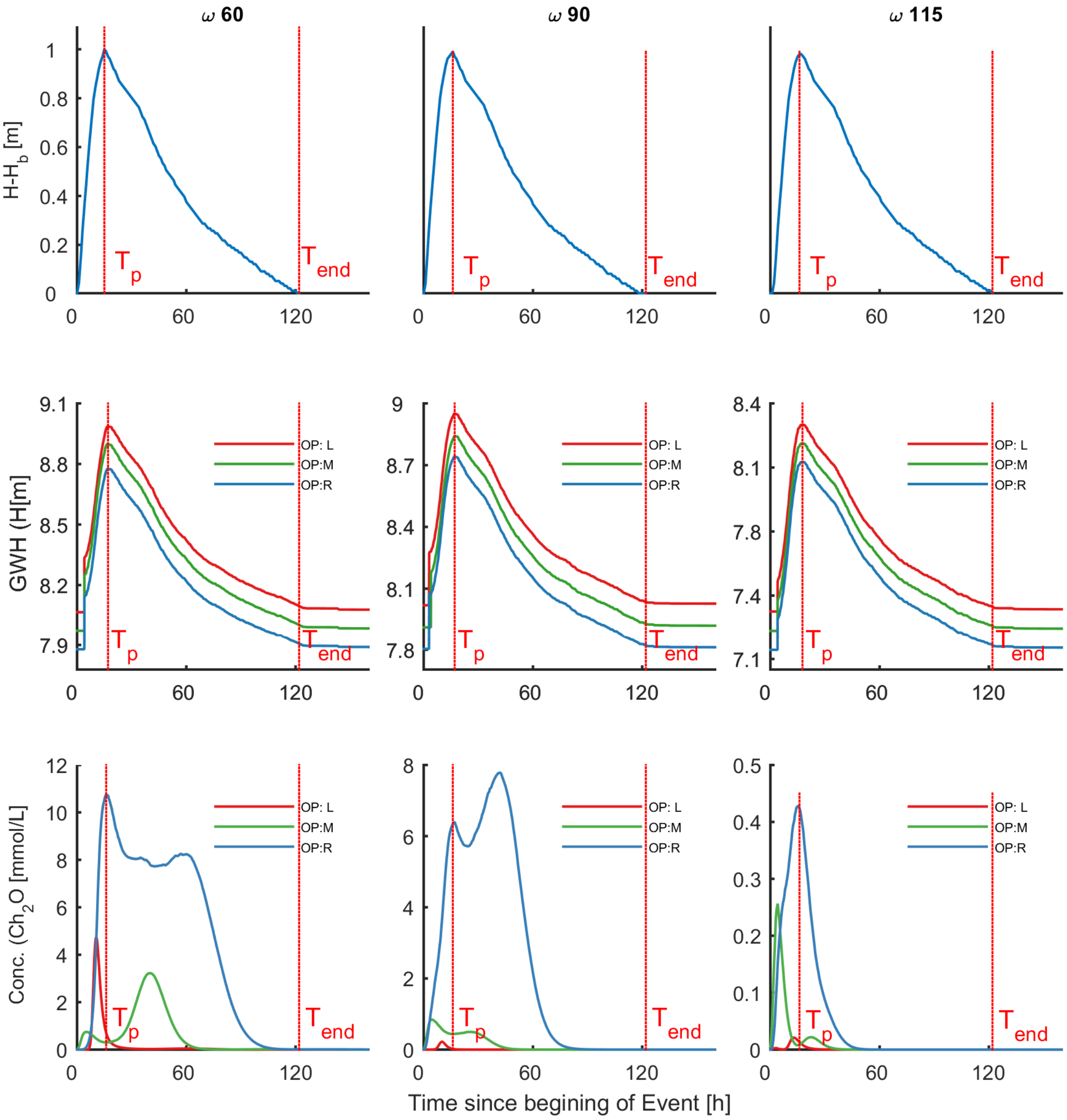

Figure 3.12: Stream stage above base flow $[H - H_b]$ at the upstream end of the meander (row 1), groundwater heads (row 2) $[GWH]$ and solute concentration $[Conc.]$ (row 3) at three locations marked as dots in in Figures 3.9, 3.10 and 3.11 for scenarios ω 60, ω 90 and ω 115 . The letters 'L', 'M' and 'R' represent the location of left, middle and right observation point along the XZ cross section.

The stream stage rises around 1 m in 16 h of the flow event above base flow level for the scenarios ω 60, ω 90 and ω 115. The stream stage falls back to the pre-event level after 120 h of the flow event. Groundwater heads start rising with increasing stream stage. Groundwater rise above the normal water table is in the range of 0.8 to 0.9 m for ω 60, 0.9 m for ω 90 and 1 m for the ω 115. Groundwater heads in all three points rise quickly i.e. peak timing coincides for all observation points 'L', 'M' and 'R' in all three shape scenarios (i.e. 16 h after the beginning of the event). Similarly, groundwater heads fall back to the pre-event level at the end of the flow event for all scenarios. The height in water level raised according to the location of observation point, i.e. peak height at observation point 'L' is the highest, whereas in observation point 'R', the lowest peak height is observed. This is partially due to the pre-existing hydraulic gradient across the opposite end of meander and partially due to the head loss with the distance from the upstream section.

In all three scenarios solute concentration were raised during the flow event. The largest solute concentration increase has been observed at the observation point 'R' (observation point nearest to the downstream section). For scenario ω 60, solute concentration at the observation point 'L' raised to the the peak level of 4.7 [mmol/L] well before the peak of groundwater head (GWH) ($\sim$ 7 h before the peak GWH at the point). A quick decline in concentration is observed after the peak and the concentration falls back to pre-event level in 22 h of the beginning of the flow event. This is because of the fact that the near stream solute mass mobilization starts immediately with rise in the stream stage increasing the solute concentration adjacent to stream-riparian interface. At the observation point 'M' solute peak raised to 3.22 [mmol/L] after $\sim$ 25 h of the GWH peak. At the observation point 'R' , the concentration peak rises to 10.72 [mmol/L] at the GWH peak. At 'R', the solute concentration falls back to the pre-event value after 125 h of the beginning of flow event.

The scenarios ω 90 and ω 115 show similar trends i.e. concentration falls back to the pre-event value quickly after the peak GWH at the point 'L', whereas at the point 'M' and 'R', the concentration falls back to pre-event value a long time after the peak GWH. Similarly, the highest concentration peaks are observed at observation point 'R' (Figure 3.12) for scenarios ω 90 and ω 115. However, both peak and duration of raised concentration show a decreasing trend with increasing sinuosity. For example, in scenario ω 90, the rise in concentration at observation point 'R' remains for shorter duration compared to the scenario ω 60 i.e. concentration falls back to the pre-event level after 66 h of the beginning of the flow event while in scenario ω 115 concentration falls back to prevent value after 56 h of the beginning of flow event. Similarly, substantially lower peak concentrations of 7.95 and 0.43 [mmol/L] are observed for scenarios ω 90 and ω 115 respectively.

Higher concentrations at the downstream observation points are due to the reason that water reaching these locations already carries the solute mass mobilized from the upstream locations leading to higher concentration peaks at the observation point 'R' for all three scenarios. Furthermore, for scenarios ω 60 and ω 90 at location 'R', concentration curves show two peaks. This is because of the fact that observation point ‘R’ in these scenarios, is located close to stream at the downstream (gaining) segment of the meander. In the beginning of the flow event, local hydraulic gradient is temporarily reversed near the observation point ‘R’ due to stream water entry into the intra-meander area from the right side boundary (similar to bank flow). As a result, initially solute mobilizes from right to left for a short period of time rising the concentration at ‘R’. Hence, first peak at ‘R’ in both ω 60 and ω 90 is caused by the right to left movement of solute due to temporary reversal of the local hydraulic gradient. It can be seen in Figures 3.9, 3.10 (R2, peak) as well, that solute has moved beyond ‘R’ (towards left). Later, the hydraulic gradient reverses back to initial conditions and the rightward movement of solute begins under the influence of discharge event, generating second peak followed by a decline in concentration. However, in the scenario ω 115, observation point ‘R’ is located near the neck area where faster intra-meander flow does not allow a temporary reversal of hydraulic gradient and therefore only single concentration peak is observed.

3.3.4.3. Solute Export during Stream Discharge Event

In this section, the total solute mass export during the flow event has been compared for all three representative scenarios. A uniform solute concentration layer has been applied as initial condition in the upper 1 m of intra-meander zone where saturation varies depending on the distance from groundwater table. Therefore actual solute mass for each cell in the unsaturated zone can be calculated as follow:

$$M_{abs} = V.C.S_w.n \tag{3.4}$$

where M_{abs} $[M]$ is the actual mass, $V[L^3]$, is the volume of the individual cell, $C[M/L^3]$, is the mass concentration, $S_w[-]$ is the water content and $n[-]$ is the effective porosity of the cell. The sum of the actual mass of all the cells in the intra-meander zone provides the total solute mass within the intra-meander zone. In this way actual solute mass at all time steps was calculated for scenarios ω 60, ω 90 and ω115.

Figure 3.13 presents the cumulative conservative solute export from the intra-meander region of scenarios ω 60, ω 90 and ω 115 during the stream discharge event. For scenarios ω 60, ω 90, although solute mass begins to mobilize with the beginning of flow event (see Figures 3.9, 3.10), solute export to the stream starts after the peak of stream stage (Figure 3.13). For scenario ω 60, solute export starts after 11 h of the peak discharge and for the scenario ω 90, the solute export starts earlier i.e. after 6 h of the peak discharge. After the peak flow, solute mass exports relatively quickly for both scenarios. Until the end of the flow event i.e. 100 h after the peak flow, solute mass remaining within the intra-meander zone reduces to 12.5 and 10 % respectively for the scenario ω 60 and scenario ω 90. After the flow event,

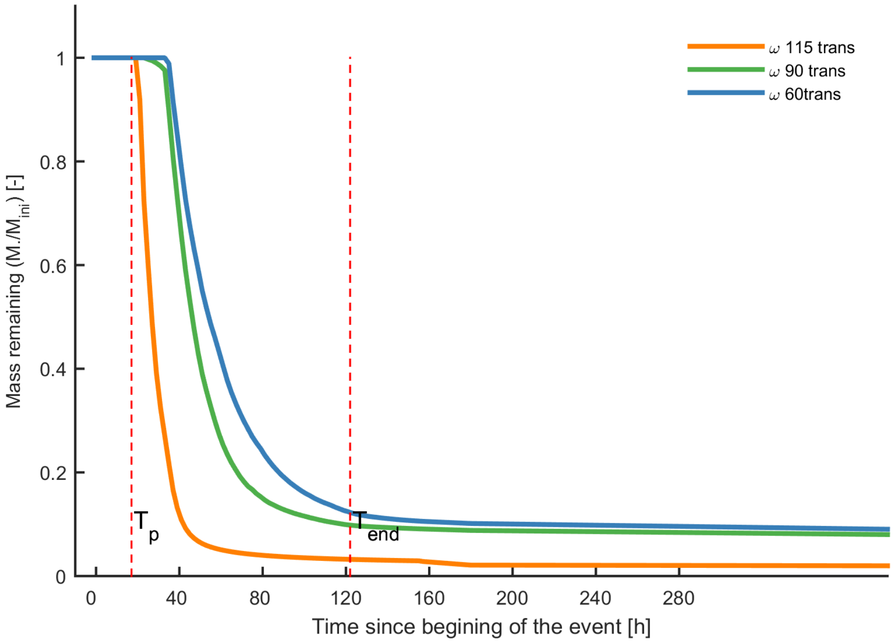

Figure 3.13: Conservative solute exported to stream during the flow event for three meander shape scenarios i.e. ω 60, ω 90, ω 115. T_p and T_{end} indicate the peak and the ending time of the flow event respectively.

solute mass export stops because the groundwater level fall back to pre-event conditions i.e. groundwater is no more in contact with the solute layer. For the scenario ω 115, solute mass export starts at the peak flow i.e. earlier than ω 90. The solute mass remaining reduces quickly to 9 % in 30 h after the peak flow whereas at the end of flow event, solute mass remaining in the intra-meander zone reduces to 3 %. Similar to scenario ω 60 and ω 90, the solute exports stops after the flow event.

The solute export through scenario ω 115 is earlier and quicker than for ω 60 and ω 90. This is because of the presence of neck in the scenario ω 115, which exhibits a very strong hydraulic gradient, resulting in earlier and greater export of solute mass through meander neck. In case of ω 60 and 90, the scenarios without meander neck, solute front is mobilized almost uniformly throughout the length of upstream section of meander, leading to delayed solute mass export (see Figures 3.9, 3.10). Average intra-meander hydraulic gradient in the scenario ω 90 is slightly greater than in ω 60, therefore the total solute mass exported from the intra-meander zone in scenario ω 90 is proportionally greater i.e. 90 % as compared 87.5 % at the end of the flow event, whereas in the scenario ω 115, almost 97 % of solute is exported during the flow event.

Hence substantial amount of solute can be transported from intra-meander region during a flow event. The meander geometry induced hydraulic gradient has a major influence on the transport of solute mass residing within the intra-meander zone.

Especially, the meander scenarios with neck feature are more efficient in solute export.

3.3.5. Intra-Meander Reactive Transport during Stream Discharge Event

The previous section addressed conservative DOC transport during a flow event. In this section, DOC removal and transport during the flow event is analyzed by simulating the aerobic respiration (AR) and denitrification (DEN) within the intra-meander zone.

3.3.5.1. Impact of Stream Discharge on Aerobic Respiration and Denitrification

According to the chemical scenarios described in the section 3.2.4 stream water is enriched with oxygen (O_2) whereas groundwater is free from O_2. Nitrate are introduced in both stream ($S-NO_3^-$) as well as in groundwater ($G-NO_3^-$). Figure 3.14 compares conservative and reactive intra-meander transport of the solute (CH_2O) during stream discharge event. XZ sections (at Y = 20 m) of the intra-meander area showing solute (CH_2O) concentration at various stages of stream discharge event are plotted for meander scenario ω 60, ω 90 and ω 115. Row 1 and 2 represent the solute concentration distribution for conservative and reactive transport scenarios while row 3 and 4 show concentration of oxygen (O_2) and surface nitrate ($S-NO_3^-$) in the intra-meander area respectively. The XY sections (at Z = 0.75 m below surface) for meander scenario ω 60, ω 90 and ω 115 are shown in the appendices 3.1A-3.3A.

With the start of discharge event, concentrations of O_2 and $S-NO_3^-$ start increasing in the domain and keep increasing until the falling limb of stream discharge hydrograph. At the end of the flow event, O_2 concentration is lowered whereas $S-NO_3^-$ remains nearly the same (Figure 3.14 R3, R4). Until the end of discharge event, intra-meander solute concentration distribution shows slightly less CH_20 remaining in the intra-meander area for reactive solute scenario (See Figures 3.1A-3.3A). The difference is further increased 20 h after the flow event, as the CH_2O concentration distribution for reactive transport scenario show a very small amount of solute remaining in the domain compared to conservative solute transport scenario. This trend holds for all three meander shape scenarios (Figures 3.14 and 3.1A-3.3A). Entry of stream water into the intra-meander area provides opportunity O_2 and $S-NO_3^-$ to come in contact with intra-meander CH_2O triggering reaction of aerobic respiration (AR) and denitrification (DEN). For the reactive transport scenarios, the process of conservative transport and consumption of CH_2O by AR and DEN continues in parallel resulting less CH_2O remaining in the domain compared with conservative transport scenarios.

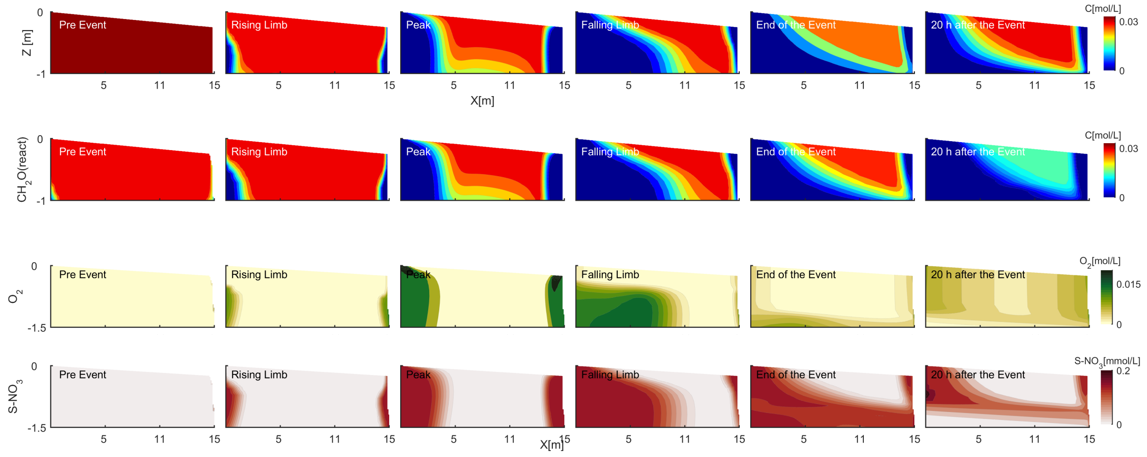

Scenario ω 60

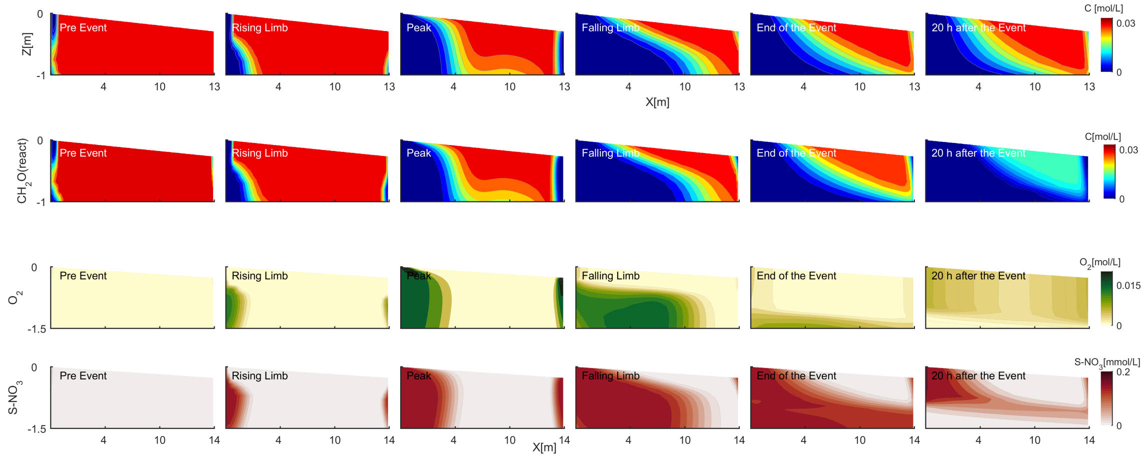

Scenario ω 90

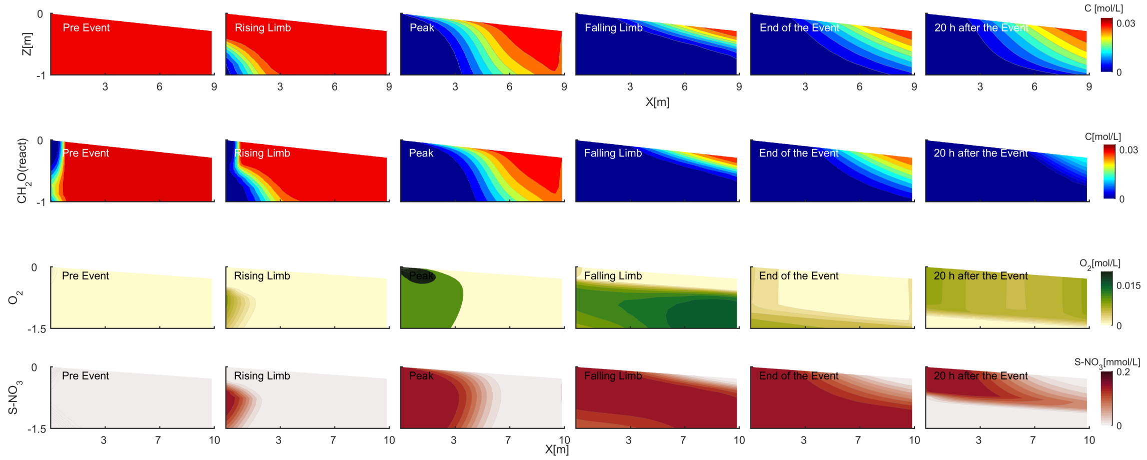

Scenario ω 115

Figure 3.14: XZ-sections (at Y = 20 m) of intra-meander area for scenarios ω 60, 90 and 115 showing concentrations of CH_2O conserv. (R1), CH_2O reactive (R2), O_2 influx (R3), $S-NO_3$ (R4) at different time steps of stream discharge event.

Figure 3.15 presents the reaction time frames of aerobic respiration initiated by entry of stream water into the unsaturated part of the intra-meander zone during the flow event as well as dentrification of stream and groundwater nitrates. For all three scenarios, aerobic respiration starts as soon as the event starts. On the falling limb of the flow event, respiration rates for all three scenarios reach their maxima. At this point, maximum volume of stream water has entered the intra-meander zone triggering high reaction rates. For ω 60, ω 90 respiration rate peaks to 170 and 204$[mol/d]$ respectively while for the scenario ω 115, the peak respiration rate reaches up to 217$[mol/d]$ just after the peak flow. Gradually, reaction rate drops because of the fact that, in the meanwhile solute mass is being exported to the stream by advection. It means, there is less CH_2O available for aerobic respiration. For example, higher hydraulic gradient in the scenario ω 115 results in the quick conservative export of CH_2O to the stream and therefore limiting the DOC source for aerobic respiration. That´s why respiration rate drops quickly after the peak, falling back to zero before the end of the flow event because of non-availability of CH_2O for aerobic respiration. Moreover, on the falling limb, groundwater level falls lower to the DOC layer, limiting the O_2 supply to DOC source layer and therefore reducing reaction rate. As a consequence, aerobic respiration diminishes at the end of the flow event.

Denitrification by groundwater borne nitrates ($G - NO_3^-$) is increased in the beginning of the flow event when stream water has not filled up the intra-meander zone. As the stream water infiltrates into the intra-meander zone, denitrifcation caused by the groundwater nitrates falls quickly reaching the minimum rate of $1x10^{-3}[mol/d]$ at the peak flow i.e. 17 h after the beginning of the flow event. This trend holds for all three scenarios. This can be explained as in absence of stream water, groundwater upwells near the streambed, resulting in denitrification of solute near the stream cell. As soon as stream water enters the unsaturated intra-meander zone, the pressure of inflowing water stops the upwelling of groundwater, limiting the denitrification caused by the groundwater borne nitrates. This is further supported by the fact that at the end of flow event i.e. at 120 h, the dentrification rates caused by the groundwater borne nitrates quickly increased back achieving a constant denitrification rate of $2.5x10^{-3}$, $2.7x10^{-3}$ and $3.4x10^{-3}[mol/d]$ for scenarios ω 60, ω 90 and ω 115 respectively at time 180 h of the beginning of flow event (see Figure 3.15). However, denitrifcation caused by the groundwater borne nitrate is considerably low (in the range of 10^{-3} $[mol/d]$), and increases gradually with increasing sinuosity (ω). This is due to the condition that DOC source is located in the unsaturated zone, which is not in contact with groundwater under pre-event conditions.

Denitrification caused by the stream water borne nitrates ($S - NO_3^-$) starts with the beginning of the flow event. For scenario ω 60 and ω 90, reaction rates increased

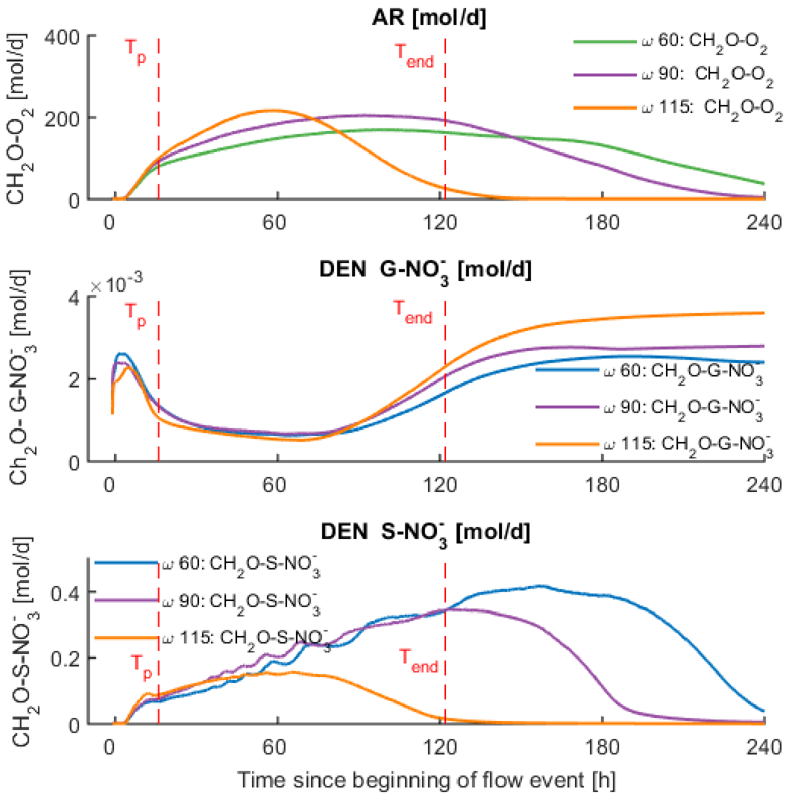

Figure 3.15: Time frames of aerobic respiration (AR) and denitrification (DEN) via stream and groundwater borne oxygen and nitrates during the flow event for meander scenarios ω 60, ω 90, ω 115. T_p and T_{end} indicate the peak and the ending time of the flow event respectively.

during the flow event and continued to increase after the end of the flow event, reaching to a maximum rate of 0.4 and 0.33 $[mol/d]$ respectively, 160 h after the beginning of flow event. Denitrification rates fall back to minimum value 240 h after the beginning of flow event. For scenario ω 115, the denitrification rates reach maximum value of 0.16 $[mol/d]$ at the peak flow time and fall back to minimum value at the end of flow event. This is because of the fact that a major portion of DOC source is transported to stream by advection and a large portion of the rest of the DOC is utilized for aerobic respiration, leaving a small amount of DOC for denitrification, which is completely consumed during the flow event.

Overall, aerobic respiration (AR) consumed the major portion of the DOC source during the flow event, followed by the stream borne nitrates and then by groundwater borne nitrates. These results are in line with the study of Trauth and Fleckenstein (2017), who found that that overall reaction efficiency of aerobic respiration and denitrification by stream nitrates increases during the stream discharge event.

3.3.5.2. DOC Mass Removal during Stream Discharge Event

Figure 3.16 presents the combined effect of advective transport and removal of DOC from intra-meander zone by AR and DEN during stream discharge event. Reactive transport curves indicate that mass export started 5 h earlier than for conservative transport for ω 60 and ω 90, whereas for ω 115, starting point of mass removal coincides with conservative transport i.e. at peak flow.

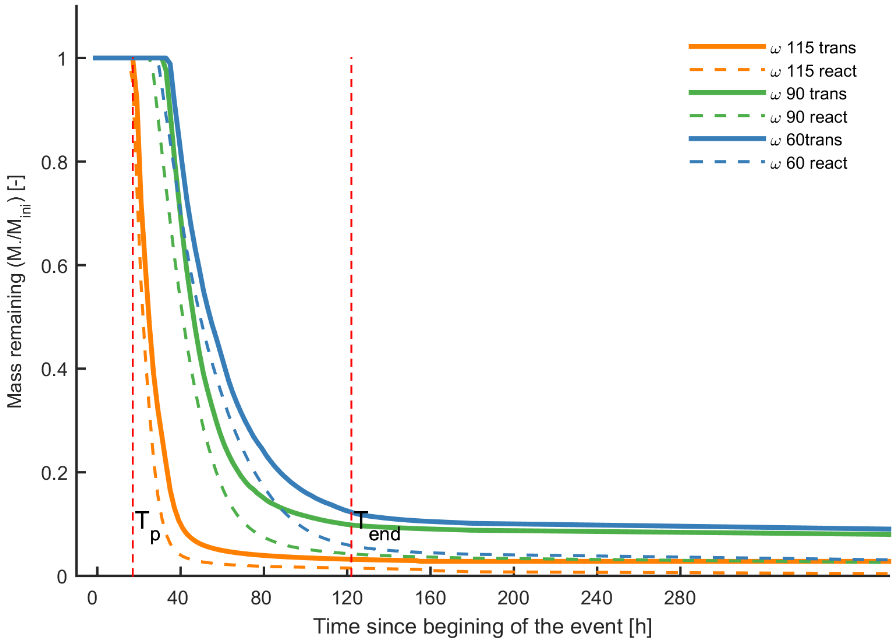

Figure 3.16: Cumulative reactive solute transport during the flow event for three meander shape scenarios i.e. ω 60, ω 90, ω 115. Solid and dotted lines represent fraction of solute remaining for conservative and reactive transport respectively.

Furthermore, the mass remaining within the intra-meander zone in this case is considerably less compared to the conservative transport scenarios. For ω 60, 12.5 % DOC mass remains within the intra-meander zone at the end of the flow event for conservative transport scenario, whereas mass remaining reduces to 5 % for reactive transport scenario i.e. 7.5 % mass has been consumed by aerobic respiration and denitrification combined until the end of flow event. Similarly for ω 90, DOC mass remaining in the intra-meander zone for conservative transport scenario until the end of flow event is 9.9 % whereas for reactive transport scenario, it reduces to 4.2 %, i.e. 5.7 % DOC mass has been consumed by aerobic respiration and denitrification. For ω 115, mass consumed by aerobic respiration and identification, at the end of the flow event is about 1 %. The low mass removal from scenario ω 90 and ω 115 is due to the fact that in these scenarios conservative transport rates are higher, therefore relatively low amount of DOC is available for reactive transport. In all scenarios, the mass removal continues after the flow event. We found that soon after the flow event, DOC is completely consumed in the scenario ω 115, whereas in the scenario ω 60 and ω 90, eventually DOC depletes completely 2880 h (120 days) after the end of flow event (not shown in the Figure 3.16).

To sum up, respiration and denitrification are important chemical reactions, which may deplete intra-meander DOC source during the flow event. Although major portion of the intra-meander solute is transported to stream conservatively during the flow event, aerobic respiration and denitrification triggered by the entry of oxygen and nitrate also consumed substantial amount of intra-meander DOC.

3.4. Summary and Conclusions

Upper layers of non-submerged intra-meander zones may contain layers of solutes and therefore, may provide an opportunity of transport and transformations of solutes between stream and intra-meander region. For example, during the intra-meander HEF, oxygen rich stream water upon coming in contact with carbon rich solute layers of RZ, can initiate biochemcial activities like aerobic respiration and denitrification. Furthermore, during a stream flow event, the submerged area of intra-meander region may increase, linking the upper layers of unsaturated area of intra-meander region, resulting in the transport and transformation of solute initially residing within the non-submerged part of intra-meander zone.

In this study, we have evaluated the influence of meander geometry (sinuosity) on intra-meander flow and residence times. Furthermore, we have investigated the impact of stream discharge event on the mobilization and transport of the DOC source residing within the non-submerged portion of intra-meander zone using three dimensional reactive transport model. In addition to that, we have also simulated the removal of carbon from intra-meander zone by aerobic respiration as well as by denitrification of stream and ground water nitrates triggered during a stream flow event.

The major difference in this study from the previous studies of meander scale exchange is that the past studies are usually limited to the steady state flow, whereas besides steady state flow analysis, we also investigated the impact of flow event on intra-meander zone. For the better representation of the problem, we used a three dimensional modeling setup instead of commonly used 2D modeling setup. Furthermore, past studies are more focused on the flow and transport processes within the fully saturated zone, whereas we also model the flow and solute transport as well as their transformation within the non-submerged partially saturated portion of intra-meander zone.

In this modeling study, we have made few assumptions to reduce complexity of the problem. For example, we assumed homogeneous porous medium with uniform hydraulic conductivity in all directions. No vertical recharge at the top surface was simulated. Additionally, groundwater flow direction was assumed in parallel to the general direction of stream flow in the transient simulations. Similarly, the effect of ambient groundwater flow from lateral directions was not simulated. These simplifications are common and necessary for explorative modeling studies in order to identify the role of individual processes.

Our findings for steady state flow simulations suggest that the hydraulic gradient induced by channel sinuosity and intra-meander area are two main controls of intra-meander flow and residence times. In the early and middle stage meanders i.e. $\omega \leq 90°$, the dominant direction of intra-meander flow paths is along the valley slope or parallel to the general direction of stream flow. This is due to relatively small and almost uniform hydraulic gradient across the upstream and downstream section of the meander, whereas in advanced stage meanders i.e. $\omega \geq 100°$, meander neck exhibits the strongest hydraulic gradient, while in the apex region hydraulic gradient is very small dividing the flow path trajectories and travel time into two flow zones i.e. water flow path trajectories in the apex region are curved and travel times are longer. This intra-meander flow characteristics are in agreement with the previous modeling work (e.g., Boano et al., 2006; Revelli et al., 2008, etc.) as well as laboratory experiments (e.g., Han and Endreny, 2014, etc.). The maximum depth of flow path depends upon the length of the flow path, i.e. longer flow paths penetrate deeper into the subsurface. The average depth of flow paths for all 22 scenarios was found to be in the range of 0.55 to 0.7 m below the streambed, hence the meander sinuosity does not affect the depth of intra-meander flow paths significantly. Another important finding from the steady state flow analysis is that the mean intra-meander residence times decrease with increasing intra-meander hydraulic gradient and increases with increasing intra-meander area regardless of the shape of the meander geometry. Intra-meander area or distance between opposite ends of the intra-meander zone are found to be a major control of intra-meander residence times.

In the transient flow analysis we found that the stream discharge event has strong influence on the mobilization and consequent conservative transport of solute initially residing within the unsaturated intra-meander area. A significant amount of solute was transported for all meander shape scenarios. Results from a similar study of Dwivedi et al. (2018), support the idea that export of carbon from intra-meander area is mainly hydrologically driven. Another important finding is that meander sinuosity is positively related to the solute export process, especially presence of neck in the meander results in the significant enhancement of conservative solute transport towards stream. These findings are consistent with the similar modeling (e.g., Boano et al., 2010) and field (e.g., Nowinski et al., 2012) studies. We also found that stream flow event enhances the reactivity of stream and groundwater borne species with species located within the unsaturated intra-meander region. Stream and groundwater chemical species react with DOC source located within submerged intra-meander area during the flow event leading to removal of carbon and nitrogen from the system. These results are in agreement with study of Trauth and Fleckenstein (2017), who simulated AR and denitrification due to stream water entry into gravel bar during stream discharge event. In our simulations, we found that aerobic respiration is more dominant process during the flow event. Denitrification due to groundwater borne nitrates is minimized during the flow event, whereas the denitrification due to surface water borne nitrates increases steadily. After the flow event, both aerobic respiration and denitrification due to surface water borne nitrates gradually fall to zero, whereas denitrification by groundwater borne nitrates increases to a constant value. In our modeling scenarios, the aerobic respiration and denitrification lead to complete removal of DOC from the intra-meander zone, within a short period of time after the flow event (i.e. within $< 300\ h$ of the beginning of flow event).

Author Contribution Statement

This chapter is the record of a manuscript in preparation. M.N. Mahmood and C. Schmidt jointly planned the study. All work related to designing the model, performing numerical simulations and analysing the results was carried out by M.N. Mahmood. N. Trauth supervised and reviewed the modeling work. The writing work was carried out by M.N. Mahmood. Both C. Schmidt and N. Trauth provided feedback and improved the manuscript.

Appendix 3

Figure 3.1A: XY- cross sections (at Z = 0.75 m below surface) for scenario ω 60 showing concentrations of CH_2O conserv. (R1), CH_2O reacted (R2), O_2 influx (R3) and $S-NO_3^-$ influx (R4) at various stages of stream flow event.

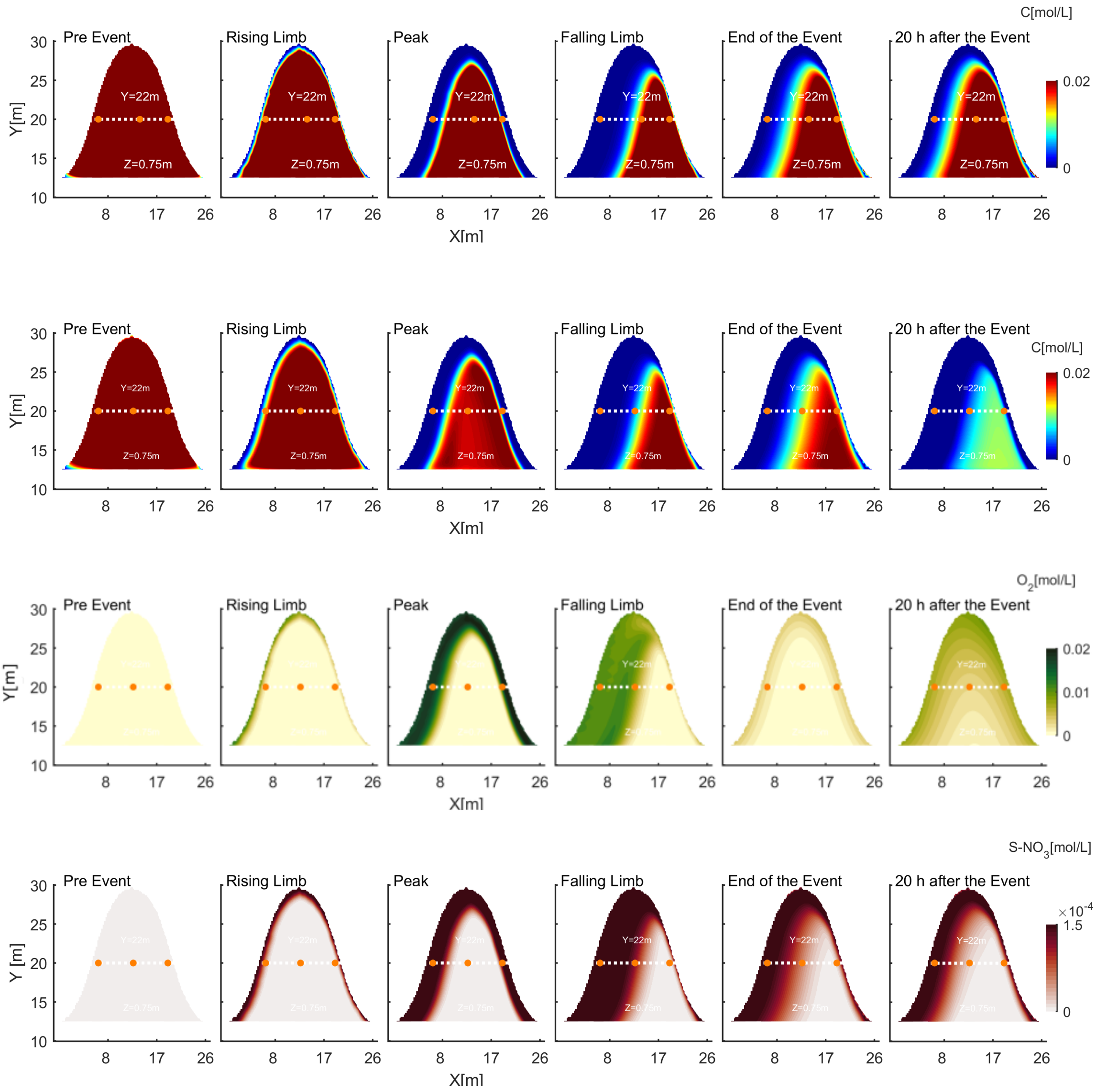

Figure 3.2A: XY- cross sections (at Z = 0.75 m below surface) of intra-meander area for scenario ω 90 showing concentrations of CH_2O conserv. (R1), CH_2O reacted (R2), O_2 influx (R3) and $S-NO_3^-$ influx at various stages of stream flow event.

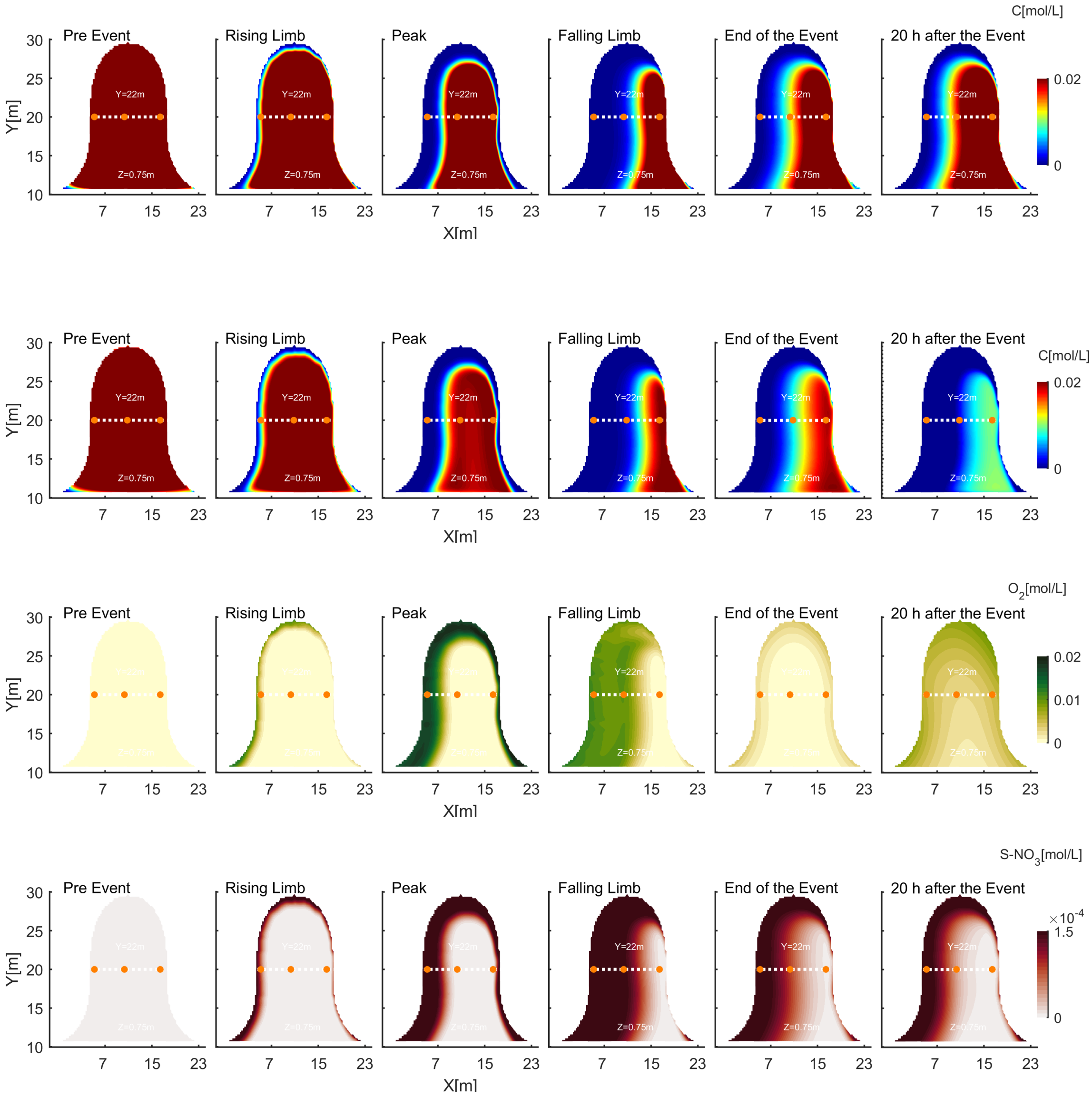

Figure 3.3A: XY-cross sections (at Z = 0.75 m below surface) of intra-meander area for scenario ω 115 showing concentrations of CH_2O conserv. (R1), CH_2O reacted (R2), O_2 influx (R3) and $S-NO_3^-$ influx (R4) at various stages of stream flow event.

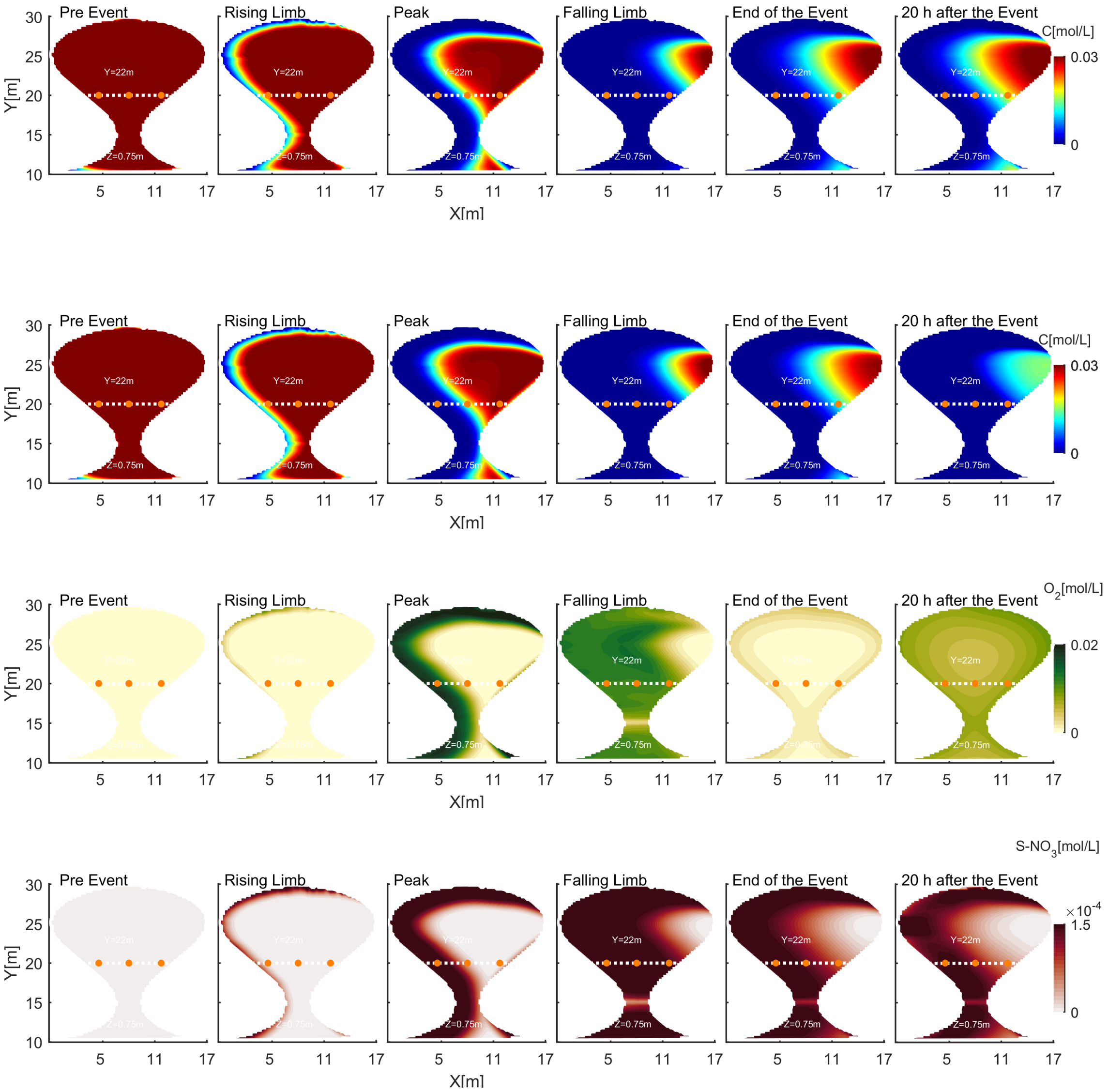

,

Code 3.1A: Matlab code for transforming meander curves to Cartesian coordinates and adjusting them in the MIN3P model as stream cells.

```
% PART A:
% Generates stream points for each run and copies them to the
% respective folder and plots the shape of meander of various degrees
% omega= [10 15 20 25 30 35 40 45 50 55 60 65 70 75 80 85 90 95 ...
    100 105 110 115 120 ];
omega= 60;
ds=0.015;   M=5;
x=1:600; y=1:600;
figure(1)
for kk=1:length(omega)
for ii=1:1000
    if ii ≠ 1
        x(ii)=x(ii-1)+cos(omega(kk)/180*pi*sin((ii-1)*ds/M*2*pi))*ds;
        y(ii)=y(ii-1)+sin(omega(kk)/180*pi*sin((ii-1)*ds/M*2*pi))*ds;
    end
end
X=(x./max(x))*100;
Y=(y./max(y))*30; %normalized to length and width
stream_points=[X'  Y'];
folderName=num2str(omega(kk));

figure (1)
plot(stream_points(:,1),stream_points(:,2),'Linewidth',2);
%save ([pathname '\stream_points'])  ;
%,'Interpreter','tex');
axis tight;
box off;
xlim([0 110]);
ylim([0 35]);
hold on;
end
%------------------------------------------------------------
%% PART B:
% Finds stream point location in  model mesh and applies ...
    parameters such as
% head values, slope etc.
% cxm and cym in the following code are grid points matching ...
    stream-points

load ([pathsp '\stream_points'])  ;
 stream_points(:,3:12)=0;
 %heads_riv=iD*0;

for s=1:length(stream_points(:,1))
  distcount=10000;
```

```

for yi=1:size(cxm,1)
    for xi=1:size(cxm,2)

        xdist=stream_points(s,1)-cxm(1,xi);
        ydist=stream_points(s,2)-cym(yi,1);
        dist_new=sqrt(xdist^2+ydist^2);

        if dist_new < distcount
        stream_points(s,3)=sqrt(xdist^2+ydist^2);
        stream_points(s,4)=cxm(1,xi);
        stream_points(s,5)=cym(yi,1);

        stream_points(s,6)=xm(1,xi);
        stream_points(s,7)=xm(1,xi+1);

        stream_points(s,8)=ym(yi,1);
        stream_points(s,9)=ym(yi+1,1);
        distcount=sqrt(xdist^2+ydist^2);

        stream_points(s,10)=iD(yi,xi);
        end
    end
end
end

[¬,b,c]=unique(stream_points(:,10));
cell_stream=stream_points(b,:); % deleting  duplicate cells

figure(3)
plot((stream_points(:,1)),(stream_points(:,2)),'-o'); hold on
plot((cell_stream(:,4)),(cell_stream(:,5)),'g*')
plot(xm,ym,'k.',cxm,cym,'ro')
axis equal

% calculate distance between points (col 11) and water level (col 12)
stream_points(1,11)=0;

for di=2:length(stream_points(:,1))
stream_points(di,11)=stream_points(di-1,11)+
sqrt((stream_points(di,1)-stream_points(di-1,1))^2+
(stream_points(di,2)-stream_points(di-1,2))^2);
end

% calculate water level (col 12)
stream_points(:,12)=-slope*stream_points(:,11)+dz(2)-incise_depth;

% creating boundary conditions

Head_BCs=zeros(length(b),6);

```

```
for hh=1:length(b)
   clear ah
   [ah,¬]=find(c == hh);
   Head_BCs(hh,1)=mean(stream_points(ah,12));
   Head_BCs(hh,2:5)=(stream_points(ah(1),6:9));
   Head_BCs(hh,6)=hh;
end

heads_riv_ID=iD*0-999;
heads_riv=iD*0-999;
heads_01=iD*0;

for headi=1:size(cell_stream,1)
[a,b]=find(cell_stream(headi,10) == iD);

    heads_riv_ID(a,b)=Head_BCs(headi,6);
    heads_riv(a,b)=Head_BCs(headi,1);
    heads_01(a,b)=1;
end
```

,

Code 3.2A: Matlab code for mesh deformation in the top layers of groundwater model in order to achieve incised stream channel as well as to adjust valley slope according to streambed slope.

```
% example of the *.ibnd file that is read by min3p.
% -----------------------------------------------------------
% title = "dataset deformed mesh"
% variables = "x", "y", "z", "ibnd_vs", "ibnd_rt"
% zone t = "vertically deformed mesh",i = 147 , j = 115 , k = 62, ...
    f=point
%
% -36.9820 -21.9988 150.9301 3520  2
% -35.1478 -21.9988 150.9301 0  0
% -33.3136 -21.9988 150.9301 0  0
% -31.4794 -21.9988 150.9301 0  0
% -29.6453 -21.9988 150.9301 0  0
% ------------------------------------------------------------
% column 4 an 5 indicate the exact number of the BC as defined in ...
    the dat
% file. Zero means no flow.
% matlab script for creating this
cxm=xm;cym=ym; % grid points
%creating topography

slope_channel=(stream_points(end,12)-stream_points(1,12))./(xmax-xmin);

topo_lin=slope_channel*cxm+dz(2);
%+dz(2)
% incise channel from top
%topo=(topo_lin)-(incise_depth.*heads_01);
% incise channel based on heads
topo=(topo_lin)-(heads_01.*(topo_lin-heads_riv));

zm=dz(1):(dz(2)-dz(1))/iz:dz(2);
[cx3m,cy3m,cz3m]=meshgrid(cxm(1,:),cym(:,1),zm); % 3D meshgrid ...
    cell centroids
%%

%%%% creating flat aquifer bottom with similar slope

aquifer_bottom=topo_lin-dz(2)+dz(2)-topo_lin(1,end);
zd=(topo-aquifer_bottom)/iz; % distance matrix between top and bottom

% fining up in Mesh, =2: qadratic function
fineup=2;

%% Define 3D-Matrix for all cells
D=zeros(iy,ix,iz+1);
```

```matlab
Dfineup=D;
[rowD,colD,arD]=size(D);

% Pressure Boundaries
BCp=zeros(iy,ix,iz+1);
[rowBC,colBC,arBC]=size(BCp);

% Chemical Boundaries
BCc=zeros(iy,ix,iz+1);

% Height of Cells is defined
for i=1:ix
    for j=1:iy
        for k=1:iz+1
            if k == 1
                D(j,i,arD)=topo(j,i);
            else
                D(j,i,arD+1-k)=topo(j,i)-(k-1)*zd(j,i);
            end
        end
        if fineup > 1
D(j,i,:)=-(((max(D(j,i,:))-D(j,i,:))./(max(D(j,i,:))-min(D(j,i,:)))).
^fineup.*(max(D(j,i,:))-min(D(j,i,:))))+max(D(j,i,:));
        end
     end
end

%%
k=1;
for i=1:iy;
    for j=1:ix;
         if heads_riv(i,j)>-999 % heads
        BCp(i,j,arBC-1)=heads_riv_ID(i,j);
        BCc(i,j,arBC-1)=1;
        k=k+1;
        else
        BCp(i,j,arBC-1)=0;
        BCc(i,j,arBC-1)=0;
         end
    end
end

%% lateral boundaries
   BCcount=max(max(max(BCp)));
if upDo_head==1
  BCp(:,1,:)=1+BCcount; %Upstream BC Nr
  BCp(:,end,:)=2+BCcount; %Downstream BC Nr
  BCc(:,1,:)=2;   %Upstream Chemie
  BCc(:,end,:)=3;  %Downstream Chemie
end

```

```
% switches of upper layer
BCp(:,:,arBC)= -1; %schaltet oberste RB aus
BCc(:,:,arBC)= -1; %schaltet obere Chemie RB aus
BCtest(:,:)=BCp(:,:,end-1);

% variabel for output
[yD,xD,zD]=size(D);
Dibnd=zeros(xD*yD*zD,5);
m=1;
for i=1:zD
    for j=1:yD
        for k=1:xD
            Dibnd(m,1)=cx3m(j,k,i);  % created by
            Dibnd(m,2)=cy3m(j,k,i);
            Dibnd(m,3)=D(j,k,i);
            Dibnd(m,4)=BCp(j,k,i);
            Dibnd(m,5)=BCc(j,k,i);
            m=m+1;
        end
    end
end
```

Chapter 4

General Summary and Conclusions

4.1. Summary

Exchange of water and solute between stream and its adjacent riparian soils has practical implications for both quantity and quality of fresh water and therefore stream-riparian interface remained in the focus of the riverine research in the past few decades.

The chemical exchange processes are primarily controlled by changes in hydrological conditions of both stream and near stream groundwater. For example, rise and fall of stream stage during a stream flow event induces groundwater table fluctuations in the near stream riparian zones. These stream water induced fluctuations enhance mixing and transport of chemical species between surface and groundwater. In addition to these, in response of stream discharge event, groundwater may rise to initially unsaturated zone, providing an opportunity of solute mobilization, transport and transformation across stream-riparian interface. Spatial and temporal extent of these interactions control the magnitude of water and solute exchange as well as biogeochemical transformations.

In this thesis, bank storage and meander scale interactions between stream and its adjacent riparian soils are studied with a particular focus on mobilization and transport of contaminants within riparian soils in response to changes in hydrologic and morphological conditions. Using a numerical modeling approach, the impact of transient stream conditions on mobilization and transport of solutes initially residing within the non-submerged partially saturated near stream riparian zone are explored.

In the first phase, the influence of stream discharge events of variable duration and magnitude on the solute dynamics in the stream bank are studied. Using a 2D groundwater flow and transport model, mobilization and transport of solute initially residing within the previously unsaturated riparian zone were simulated.

A total of 160 scenarios of single discharge events with systematically increasing peak height and event duration were applied as a time varying head boundary to the stream-riparian interface. The resulting effect on solute mobilization within the riparian zone as well as its consequent export to the stream with return flow was estimated. In the subsequent analysis, relation between solute export and stream event parameters as well as temporal dynamics of the export process were analyzed.

In the second phase, impact of meander sinuosity on intra-meander riparian flow and residence times was investigated using a 3D modeling setup. For this purpose, intra-meander flow was simulated for 22 meander shape scenarios of varying sinuosity. The meandering stream was implemented in the model by adjusting the top layers of the modeling domain to the streambed elevation and assigning linearly decreasing head boundary conditions to the streambed cells. Residence times for the intra-meander zone were computed by advective particle tracking across the inner bank of meander. Selected steady state scenarios were extended to transient flow simulations to evaluate the impact of changes in stream flow conditions on the behavior of the water and solute exchange across the intra-meander zone. In order to represent varying stream flow conditions, a stream discharge event for three representative meander shape scenarios was simulated using surface water model. Transient hydraulic heads obtained from the surface water model were then applied as transient head boundary conditions to the streambed cells of the groundwater model. A constant solute concentration source was added in the unsaturated intra-meander zone to evaluate the effect of transient flow conditions on solute mobilization within intra-meander zone. The temporal and spatial patterns of conservative solute transport were computed and analyzed. In the next step, the model was further extended to investigate biogeochmical transformations within intra-meander zone using pre-defined chemical scenarios. Consumption of solutes (DOC) and nitrates through aerobic respiration (AR) and dentrification (DEN) under variable flow conditions was computed and analyzed.

4.2. Conclusions

4.2.1. Flow and Transport Dynamics in Near Stream Riparian Zone (Bank Flows)

Stream discharge events induce fluctuations in the water table in near stream riparian zone resulting in mobilization of the solutes residing in the non-submerged portion of riparian zone. The shape of stream discharge event (i.e., event peak height and duration) is a major control of magnitude and timing of bank inflows and outflows. Hence associated solute mass outflux from the riparian zone into the stream is also controlled by the shape of the discharge event.

The results suggest that the bank outflows typically start during the falling limb of the stream flow event, when the local hydraulic gradient reverses back to gaining conditions. The timing of change in stream concentration is directly linked to the timing of the bank outflows which in turn depends on the hydraulic gradient near the stream. The time lag between peak stream discharge and peak stream concentration increases with event duration as longer durations delay the reversal of the local hydraulic gradient.

The total solute mass export to the stream is proportional to the magnitude and duration of flow event. Both event peak height and event duration enhance solute mass export. However, peak height is the dominant driver for the solute mass mobilization and export. Longer event duration resulted in delayed peak of solute outflux, providing longer time period for stream and groundwater mixing within the riparian zone. This is particularly important for time dependent solute transformations within the riparian zone. The export of riparian solutes into the stream occurs in two phases. Initially, the bulk of the mobilized solute as a result of rise in water table is transported by the direct bank outflow. Bank outflow driven export lasts for a relatively short period of up to 12 days. The rest of solute mass drains at slow rate after the flow event under the influence of gravity. This slow drainage process from the unsaturated zone is responsible for the long tailing of stream concentration (> 400 days) after the event.

The above findings are in line with previous studies (Boutt and Fleming, 2009; Gu et al., 2012; Mei et al., 2014; Sawyer et al., 2014). It also supports the idea that the export of the riparian solutes during bank outflows is dominantly controlled by the fluctuations in near stream hydraulic gradients (Welch et al., 2015).

4.2.2. Flow and Transport Dynamics within Intra-Meander Zone

Intra-meander hyporheic exchange flow is controlled by the head difference between opposite banks of meander. The residence time of hyporheic exchange plays an important role in biogeochemical transformations as it defines the contact time between stream and groundwater borne species. The residence times of intra-meander flow were computed through advective steady state particle tracking between losing and gaining part of the meander for various meander shape scenarios. The analysis revealed that as meander sinuosity increases, average intra-meander hydraulic gradient increases, resulting in faster flow through the intra-meander zone. Hence, intra-meander residence times are negatively related to intra-meander hydraulic gradient and positively related to the intra-meander area, regardless the shape of meander. Intra-meander residence times ranged from 20 to 65 days for the intra-meander area range of 480 to 760 m^2 depending upon the meander shape. The vertical extent of hyporheic flow paths generally decreases with increasing sinuosity, however maximum penetration depth does not change much with the increasing sinuosity. The maximum penetration depth range of the flow paths was observed from 0.55 to 0.7 m. Therefore, meander sinuosity and intra-meander area are major controls of intra-meander residence times. Results of 3D steady state analysis in this study support the previous 2D modeling studies (e.g., Boano et al., 2006; Revelli et al., 2008) as well as laboratory experiment study of Han and Endreny (2014).

Stream flow variations resulted in mobilization and conservative transport of solute from initially unsaturated portion of intra-meander zone into the stream. In all of our transient flow scenarios, 87 % or more solute mass was conservatively transported towards stream until the end of flow event. Sinuosity was found to be positively related to the mobilization and transport of intra-meander solute towards stream, especially presence of neck feature in the meander resulted in quicker conservative solute transport towards the stream. These finding are consistent with the field studies of Nowinski et al. (2012) and Dwivedi et al. (2018).

Although most of the intra-meander solute was conservatively transported towards stream, reactive transport simulations show that stream flow variations also enhance the reactivity of stream and groundwater borne species with the DOC source located within the unsaturated intra-meander zone. Entry of stream water into intra-meander zone triggered consumption of intra-meander DOC by aerobic respiration and denitrification due to surface water borne nitrates. Aerobic respiration was found to be a dominant process during the flow event followed by the denitrification due to surface water borne nitrates, whereas the denitrifcation due to groundwater borne nitrates was minimized during the flow event. After the flow event, both aerobic respiration and the denitrification due to surface water borne nitrates were minimized, whereas the denitrification by groundwater borne nitrates increased until reaching a constant value. In the modeling scenarios, the aerobic respiration and the denitrification led to complete removal of DOC from the intra-meander zone, within $< 300\ h$ of the beginning of flow event.

4.3. Model Limitations and Future Studies

The modeling setup applied in this study, represents a simplified riparian zone with reduced process complexity. For example, in modeling setup for bank flows and intra-meander flow, the riparian aquifer is homogeneous and isotropic in both effective porosity and hydraulic conductivity. Therefore, any highly conductive zones were not accounted for, although they may facilitate fast preferential flow and transport that potentially exists in riparian aquifers (Beven and Germann, 1982). Conversely, layers of lower permeability may reduce the zone of water exchange and solute removal (Chen and Chen, 2003). However, since sediment properties will hardly change during short-term stream discharge events, the comparative metrics derived in this study are likely the same as for the heterogeneous case. Furthermore, recharge by precipitation was not simulated, although it is potentially an important process for water and solute mobilization (Nielsen et al., 1986). In the intra-meander flow study, groundwater flow direction was assumed in parallel to the general direction of stream flow for the transient flow simulations. Hence, the effect of ambient groundwater flow from lateral directions was not simulated, however, in natural streams, ambient groundwater can potentially alter the direction as well as magnitude of intra-meander flow (Cardenas, 2009). Furthermore, in our study for bank flows, solute transport is purely conservative, although in natural aquifers, sorption and reaction may alter solute export to the stream. Besides that, for the transient flow simulations in the intra-meander zone, only one discharge event scenario was applied to the representative meander shape scenarios instead of simulating the effect of discharge scenarios of varying peak and duration.

However, these simplification are common and necessary for this kind of explorative modeling studies in order to identify the role of individual drivers in complex exchange processes. Although the study has above mentioned limitations, the results obtained through this modeling work support previous field studies as well as give new insights in understanding the the effect of stream stage induced water table flucutations on transport and transformation processes between surface and groundwater. Hence, a step forward was made in understanding the bank and intra-meander scale exchanges. In the future studies of bank flows, incorporating reactions in combination with varying hydrological scenarios would highlight the effect of water table fluctuations on efficiency of solute transformation and removal of DOC. Moreover, influence of vertical recharge as well as variability in hydraulic conductivity should be explored for comprehensive understanding of bank and meander scale transport processes. Furthermore, incorporating the influence of ambient groundwater flow in combination with multiple stream discharge, meander shape and chemical scenarios in future work on the intra-meander flow, will improve our understanding of intra-meander hyporheic exchange.

Bibliography

Aber, J., W. McDowell, K. Nadelhoffer, A. Magill, G. Berntson, M. Kamakea, S. McNulty, W. Currie, L. Rustad, and I. Fernandez (1998). Nitrogen saturation in temperate forest ecosystems: hypotheses revisited. *BioScience 48*(11), 921–934.

Baker, M. E., M. J. Wiley, and P. W. Seelbach (2001). GIS-Based hydrologic modeling of riparian areas: Implications for stream water quality. *JAWRA Journal of the American Water Resources Association 37*(6), 1615–1628.

Barling, R. D. and I. D. Moore (1994). Role of buffer strips in management of waterway pollution: a review. *Environmental Management 18*(4), 543–558.

Barnett, T. P., J. C. Adam, and D. P. Lettenmaier (2005). Potential impacts of a warming climate on water availability in snow-dominated regions. *Nature 438*(7066), 303.

Bartsch, S., S. Frei, M. Ruidisch, C. L. Shope, S. Peiffer, B. Kim, and J. H. Fleckenstein (2014). River-aquifer exchange fluxes under monsoonal climate conditions. *Journal of Hydrology 509*, 601–614.

Battin, T. J., L. A. Kaplan, J. D. Newbold, and S. P. Hendricks (2003). A mixing model analysis of stream solute dynamics and the contribution of a hyporheic zone to ecosystem function. *Freshwater Biology 48*(6), 995–1014.

Becker, M., T. Georgian, H. Ambrose, J. Siniscalchi, and K. Fredrick (2004). Estimating flow and flux of ground water discharge using water temperature and velocity. *Journal of Hydrology 296*(1-4), 221–233.

Bencala, K. E. (1993). A perspective on stream-catchment connections. *Journal of the North American Benthological Society 12*(1), 44–47.

Bencala, K. E. (2000). Hyporheic zone hydrological processes. *Hydrological Processes 14*(15), 2797–2798.

Bencala, K. E. (2005). Hyporheic exchange flows. *Encyclopedia of Hydrological Sciences*.

Bencala, K. E., M. N. Gooseff, and B. A. Kimball (2011). Rethinking hyporheic flow and transient storage to advance understanding of stream-catchment connections. *Water Resources Research 47*(3).

Bencala, K. E. and R. A. Walters (1983). Simulation of solute transport in a mountain pool-and-riffle stream: A transient storage model. *Water Resources Research 19*(3), 718–724.

Berman, T. and D. A. Bronk (2003). Dissolved organic nitrogen: a dynamic participant in aquatic ecosystems. *Aquatic Microbial Ecology 31*(3), 279–305.

Beven, K. and P. Germann (1982). Macropores and water flow in soils. *Water Resources Research 18*(5), 1311–1325.

Biron, P. M., A. G. Roy, F. Courschesne, W. H. Hendershot, B. Côté, and J. Fyles (1999). The effects of antecedent moisture conditions on the relationship of hydrology to hydrochemistry in a small forested watershed. *Hydrological Processes 13*(11), 1541–1555.

Bishop, K., H. Grip, and A. O'neill (1990). The origins of acid runoff in a hillslope during storm events. *Journal of Hydrology 116*(1-4), 35–61.

Bishop, K., C. Pettersson, B. Allard, and Y.-H. Lee (1994). Identification of the riparian sources of aquatic dissolved organic carbon. *Environment International 20*(1), 11–19.

Blodau, C. and T. R. Moore (2003). Experimental response of peatland carbon dynamics to a water table fluctuation. *Aquatic Sciences 65*(1), 47–62.

Boano, F., C. Camporeale, R. Revelli, and L. Ridolfi (2006). Sinuosity-driven hyporheic exchange in meandering rivers. *Geophysical Research Letters 33*(18).

Boano, F., A. Demaria, R. Revelli, and L. Ridolfi (2010). Biogeochemical zonation due to intrameander hyporheic flow. *Water Resources Research 46*(2).

Boano, F., J. W. Harvey, A. Marion, A. I. Packman, R. Revelli, L. Ridolfi, and A. Wörman (2014). Hyporheic flow and transport processes: Mechanisms, models, and biogeochemical implications. *Reviews of Geophysics 52*(4), 603–679.

Böhlke, J. K., R. C. Antweiler, J. W. Harvey, A. E. Laursen, L. K. Smith, R. L. Smith, and M. A. Voytek (2009). Multi-scale measurements and modeling of denitrification in streams with varying flow and nitrate concentration in the upper Mississippi River basin, USA. *Biogeochemistry 93*(1-2), 117–141.

Bolin, B. (1959). On the use of tritium as a tracer for water in nature. Technical report, International Meteorological Inst., Stockholm.

Boulton, A. J., S. Findlay, P. Marmonier, E. H. Stanley, and H. M. Valett (1998). The functional significance of the hyporheic zone in streams and rivers. *Annual Review of Ecology and Systematics 29*(1), 59–81.

Boutt, D. F. and B. J. Fleming (2009). Implications of anthropogenic river stage fluctuations on mass transport in a valley fill aquifer. *Water Resources Research 45*(4).

Brinson, M. M. (1993). Changes in the functioning of wetlands along environmental gradients. *Wetlands 13*(2), 65–74.

Brunke, M. and T. Gonser (1997). The ecological significance of exchange processes between rivers and groundwater. *Freshwater Biology 37*(1), 1–33.

Brunner, P., R. Therrien, P. Renard, C. T. Simmons, and H.-J. H. Franssen (2017). Advances in understanding river-groundwater interactions. *Reviews of Geophysics 55*(3), 818–854.

Buffington, J. M. and D. Tonina (2009). Hyporheic exchange in mountain rivers ii: effects of channel morphology on mechanics, scales, and rates of exchange. *Geography Compass 3*(3), 1038–1062.

Burnett, W., P. Aggarwal, A. Aureli, H. Bokuniewicz, J. Cable, M. Charette, E. Kontar, S. Krupa, K. Kulkarni, A. Loveless, et al. (2006). Quantifying submarine groundwater discharge in the coastal zone via multiple methods. *Science of the total Environment 367*(2-3), 498–543.

Burt, T., P. Bates, M. Stewart, A. Claxton, M. Anderson, and D. Price (2002). Water table fluctuations within the floodplain of the River Severn, England. *Journal of Hydrology 262*(1-4), 1–20.

Burt, T., L. Matchett, K. Goulding, C. Webster, and N. Haycock (1999). Denitrification in riparian buffer zones: the role of floodplain hydrology. *Hydrological Processes 13*(10), 1451–1463.

Camino Serrano, M., E. Graf Pannatier, S. Vicca, S. Luyssaert, M. Jonard, P. Ciais, B. Guenet, B. Gielen, J. Peñuelas, J. Sardans, et al. (2016). Trends in soil solution dissolved organic carbon (DOC) concentrations across European forests. *Biogeosciences 13*, 5567–5585.

Camporeale, C., P. Perona, A. Porporato, and L. Ridolfi (2005). On the long-term behavior of meandering rivers. *Water Resources Research 41*(12).

Cardenas, M. B. (2008). Surface water-groundwater interface geomorphology leads to scaling of residence times. *Geophysical Research Letters 35*(8).

Cardenas, M. B. (2009). Stream-aquifer interactions and hyporheic exchange in gaining and losing sinuous streams. *Water Resources Research 45*(6).

Cardenas, M. B. (2010). Lessons from and assessment of Boussinesq aquifer modeling of a large fluvial island in a dam-regulated river. *Advances in Water Resources 33*(11), 1359–1366.

Cardenas, M. B. and J. L. Wilson (2007). Dunes, turbulent eddies, and interfacial exchange with permeable sediments. *Water Resources Research 43*(8).

Carpenter, S. R., N. F. Caraco, D. L. Correll, R. W. Howarth, A. N. Sharpley, and V. H. Smith (1998). Nonpoint pollution of surface waters with phosphorus and nitrogen. *Ecological Applications 8*(3), 559–568.

Castelle, A. J., A. Johnson, and C. Conolly (1994). Wetland and stream buffer size requirements—a review. *Journal of Environmental Quality 23*(5), 878–882.

Chen, X. and X. Chen (2003). Stream water infiltration, bank storage, and storage zone changes due to stream-stage fluctuations. *Journal of Hydrology 280*(1-4), 246–264.

Cisneros, J., T. O. BE, N. W. Arnell, G. Benito, J. G. Cogley, P. Döll, T. Jiang, S. S. Mwakalila, T. Fischer, D. Gerten, et al. (2014). Freshwater resources. in: Climate change 2014: Impacts,adaptation, and vulnerability. pp. 229–269. Cambridge University Press, Cambridge, United Kingdom and New York, NY, USA.

Constantz, J. (1998). Interaction between stream temperature, streamflow, and groundwater exchanges in alpine streams. *Water Resources Research 34*(7), 1609–1615.

Constantz, J. (2008). Heat as a tracer to determine streambed water exchanges. *Water Resources Research 44*(4).

Constantz, J., D. Stonestorm, A. E. Stewart, R. Niswonger, and T. R. Smith (2001). Analysis of streambed temperatures in ephemeral channels to determine streamflow frequency and duration. *Water Resources Research 37*(2), 317–328.

Cook, P., G. Favreau, J. Dighton, and S. Tickell (2003). Determining natural groundwater influx to a tropical river using radon, chlorofluorocarbons and ionic environmental tracers. *Journal of Hydrology 277*(1-2), 74–88.

Cook, P. G. (2013). Estimating groundwater discharge to rivers from river chemistry surveys. *Hydrological Processes 27*(25), 3694–3707.

Cooper, H. H. and M. I. Rorabaugh (1963). Groundwater movements and bank storage due to flood stages in surface streams. *Water Supply Paper. USGS 1536–J*, 343–363.

Correll, D. L., T. E. Jordan, and D. E. Weller (1997). Failure of agricultural riparian buffers to protect surface waters from groundwater nitrate contamination. In: Groundwater / surface water ecotones: Biological and hydrological interactions and management options. pp. 162–165.

Creed, I. and L. Band (1998). Export of nitrogen from catchments within a temperate forest: evidence for a unifying mechanism regulated by variable source area dynamics. *Water Resources Research 34*(11), 3105–3120.

Creed, I., L. Band, N. Foster, I. Morrison, J. Nicolson, R. Semkin, and D. Jeffries (1996). Regulation of nitrate-n release from temperate forests: A test of the n flushing hypothesis. *Water Resources Research 32*(11), 3337–3354.

Derx, J., A. Blaschke, and G. Blöschl (2010). Three-dimensional flow patterns at the river–aquifer interface—a case study at the Danube. *Advances in Water Resources 33*(11), 1375–1387.

Diem, S., M. R. Von Rohr, J. G. Hering, H.-P. E. Kohler, M. Schirmer, and U. Von Gunten (2013). Nom degradation during river infiltration: Effects of the climate variables temperature and discharge. *Water Research 47*(17), 6585–6595.

Doble, R., P. Brunner, J. McCallum, and P. G. Cook (2012). An analysis of river bank slope and unsaturated flow effects on bank storage. *Groundwater 50*(1), 77–86.

Döll, P. (2009). Vulnerability to the impact of climate change on renewable groundwater resources: a global-scale assessment. *Environmental Research Letters 4*(3), 035006.

Domenico, P. A., F. W. Schwartz, et al. (1998). *Physical and Chemical Hydrogeology, 2nd ed.*, Volume 506. John Wiley & Sons Inc., New York.

Duval, T. and A. Hill (2006). Influence of stream bank seepage during low-flow conditions on riparian zone hydrology. *Water Resources Research 42*(10).

Dwivedi, D., C. I. Steefel, B. Arora, M. Newcomer, J. D. Moulton, B. Dafflon, B. Faybishenko, P. Fox, P. Nico, N. Spycher, et al. (2018). Geochemical exports to river from the intrameander hyporheic zone under transient hydrologic conditions: East River Mountainous Watershed, Colorado. *Water Resources Research 54*(10), 8456–8477.

Edwardson, K. J., W. B. Bowden, C. Dahm, and J. Morrice (2003). The hydraulic characteristics and geochemistry of hyporheic and parafluvial zones in Arctic tundra streams, north slope, Alaska. *Advances in Water Resources 26*(9), 907–923.

Einsiedl, F. (2005). Flow system dynamics and water storage of a fissured-porous karst aquifer characterized by artificial and environmental tracers. *Journal of Hydrology 312*(1-4), 312–321.

Elliott, A. H. and N. H. Brooks (1997). Transfer of nonsorbing solutes to a streambed with bed forms: Theory. *Water Resources Research 33*(1), 123–136.

Engelhardt, I., M. Piepenbrink, N. Trauth, S. Stadler, C. Kludt, M. Schulz, C. Schüth, and T. Ternes (2011). Comparison of tracer methods to quantify hydrodynamic exchange within the hyporheic zone. *Journal of Hydrology 400*(1-2), 255–266.

Fisher, S. G., N. B. Grimm, E. Martí, R. M. Holmes, and J. B. Jones Jr (1998). Material spiraling in stream corridors: a telescoping ecosystem model. *Ecosystems 1*(1), 19–34.

Fleckenstein, J. H., S. Krause, D. M. Hannah, and F. Boano (2010). Groundwater-surface water interactions: New methods and models to improve understanding of processes and dynamics. *Advances in Water Resources 33*(11), 1291–1295.

Fowler, R. T. and M. R. Scarsbrook (2002). Influence of hydrologic exchange patterns on water chemistry and hyporheic invertebrate communities in three gravel-bed rivers. *New Zealand Journal of Marine and Freshwater Research 36*(3), 471–482.

Franklin, D. H., J. L. Steiner, S. E. Duke, D. N. Moriasi, and P. J. Starks (2013). Spatial considerations in wet and dry periods for phosphorus in streams of the fort cobb watershed, United States. *JAWRA Journal of the American Water Resources Association 49*(4), 908–922.

Frei, S., K. Knorr, S. Peiffer, and J. Fleckenstein (2012). Surface micro-topography causes hot spots of biogeochemical activity in wetland systems: A virtual modeling experiment. *Journal of Geophysical Research: Biogeosciences 117*(G4).

Galloway, J. N., F. J. Dentener, D. G. Capone, E. W. Boyer, R. W. Howarth, S. P. Seitzinger, G. P. Asner, C. C. Cleveland, P. Green, E. A. Holland, et al. (2004). Nitrogen cycles: past, present, and future. *Biogeochemistry 70*(2), 153–226.

Gassen, N., C. Griebler, U. Werban, N. Trauth, and C. Stumpp (2017). High resolution monitoring above and below the groundwater table uncovers small-scale hydrochemical gradients. *Environmental Science & Technology 51*(23), 13806–13815.

Gerecht, K. E., M. B. Cardenas, A. J. Guswa, A. H. Sawyer, J. D. Nowinski, and T. E. Swanson (2011). Dynamics of hyporheic flow and heat transport across a bed-to-bank continuum in a large regulated river. *Water Resources Research 47*(3).

Gift, D. M., P. M. Groffman, S. S. Kaushal, and P. M. Mayer (2010). Denitrification potential, root biomass, and organic matter in degraded and restored urban riparian zones. *Restoration Ecology 18*(1), 113–120.

Gleick, P. H. (1993). Water in crisis: a guide to the worlds fresh water resources.

Gomez, J. D., J. L. Wilson, and M. B. Cardenas (2012). Residence time distributions in sinuosity-driven hyporheic zones and their biogeochemical effects. *Water Resources Research 48*(9).

Gomez-Velez, J., J. Wilson, M. Cardenas, and J. Harvey (2017). Flow and residence times of dynamic river bank storage and sinuosity-driven hyporheic exchange. *Water Resources Research 53*(10), 8572–8595.

Gomez-Velez, J. D., J. W. Harvey, M. B. Cardenas, and B. Kiel (2015). Denitrification in the Mississippi River network controlled by flow through river bedforms. *Nature Geoscience 8*(12), 941–945.

Grabs, T., K. Bishop, H. Laudon, S. W. Lyon, and J. Seibert (2012). Riparian zone hydrology and soil water total organic carbon (TOC): implications for spatial variability and upscaling of lateral riparian TOC exports. *Biogeosciences 9*(10), 3901–3916.

Grizzetti, B., F. Bouraoui, G. Billen, H. van Grinsven, A. C. Cardoso, V. Thieu, J. Garnier, C. Curtis, R. Howarth, and P. Johnes (2011). Nitrogen as a threat to European water quality.

Gu, C., W. Anderson, and F. Maggi (2012). Riparian biogeochemical hot moments induced by stream fluctuations. *Water Resources Research 48*(9).

Hallberg, G. R. (1989). Nitrate in ground water in the united states. In *Developments in Agricultural and Managed Forest Ecology*, Volume 21, pp. 35–74. Elsevier.

Han, B. and T. A. Endreny (2014). Detailed river stage mapping and head gradient analysis during meander cutoff in a laboratory river. *Water Resources Research 50*(2), 1689–1703.

Hangen, E., M. Lindenlaub, C. Leibundgut, and K. Von Wilpert (2001). Investigating mechanisms of stormflow generation by natural tracers and hydrometric data: a small catchment study in the Black Forest, Germany. *Hydrological Processes 15*(2), 183–199.

Hanrahan, G., M. Gledhill, W. A. House, and P. J. Worsfold (2003). Evaluation of phosphorus concentrations in relation to annual and seasonal physico-chemical water quality parameters in a UK chalk stream. *Water Research 37*(15), 3579–3589.

Harvey, J. W. (2000). Quantifying hydrologic interactions between streams and their subsurface hyporheic structure, in: Streams and Ground Waters. pp. 3–44.

Harvey, J. W. and K. E. Bencala (1993). The effect of streambed topography on surface-subsurface water exchange in mountain catchments. *Water Resources Research 29*(1), 89–98.

Harvey, J. W., B. J. Wagner, and K. E. Bencala (1996). Evaluating the reliability of the stream tracer approach to characterize stream-subsurface water exchange. *Water Resources Research 32*(8), 2441–2451.

Harvey, R. W. (1997). Microorganisms as tracers in groundwater injection and recovery experiments: a review. *FEMS Microbiology Reviews 20*(3-4), 461–472.

Hassan, M. A., D. Tonina, R. D. Beckie, and M. Kinnear (2015). The effects of discharge and slope on hyporheic flow in step-pool morphologies. *Hydrological Processes 29*(3), 419–433.

Hedin, L. O., J. C. von Fischer, N. E. Ostrom, B. P. Kennedy, M. G. Brown, and G. P. Robertson (1998). Thermodynamic constraints on nitrogentransformations and other biogeochemicalprocesses at soil–stream interfaces. *Ecology 79*(2), 684–703.

Hefting, M., J.-C. Clément, D. Dowrick, A.-C. Cosandey, S. Bernal, C. Cimpian, A. Tatur, T. Burt, and G. Pinay (2004). Water table elevation controls on soil nitrogen cycling in riparian wetlands along a European climatic gradient. *Biogeochemistry 67*(1), 113–134.

Hill, A. R. (1996). Nitrate removal in stream riparian zones. *Journal of Environmental Quality 25*(4), 743–755.

Hill, A. R. (2000). *Stream chemistry and riparian zones, In: Streams and Ground Waters*. Academic Press, San Diego, California.

Hill, A. R. and K. J. Devito (1997). Hydrological-chemical interactions in headwater forest wetlands. *Northern Forested Wetlands: Ecology and Management. Boca Raton, FL, USA*, 213–230.

Hornberger, G., K. Bencala, and D. McKnight (1994). Hydrological controls on dissolved organic carbon during snowmelt in the Snake River near Montezuma, Colorado. *Biogeochemistry 25*(3), 147–165.

Hrachowitz, M., P. Benettin, B. M. Van Breukelen, O. Fovet, N. J. Howden, L. Ruiz, Y. Van Der Velde, and A. J. Wade (2016). Transit times—the link between hydrology and water quality at the catchment scale. *Wiley Interdisciplinary Reviews: Water 3*(5), 629–657.

Ikeda, S., G. Parker, and K. Sawai (1981). Bend theory of river meanders. part 1. linear development. *Journal of Fluid Mechanics 112*, 363–377.

Inamdar, S. P., S. F. Christopher, and M. J. Mitchell (2004). Export mechanisms for dissolved organic carbon and nitrate during summer storm events in a glaciated forested catchment in New York, USA. *Hydrological Processes 18*(14), 2651–2661.

Inamdar, S. P. and M. J. Mitchell (2006). Hydrologic and topographic controls on storm-event exports of dissolved organic carbon (DOC) and nitrate across catchment scales. *Water Resources Research 42*(3).

Jansson, R., H. Laudon, E. Johansson, and C. Augspurger (2007). The importance of groundwater discharge for plant species number in riparian zones. *Ecology 88*(1), 131–139.

Johannesson, H. and G. Parker (1989). Linear theory of river meanders. *River Meandering 12*, 181–213.

Jones Jr, J. B., S. G. Fisher, and N. B. Grimm (1995). Vertical hydrologic exchange and ecosystem metabolism in a Sonoran Desert stream. *Ecology 76*(3), 942–952.

Kalbus, E., F. Reinstorf, and M. Schirmer (2006). Measuring methods for groundwater-surface water interactions: a review. *Hydrology & Earth System Sciences 10*, 873–887.

Kaplan, L. A. and T. L. Bott (1982). Diel fluctuations of DOC generated by algae in a piedmont stream . *Limnology and Oceanography 27*(6), 1091–1100.

Kaplan, L. A. and J. D. Newbold (2000). Surface and subsurface dissolved organic carbon. In *Streams and Ground waters*, pp. 237–258. Elsevier.

Karr, J. R. and I. J. Schlosser (1978). Water resources and the land-water interface. *Science 201*(4352), 229–234.

Kaushal, S. S. and W. M. Lewis (2005). Fate and transport of organic nitrogen in minimally disturbed montane streams of Colorado, USA. *Biogeochemistry 74*(3), 303–321.

Kelly, S. E. and L. C. Murdoch (2003). Measuring the hydraulic conductivity of shallow submerged sediments. *Groundwater 41*(4), 431–439.

Kendall, C. (1998). Tracing nitrogen sources and cycling in catchments. In *Isotope tracers in catchment hydrology*, pp. 519–576.

Kiel, B. A. and M. B. Cardenas (2014). Lateral hyporheic exchange throughout the Mississippi river network. *Nature Geoscience 7*(6), 413.

Konsoer, K. M., B. L. Rhoads, J. L. Best, E. J. Langendoen, J. D. Abad, D. R. Parsons, and M. H. Garcia (2016). Three-dimensional flow structure and bed morphology in large elongate meander loops with different outer bank roughness characteristics. *Water Resources Research 52*(12), 9621–9641.

Kraemer, T. F. (2005). Radium isotopes in Cayuga Lake, New York: Indicators of inflow and mixing processes. *Limnology and Oceanography 50*(1), 158–168.

Krause, S. (2005). Investigation and modeling of water balance and mass transport processes in groundwater-prone landscapes using the example of the lower Havel.

Krause, S., D. Hannah, and T. Blume (2011). Heat transport patterns at pool-riffle sequences of an UK lowland stream. *Ecohydrolology Journal 4*(4), 549–563.

Krause, S., D. Hannah, and J. Fleckenstein (2009). Hyporheic hydrology: interactions at the groundwater-surface water interface. *Hydrological Processes: An International Journal 23*(15), 2103–2107.

Langbein, W. B. and L. B. Leopold (1966). *River meanders–theory of minimum variance.* US Government Printing Office.

Lange, J., C. Leibundgut, T. Grodek, J. Lekach, and A. Schick (1998). Using artificial tracers to study water losses of ephemeral floods in small arid streams. *IAHS Publications-Series of Proceedings and Reports-Intern Assoc. Hydrological Sciences 247*, 31–40.

Lansdown, K., M. Trimmer, C. Heppell, F. Sgouridis, S. Ullah, A. Heathwaite, A. Binley, and H. Zhang (2012). Characterization of the key pathways of dissimilatory nitrate reduction and their response to complex organic substrates in hyporheic sediments. *Limnology and Oceanography 57*(2), 387–400.

Laudon, H. and I. Buffam (2007). Impact of changing DOC concentrations on the potential distribution of acid sensitive biota in a boreal stream network. *Hydrology & Earth System Sciences Discussions 4*(5), 3145–3173.

Laudon, H., S. Köhler, and I. Buffam (2004). Seasonal TOC export from seven boreal catchments in northern Sweden. *Aquatic Sciences 66*(2), 223–230.

Laursen, A. E. and S. P. Seitzinger (2002). Measurement of denitrification in rivers: an integrated, whole reach approach. *Hydrobiologia 485*(1-3), 67–81.

Ledesma, J. L., S. J. Köhler, and M. N. Futter (2012). Long-term dynamics of dissolved organic carbon: implications for drinking water supply. *Science of the total Environment 432*, 1–11.

Lee, D. R. (1977). A device for measuring seepage flux in lakes and estuaries 1. *Limnology and Oceanography 22*(1), 140–147.

Leibundgut, C., P. Maloszewski, and C. Külls (2011). *Tracers in hydrology.* John Wiley & Sons.

Lintern, A., J. Webb, D. Ryu, S. Liu, U. Bende-Michl, D. Waters, P. Leahy, P. Wilson, and A. Western (2018). Key factors influencing differences in stream water quality across space. *Wiley Interdisciplinary Reviews: Water 5*(1), e1260.

Lowrance, R., R. Todd, J. Fail Jr, O. Hendrickson Jr, R. Leonard, and L. Asmussen (1984). Riparian forests as nutrient filters in agricultural watersheds. *BioScience 34*(6), 374–377.

Mahmood, M. N., C. Schmidt, J. H. Fleckenstein, and N. Trauth (2019). Modeling the impact of stream discharge events on riparian solute dynamics. *Groundwater 57*(1), 140–152.

Marzadri, A., D. Tonina, and A. Bellin (2012). Morphodynamic controls on redox conditions and on nitrogen dynamics within the hyporheic zone: Application to gravel bed rivers with alternate-bar morphology. *Journal of Geophysical Research: Biogeosciences 117*(G3).

Marzadri, A., D. Tonina, A. Bellin, G. Vignoli, and M. Tubino (2010). Semianalytical analysis of hyporheic flow induced by alternate bars. *Water Resources Research 46*(7).

Mayer, K. U., E. O. Frind, and D. W. Blowes (2002). Multicomponent reactive transport modeling in variably saturated porous media using a generalized formulation for kinetically controlled reactions. *Water Resources Research 38*(9), 13–1.

Mayer, P. M., S. K. Reynolds, M. McCutchen, and T. Canfield (2005). Riparian buffer width, vegetative cover, and nitrogen removal effectiveness: A review of current science and regulations. *US Environmental Protection Agency 27*.

McCallum, J. L., P. G. Cook, P. Brunner, and D. Berhane (2010). Solute dynamics during bank storage flows and implications for chemical base flow separation. *Water Resources Research 46*(7).

McCallum, J. L. and M. Shanafield (2016). Residence times of stream-groundwater exchanges due to transient stream stage fluctuations. *Water Resources Research 52*(3), 2059–2073.

McClain, M. E., E. W. Boyer, C. L. Dent, S. E. Gergel, N. B. Grimm, P. M. Groffman, S. C. Hart, J. W. Harvey, C. A. Johnston, E. Mayorga, et al. (2003). Biogeochemical hot spots and hot moments at the interface of terrestrial and aquatic ecosystems. *Ecosystems 6*(4), 301–312.

Mei, Y., G. M. Hornberger, L. A. Kaplan, J. D. Newbold, and A. K. Aufdenkampe (2014). The delivery of dissolved organic carbon from a forested hillslope to a headwater stream in southeastern Pennsylvania, USA. *Water Resources Research 50*(7), 5774–5796.

Mierle, G. and R. Ingram (1991). The role of humic substances in the mobilization of mercury from watersheds. *Water Air & Soil Pollution 56*(1), 349–357.

Millington, R. (1959). Gas diffusion in porous media. *Science 130*(3367), 100–102.

Mualem, Y. (1976). A new model for predicting the hydraulic conductivity of unsaturated porous media. *Water Resources Research 12*(3), 513–522.

Mulholland, P. J., A. M. Helton, G. C. Poole, R. O. Hall, S. K. Hamilton, B. J. Peterson, J. L. Tank, L. R. Ashkenas, L. W. Cooper, C. N. Dahm, et al. (2008). Stream denitrification across biomes and its response to anthropogenic nitrate loading. *Nature 452*(7184), 202.

Mulholland, P. J., E. R. Marzolf, J. R. Webster, D. R. Hart, and S. P. Hendricks (1997). Evidence that hyporheic zones increase heterotrophic metabolism and phosphorus uptake in forest streams. *Limnology and Oceanography 42*(3), 443–451.

Mulholland, P. J., J. L. Tank, D. M. Sanzone, W. M. Wollheim, B. J. Peterson, J. R. Webster, and J. L. Meyer (2000). Nitrogen cycling in a forest stream determined by a 15n tracer addition. *Ecological Monographs 70*(3), 471–493.

Munch, J. and J. Ottow (1983). Reductive transformation mechanism of ferric oxides in hydromorphic soils. *Ecological Bulletins*, 383–394.

Munz, M. and C. Schmidt (2017). Estimation of vertical water fluxes from temperature time series by the inverse numerical computer program flux-bot. *Hydrological Processes 31*(15), 2713–2724.

Musial, C. T., A. H. Sawyer, R. T. Barnes, S. Bray, and D. Knights (2016). Surface water–groundwater exchange dynamics in a tidal freshwater zone. *Hydrological Processes 30*(5), 739–750.

Naiman, R. J., H. Decamps, and M. E. McClain (2010). *Riparia: ecology, conservation, and management of streamside communities*. Elsevier.

Neilson, B. T., S. Chapra, D. K. Stevens, and C. Bandaragoda (2010). Two-zone transient storage modeling using temperature and solute data with multiobjective calibration: 1. temperature. *Water Resources Research 46*(12).

Nielsen, D., M. Th. Van Genuchten, and J. Biggar (1986). Water flow and solute transport processes in the unsaturated zone. *Water Resources Research 22*(9S), 89S–108S.

Nowinski, J. D., M. B. Cardenas, A. F. Lightbody, T. E. Swanson, and A. H. Sawyer (2012). Hydraulic and thermal response of groundwater–surface water exchange to flooding in an experimental aquifer. *Journal of Hydrology 472*, 184–192.

O'Connor, B. L., J. W. Harvey, and L. E. McPhillips (2012). Thresholds of flow-induced bed disturbances and their effects on stream metabolism in an agricultural river. *Water Resources Research 48*(8).

Packman, A. I. and M. Salehin (2003). Relative roles of stream flow and sedimentary conditions in controlling hyporheic exchange. *Hydrobiologia 494*(1), 291–297.

Parkin, T. B. (1987). Soil microsites as a source of denitrification variability 1. *Soil Science Society of America Journal 51*(5), 1194–1199.

Paulsen, R. J., C. F. Smith, D. O'Rourke, and T.-F. Wong (2001). Development and evaluation of an ultrasonic ground water seepage meter. *Groundwater 39*(6), 904–911.

Pellerin, B. A., J. F. Saraceno, J. B. Shanley, S. D. Sebestyen, G. R. Aiken, W. M. Wollheim, and B. A. Bergamaschi (2012). Taking the pulse of snowmelt: in situ sensors reveal seasonal, event and diurnal patterns of nitrate and dissolved organic matter variability in an upland forest stream. *Biogeochemistry 108*(1-3), 183–198.

Peterson, B., J. Tank, L. Ashkenas, L. Cooper, C. Dahm, W. Dodds, S. Findlay, S. Gregory, N. Grimm, S. Johnson, et al. (2008). Stream denitrification across biomes and its response to anthropogenic nitrate loading. *Nature 452*(7184), 202206Mulholland.

Pinder, G. F. and S. P. Sauer (1971). Numerical simulation of flood wave modification due to bank storage effects. *Water Resources Research 7*(1), 63–70.

Pratt, B. and H. Chang (2012). Effects of land cover, topography, and built structure on seasonal water quality at multiple spatial scales. *Journal of hazardous materials 209*, 48–58.

Pye, V. I. and R. Patrick (1983). Ground water contamination in the United States. *Science 221*(4612), 713–718.

Rassam, D. W., C. S. Fellows, R. De Hayr, H. Hunter, and P. Bloesch (2006). The hydrology of riparian buffer zones; two case studies in an ephemeral and a perennial stream. *Journal of Hydrology 325*(1-4), 308–324.

Rau, G. C., M. S. Andersen, A. M. McCallum, H. Roshan, and R. I. Acworth (2014). Heat as a tracer to quantify water flow in near-surface sediments. *Earth-Science Reviews 129*, 40–58.

Raymond, P. A. and J. E. Saiers (2010). Event controlled DOC export from forested watersheds. *Biogeochemistry 100*(1-3), 197–209.

Reddy, K., R. Kadlec, E. Flaig, and P. Gale (1999). Phosphorus retention in streams and wetlands: a review. *Critical Reviews in Environmental Science and Technology 29*(1), 83–146.

Revelli, R., F. Boano, C. Camporeale, and L. Ridolfi (2008). Intra-meander hyporheic flow in alluvial rivers. *Water Resources Research 44*(12).

Rinke, K., B. Kuehn, S. Bocaniov, K. Wendt-Potthoff, O. Büttner, J. Tittel, M. Schultze, P. Herzsprung, H. Rönicke, K. Rink, et al. (2013). Reservoirs as sentinels of catchments: the Rappbode Reservoir Observatory (Harz Mountains, Germany). *Environmental Earth Sciences 69*(2), 523–536.

Robertson, A., P. Wood, et al. (2010). Ecology of the hyporheic zone: origins, current knowledge and future directions. *Fundamental and Applied Limnology 176*(4), 279–289.

Rosenberry, D. O. and R. H. Morin (2004). Use of an electromagnetic seepage meter to investigate temporal variability in lake seepage. *Groundwater 42*(1), 68–77.

Rosenberry, D. O. and J. Pitlick (2009). Effects of sediment transport and seepage direction on hydraulic properties at the sediment–water interface of hyporheic settings. *Journal of Hydrology 373*(3-4), 377–391.

Runkel, R. L. (1998). One-dimensional transport with inflow and storage (OTIS): A solute transport model for streams and rivers. *Water Res. Invest. Rep. USGS*, 98–4018.

Salehin, M., A. I. Packman, and M. Paradis (2004). Hyporheic exchange with heterogeneous streambeds: Laboratory experiments and modeling. *Water Resources Research 40*(11).

Sandén, P., S. Karlsson, A. Düker, A. Ledin, and L. Lundman (1997). Variations in hydrochemistry, trace metal concentration and transport during a rain storm event in a small catchment. *Journal of Geochemical Exploration 58*(2-3), 145–155.

Sawyer, A., L. Kaplan, O. Lazareva, and H. Michael (2014). Hydrologic dynamics and geochemical responses within a floodplain aquifer and hyporheic zone during hurricane sandy. *Water Resources Research 50*(6), 4877–4892.

Schlesinger, W. H. and E. S. Bernhardt (2013). *Biogeochemistry: an analysis of global change, 3rd Ed.* Academic Press.

Schmadel, N. M., A. S. Ward, C. S. Lowry, and J. M. Malzone (2016). Hyporheic exchange controlled by dynamic hydrologic boundary conditions. *Geophysical Research Letters 43*(9), 4408–4417.

Schmidt, C., B. Conant Jr, M. Bayer-Raich, and M. Schirmer (2007). Evaluation and field-scale application of an analytical method to quantify groundwater discharge using mapped streambed temperatures. *Journal of Hydrology 347*(3-4), 292–307.

Schmidt, C., A. Musolff, N. Trauth, M. Vieweg, and J. Fleckenstein (2012). Transient analysis of fluctuations of electrical conductivity as tracer in the stream bed. *Hydrology & Earth System Sciences 16*(10).

Seitzinger, S. P., R. V. Styles, E. W. Boyer, R. B. Alexander, G. Billen, R. W. Howarth, B. Mayer, and N. Van Breemen (2002). Nitrogen retention in rivers: model development and application to watersheds in the northeastern USA. In *The Nitrogen Cycle at Regional to Global Scales*, pp. 199–237. Springer.

Shope, C. L., J. E. Constantz, C. A. Cooper, D. M. Reeves, G. Pohll, and W. A. McKay (2012, jun). Influence of a large fluvial island, streambed, and stream bank on surface water-groundwater fluxes and water table dynamics. *Water Resources Research 48*(6).

Shuai, P., M. B. Cardenas, P. S. Knappett, P. C. Bennett, and B. T. Neilson (2017). Denitrification in the banks of fluctuating rivers: The effects of river stage amplitude, sediment hydraulic conductivity and dispersivity, and ambient groundwater flow. *Water Resources Research 53*(9), 7951–7967.

Silliman, S. E., B. Berkowitz, J. Simunek, and M. T. Van Genuchten (2002). Fluid flow and solute migration within the capillary fringe. *Groundwater 40*(1), 76–84.

Simmons, R. C., A. J. Gold, and P. M. Groffman (1992). Nitrate dynamics in riparian forests: groundwater studies. *Journal of Environmental Quality 21*(4), 659–665.

Skogen, M. D., K. Eilola, J. L. Hansen, H. M. Meier, M. S. Molchanov, and V. A. Ryabchenko (2014). Eutrophication status of the North Sea, Skagerrak, Kattegat and the Baltic Sea in present and future climates: A model study. *Journal of Marine Systems 132*, 174–184.

Sliva, L. and D. D. Williams (2001). Buffer zone versus whole catchment approaches to studying land use impact on river water quality. *Water Research 35*(14), 3462–3472.

Smith, V. H., S. B. Joye, and R. W. Howarth (2006). Eutrophication of freshwater and marine ecosystems. *Limnology and Oceanography 51*(1part2), 351–355.

Squillace, P. J., E. Thurman, and E. T. Furlong (1993). Groundwater as a nonpoint source of atrazine and deethylatrazine in a river during base flow conditions. *Water Resources Research 29*(6), 1719–1729.

Stanford, J. A. and J. Ward (1993). An ecosystem perspective of alluvial rivers: connectivity and the hyporheic corridor. *Journal of the North American Benthological Society 12*(1), 48–60.

Stegen, J. C., J. K. Fredrickson, M. J. Wilkins, A. E. Konopka, W. C. Nelson, E. V. Arntzen, W. B. Chrisler, R. K. Chu, R. E. Danczak, S. J. Fansler, et al. (2016). Groundwater–surface water mixing shifts ecological assembly processes and stimulates organic carbon turnover. *Nature Communications 7*, 11237.

Stonedahl, S. H., J. W. Harvey, and A. I. Packman (2013). Interactions between hyporheic flow produced by stream meanders, bars, and dunes. *Water Resources Research 49*(9), 5450–5461.

Stonedahl, S. H., J. W. Harvey, A. Wörman, M. Salehin, and A. I. Packman (2010). A multiscale model for integrating hyporheic exchange from ripples to meanders. *Water Resources Research 46*(12).

Storey, R. G., K. W. Howard, and D. D. Williams (2003). Factors controlling riffle-scale hyporheic exchange flows and their seasonal changes in a gaining stream: A three-dimensional groundwater flow model. *Water Resources Research 39*(2).

Suarez, J. and J. Puertas (2005). Determination of COD, BOD, and suspended solids loads during combined sewer overflow (CSO) events in some combined catchments in Spain. *Ecological Engineering 24*(3), 199–217.

Swanson, F., S. Gregory, J. Sedell, and A. Campbell (1982). Land-water interactions: the riparian zone, in: Analysis of coniferous forest ecosystems in the western united states. pp. 267–291. Stroudsburg, Hutchinson Ross Pub. Co., New York.

Tabacchi, E., L. Lambs, H. Guilloy, A.-M. Planty-Tabacchi, E. Muller, and H. Decamps (2000). Impacts of riparian vegetation on hydrological processes. *Hydrological Processes 14*(16-17), 2959–2976.

Taniguchi, M. and Y. Fukuo (1993). Continuous measurements of ground-water seepage using an automatic seepage meter. *Groundwater 31*(4), 675–679.

Tank, J. L., E. J. Rosi-Marshall, N. A. Griffiths, S. A. Entrekin, and M. L. Stephen (2010). A review of allochthonous organic matter dynamics and metabolism in streams. *Journal of the North American Benthological Society 29*(1), 118–146.

Tonina, D. and J. M. Buffington (2007). Hyporheic exchange in gravel bed rivers with pool-riffle morphology: Laboratory experiments and three-dimensional modeling. *Water Resources Research 43*(1).

Tonina, D. and J. M. Buffington (2011). Effects of stream discharge, alluvial depth and bar amplitude on hyporheic flow in pool-riffle channels. *Water Resources Research 47*(8).

Trauth, N. and J. H. Fleckenstein (2017). Single discharge events increase reactive efficiency of the hyporheic zone. *Water Resources Research 53*(1), 779–798.

Trauth, N., C. Schmidt, U. Maier, M. Vieweg, and J. H. Fleckenstein (2013). Coupled 3-d stream flow and hyporheic flow model under varying stream and ambient groundwater flow conditions in a pool-riffle system. *Water Resources Research 49*(9), 5834–5850.

Trauth, N., C. Schmidt, M. Vieweg, U. Maier, and J. H. Fleckenstein (2014). Hyporheic transport and biogeochemical reactions in pool-riffle systems under varying ambient groundwater flow conditions. *Journal of Geophysical Research: Biogeosciences 119*(5), 910–928.

Trauth, N., C. Schmidt, M. Vieweg, S. E. Oswald, and J. H. Fleckenstein (2015). Hydraulic controls of in-stream gravel bar hyporheic exchange and reactions. *Water Resources Research 51*(4), 2243–2263.

Ulrich, K.-U., L. Paul, and A. Meybohm (2006). Response of drinking-water reservoir ecosystems to decreased acidic atmospheric deposition in SE Germany: trends of chemical reversal. *Environmental Pollution 141*(1), 42–53.

USEPA (2002). National primary drinking water regulations: Long term 1 enhanced surface water treatment rule. final rule. *Federal Register 67*(9), 1811.

Valett, H., C. Dahm, M. Campana, J. Morrice, M. A. Baker, and C. Fellows (1997). Hydrologic influences on groundwater-surface water ecotones: heterogeneity in nutrient composition and retention. *Journal of the North American Benthological Society 16*(1), 239–247.

Valett, H. M., S. G. Fisher, N. B. Grimm, and P. Camill (1994). Vertical hydrologic exchange and ecological stability of a desert stream ecosystem. *Ecology 75*(2), 548–560.

Van Genuchten, M. T. (1980). A closed-form equation for predicting the hydraulic conductivity of unsaturated soils 1. *Soil Science Society of America Journal 44*(5), 892–898.

Vidon, P., C. Allan, D. Burns, T. P. Duval, N. Gurwick, S. Inamdar, R. Lowrance, J. Okay, D. Scott, and S. Sebestyen (2010). Hot spots and hot moments in riparian zones: potential for improved water quality management. *JAWRA Journal of the American Water Resources Association 46*(2), 278–298.

Vidon, P. and A. R. Hill (2004a). Denitrification and patterns of electron donors and acceptors in eight riparian zones with contrasting hydrogeology. *Biogeochemistry 71*(2), 259–283.

Vidon, P., S. Marchese, and S. Rook (2017). Impact of Hurricane Irene and Tropical Storm Lee on riparian zone hydrology and biogeochemistry. *Hydrological Processes 31*(2), 476–488.

Vidon, P. G. and A. R. Hill (2004b). Landscape controls on nitrate removal in stream riparian zones. *Water Resources Research 40*(3).

Vogt, T., E. Hoehn, P. Schneider, A. Freund, M. Schirmer, and O. A. Cirpka (2010). Fluctuations of electrical conductivity as a natural tracer for bank filtration in a losing stream. *Advances in Water Resources 33*(11), 1296–1308.

Wang, Y.-J. and D.-H. Qin (2017). Influence of climate change and human activity on water resources in arid region of Northwest China: an overview. *Advances in Climate Change Research 8*(4), 268–278.

Ward, A. S., N. M. Schmadel, S. M. Wondzell, M. N. Gooseff, and K. Singha (2017). Dynamic hyporheic and riparian flow path geometry through base flow recession in two headwater mountain stream corridors. *Water Resources Research 53*(5), 3988–4003.

Webster, J., E. Benfield, T. Ehrman, M. Schaeffer, J. Tank, J. Hutchens, and D. D'angelo (1999). What happens to allochthonous material that falls into streams? a synthesis of new and published information from Coweeta. *Freshwater Biology 41*(4), 687–705.

Welch, C., G. A. Harrington, and P. G. Cook (2015). Influence of groundwater hydraulic gradient on bank storage metrics. *Groundwater 53*(5), 782–793.

Winter, T. C. (1998). *Ground water and surface water: a single resource*, Volume 1139. USGS.

Winter, T. C. (1999). Relation of streams, lakes, and wetlands to groundwater flow systems. *Hydrogeology Journal 7*(1), 28–45.

Woessner, W. W. (2000). Stream and fluvial plain ground water interactions: rescaling hydrogeologic thought. *Groundwater 38*(3), 423–429.

Wondzell, S. M. and F. J. Swanson (1996). Seasonal and storm dynamics of the hyporheic zone of a 4th-order mountain stream. ii: Nitrogen cycling. *Journal of the North American Benthological Society 15*(1), 20–34.

Wood, P. (1977). Controls of variation in suspended sediment concentration in the River Rother, West Sussex, England. *Sedimentology 24*(3), 437–445.

Wroblicky, G. J., M. E. Campana, H. M. Valett, and C. N. Dahm (1998). Seasonal variation in surface-subsurface water exchange and lateral hyporheic area of two stream-aquifer systems. *Water Resources Research 34*(3), 317–328.

Wu, Y., X. Wen, and Y. Zhang (2004). Analysis of the exchange of groundwater and river water by using Radon-222 in the middle Heihe Basin of northwestern China. *Environmental Geology 45*(5), 647–653.

Xie, Y., P. G. Cook, and C. T. Simmons (2016). Solute transport processes in flow-event-driven stream–aquifer interaction. *Journal of Hydrology 538*, 363–373.

Yoon, B. and P. A. Raymond (2012). Dissolved organic matter export from a forested watershed during Hurricane Irene. *Geophysical Research Letters 39*(18).

Zolezzi, G. and G. Seminara (2001). Downstream and upstream influence in river meandering. part 2. planimetric development. *Journal of Fluid Mechanics 438*, 183–211.

Acknowledgement

This research project could have not been possible without the support and guidance of many people.

I wish to show my deepest gratitude to Dr. Christian Schmidt, my supervisor at UFZ, for accepting me as doctoral candidate under his supervision and guiding me well during the research work. His continuous in and off campus support, motivation and guidance remained with me during these years. I am also deeply grateful to Dr. Nico Trauth (UFZ) for co-supervising this project. This project would not have been possible without his support and guidance in modeling work. I am also thankful to both Christian and Nico for reviewing and improving my scientific writings.

I am grateful to the Prof. Dr. Jan H. Fleckenstein, (Helmholtz Centre for Environmental Research-UFZ) for providing me the opportunity of conducting this research at the department of Hydrogeology (UFZ) and for his support in resolving managerial issues during my stay at UFZ as well as arranging funds after the end of my HEC scholarship. I am equally thankful to Prof. Dr. Rudolf Liedl (Institute for Groundwater Management, IGW, Technical University Dresden) for his kind support at TU Dresden from enrollment into the Ph.D. program to final defense of this thesis.

I would always remember ever helping and cheerful team of department of Hydrogeology UFZ, for the fun-time we spent together, for useful discussions as well for their off campus support. I extend my sincere thanks to Barbara Timmel (International Office, UFZ) for her support with Ausländerbehörde.

This acknowledgment will be incomplete without mentioning my parents and siblings for their support throughout. Especially, I would like to mention Khurshid Anwar, my brother and mentor, for his immense moral support and guidance. I am also thankful to my wife Zobia Latif, who has been extremely supportive of me throughout this entire period.

Last but not least, I thank all my teachers for their guidance, specially ever-inspiring late Mr. Fazal Hussain Naseem.